



Strål  
säkerhets  
myndigheten

Swedish Radiation Safety Authority

Research

# Assessment of modelling approaches for axial gas flow inside LWR fuel rods

## 2022:09

**Author:** Lars Olof Jernkvist  
Quantum Technologies AB Uppsala

**Report number:** 2022:09

**ISSN:** 2000-0456

**Available at:** [www.ssm.se](http://www.ssm.se)



## **SSM perspective**

### **Background**

The fuel rod analysis program SCANAIR has been developed by IRSN (Institut de Radioprotection et de Sûreté Nucléaire) for analysis of reactivity initiated accidents (RIA) in light water reactors. The Swedish Radiation Safety Authority (SSM) has access to SCANAIR in exchange for annual contributions for its further development. The development and administration of the program is done by Quantum Technologies AB on assignment from SSM.

The production and release of gaseous fission products in fuel rods are important phenomena that can be analysed by most computer codes for fuel rod thermal-mechanical behaviour. Bulk flow of gas caused by axial pressure gradients is a phenomenon acting in transient scenarios, and it is still an area of development in these computer codes. The 2021 contribution to the development of SCANAIR is a review of experimental and analytical work for pressure-driven axial gas flow.

### **Results**

This report is an in-depth investigation into models for bulk flow that could be used in computer programs. The report discusses theoretical approaches that are suitable for development of such a model and gives recommendations to further development and implementation. The work describes the complexity of modelling and observes that parameters for gas flow is necessary to compute in connection with other state parameters. For example, the state of the pellet-cladding gap strongly affects the accuracy of the computations and the gap state depends on non-trivial parameters like pellet and cladding deformations and extent of pellet cracking.

Besides being a theoretical foundation for further development, the report also discusses the experimental basis for development and validation. A conclusion is that there is little such information available in open literature and that more tests would be useful.

### **Relevance**

Knowledge of what is happening in a fuel rod during an event and how it is implemented in analytical tools is essential to SSM for the supervision of nuclear power plants and their safety analysis. The participation in the development of SCANAIR also enables SSM to actively be a part of the large efforts that are made internationally with testing, understanding and improving the tools for analysis of reactivity initiated accidents.

**Need for further research**

Continued work on developing SCANAIR's analysis capabilities is planned in cooperation with IRSN. The current work is a foundation for development of a computational model and a continuation in this direction is planned. There is also a need for tests of fuel behaviour to include gas transport in order to expand the basis for models development.

**Project information**

Contact person SSM: Anna Alvestav

Reference: SSM2021-817 / 7030379-00



Strål  
säkerhets  
myndigheten

Swedish Radiation Safety Authority

**Author:** Lars Olof Jernkvist  
Quantum Technologies AB Uppsala

# 2022:09

## Assessment of modelling approaches for axial gas flow inside LWR fuel rods

**Date:** June 2022  
**Report number:** 2022:09  
**ISSN:** 2000-0456  
Available at [www.stralsakerhetsmyndigheten.se](http://www.stralsakerhetsmyndigheten.se)

This report concerns a study which has been conducted for the Swedish Radiation Safety Authority, SSM. The conclusions and viewpoints presented in the report are those of the author/authors and do not necessarily coincide with those of the SSM.

# Assessment of modelling approaches for axial gas flow inside LWR fuel rods

L. O. Jernkvist

1 March, 2022

Quantum Technologies AB  
Uppsala Science Park  
SE-751 83 Uppsala, Sweden

# Assessment of modelling approaches for axial gas flow inside LWR fuel rods

L. O. Jernkvist

Quantum Technologies AB  
Uppsala Science Park  
SE-751 83 Uppsala, Sweden

# Contents

<b>Abstract</b>	<b>III</b>
<b>Sammanfattning</b>	<b>IV</b>
<b>1 Introduction</b>	<b>1</b>
1.1 Background . . . . .	1
1.2 Existing models for axial gas transport . . . . .	3
1.3 Scope and organization of the report . . . . .	4
<b>2 Modelling approaches for axial gas flow</b>	<b>7</b>
2.1 Fundamental equations for gas flow . . . . .	7
2.1.1 General conservation equations . . . . .	7
2.1.2 Constitutive relations for the gas . . . . .	8
2.1.3 Common approximations . . . . .	9
2.2 Models for flow in annular ducts . . . . .	13
2.2.1 Governing equations for laminar flow . . . . .	13
2.2.2 Approximations applied in existing fuel rod gas flow models . . . . .	15
2.2.3 Extensions to turbulent flow . . . . .	16
2.2.4 Application to LWR fuel rods . . . . .	20
2.3 Models for flow in porous and/or cracked media . . . . .	23
2.3.1 Governing equations for gas flow in porous media . . . . .	24
2.3.2 Common approximations to the momentum conservation equation . . . . .	25
2.3.3 Application to LWR fuel rods . . . . .	26
2.3.4 Models for permeability of porous and/or cracked materials . . . . .	28
<b>3 Data for axial permeability of the fuel pellet column</b>	<b>33</b>
3.1 Direct measurements . . . . .	33
3.1.1 Rondinella et al (2015) . . . . .	33
3.1.2 Montgomery & Morris (2019) . . . . .	35
3.2 Other data . . . . .	37
3.2.1 Double gas expansion tests by Desgranges et al. (2005) . . . . .	37
3.2.2 Halden in-reactor gas flow experiments . . . . .	38
3.2.3 INEL out-of-reactor gas flow experiments . . . . .	43
3.2.4 KfK out-of-reactor gas flow experiments . . . . .	45
<b>4 Comparison of modelling approaches</b>	<b>49</b>
4.1 Governing equations for mass flow rate . . . . .	49
4.2 Transmissivity measures . . . . .	50
<b>5 Conclusions and outlook</b>	<b>53</b>
5.1 Conclusions . . . . .	53
5.2 Outlook . . . . .	56

<b>6 Nomenclature</b>	<b>59</b>
6.1 Latin symbols . . . . .	59
6.2 Greek symbols . . . . .	60
<b>References</b>	<b>61</b>

# Abstract

This report deals with computational models and data for pressure-driven axial gas flow inside light-water reactor fuel rods. Following a brief introduction to the physical phenomenon and a review of past experimental and analytical work on the subject, we start by assessing the two principally different categories of models that are currently in use.

The first category of models for axial gas flow inside fuel rods are based on Hagen-Poiseuille type equations for one-dimensional flow in annular ducts. We show that these equations result from considerable approximations to the fundamental conservation laws for mass, momentum and energy, and to the constitutive relations for the gas. These approximations are thoroughly discussed with regard to their physical significance and the restrictions on the applicability that they entail.

The second category of existing models comprise empirically based relations for gas flow through a tortuous network of cracks and pores in the fuel pellets. We show that, for most flow conditions expected inside the fuel rods, the governing Darcy-Forchheimer type equations used in these models are equivalent to the aforementioned Hagen-Poiseuille type equations.

Hence, in practice, the two categories of models differ mainly in the way the axial gas transmissivity or permeability of the fuel rod is described. We conclude that the Hagen-Poiseuille modelling approach has an advantage with regard to implementation in computer programs for thermal-mechanical fuel rod analysis, in that the approach furnishes analytical relations, through which the transmissivity can be estimated from pellet-cladding gap state parameters calculated by such programs.

Finally, we assess experiments and data that are available for validation of axial gas flow models. A few useful in-reactor studies on axial gas flow inside operating fuel rods exist, but most of the current public domain database consists of out-of-reactor laboratory experiments on discharged pressure water reactor fuel rods. For reasons described in the report, the latter are currently of limited value for model validation.

# Sammanfattning

Denna rapport behandlar beräkningsmodeller för tryckinducerad axiell gasströmning i bränslestavar för lättvattenreaktorer. Efter en kortfattad introduktion till fenomenet och en genomgång av tidigare experimentella och analytiska studier av ämnet, inleder vi genom att utvärdera de två principiellt skilda modellkategorierna som för närvarande används.

Den första modellkategorin för axiell gasströmning i bränslestavar är baserad på ekvationer för endimensionell strömning i annulära kanaler av Hagen-Poiseuille-karaktär. Vi visar att dessa ekvationer erhålls genom omfattande förenklingar av de grundläggande konserveringslagarna för massa, rörelsemängd och energi, liksom av gasens konstitutiva samband. Dessa förenklingar diskuteras ingående, med avseende på deras fysikaliska betydelse och de begränsningar i tillämpbarhet de medför.

Den andra modellkategorin i bruk omfattar empiriskt baserade samband för gasströmning genom ett snirklande nätverk av sprickor och porer i bränslekutsarna. Vi visar att de styrande ekvationerna av Darcy-Forchheimer-karaktär i dessa modeller är ekvivalenta med de ovan nämnda Hagen-Poiseuille ekvationerna för merparten av de strömningsförhållanden som kan förväntas i bränslestavarna.

I praktiken skiljer sig således de två modellkategorierna huvudsakligen med avseende på deras beskrivning av bränslestavens axiella genomsläpplighet (permeabilitet) för gas. Vi finner att modelleringsansatsen enligt Hagen-Poiseuille har en fördel med avseende på användning i beräkningsprogram för termomekanisk analys av bränslestavar, då denna ansats erbjuder analytiska samband, varigenom gasgenomsläppligheten kan uppskattas på grundval av beräknade parametrar för kuts-kapslingsgapet från dessa program.

Slutligen utvärderar vi de experiment och data som finns tillgängliga för validering av axiella gasströmningsmodeller. Det finns ett fåtal användbara studier av axiell gasströmning, utförda på bränslestavar under drift i reaktorhärden, men större delen av den öppet tillgängliga databasen utgörs av laboratorieexperiment utförda på utbrända bränslestavar från tryckvattenreaktorer, efter att dessa tagits ut ur härden. Av orsaker som beskrivs i denna rapport är de sistnämnda experimenten i nuläget av begränsat värde för modellvalidering.

# 1 Introduction

## 1.1 Background

The thermal-mechanical behaviour of light water reactor (LWR) fuel rods may, under certain conditions, be affected by axial transport of gas that resides in the pellet-cladding gap and other internal volumes of the rods. The conditions of interest range from mild over-power transients to reactor accident scenarios, such as loss-of-coolant accidents (LOCAs) and reactivity-initiated accidents (RIAs) [1, 2].

The importance of axial gas transport can be understood from the design of LWR fuel rods [3]: the rods are nearly 4 m long and comprise a  $\approx 3.6$  m long column of fissile ceramic fuel pellets, which are enclosed in a thin-wall zirconium alloy cladding tube with an outer diameter of about 10 mm. The pellet-cladding radial gap at operating (hot) condition is narrow ( $< 50 \mu\text{m}$ ) to ease radial heat transfer from the fuel pellets to the cladding and further to the surrounding light water coolant. For the same reason, the hermetically sealed fuel rod is filled with helium gas, having excellent thermal conductivity. With progressive in-reactor use (rod burnup), the helium fill gas is polluted with gaseous fission products with low thermal conductivity, notably xenon and krypton, which are released from the fuel pellets during operation. To reduce the deteriorating effect of these fission gases on pellet-cladding heat transfer, LWR fuel rods are manufactured with fairly large ( $\approx 20 \text{ cm}^3$ ) gas plena at one or both ends to increase the volume of helium. Under in-reactor operation, there is axial transport of gas between these plena, which are comparatively cool, and the hot fuelled part of the rod. Due to the long and narrow flow path, which is made up of the pellet-cladding gap and cracks in the ceramic fuel pellets, this transport is slow.

To assess the typical time scale for axial gas transport in LWR fuel rods, it is necessary to recognize that there are two principally different transport mechanisms:

1. Mixing of gas species under uniform pressure, caused by diffusion;
2. Bulk flow of gas, caused by axial pressure gradients.

The first mechanism is important for normal steady-state reactor operation and mild over-power transients, since it has the potential to affect the thermal conductance of the pellet-cladding gap, and hence, the fuel temperature, under these conditions. More precisely, fission gases with low thermal conductivity are released predominantly in the hot central part of LWR fuel rods, and they mix with the helium fill gas that resides in other parts of the rod. Under normal steady-state operation, this axial gas mixing takes place under virtually uniform pressure conditions, i.e. in the absence of pressure gradients. Consequently, there is no net transport of mass inside the fuel rod, but if there are axial concentration gradients among individual gas species in the gas, there will be equilibrating flows of these gas components due to diffusion.

Diffusive mixing of fission gases with the fuel rod helium fill gas is a rather slow phenomenon, the time dependence of which may be necessary to take into account in order to correctly determine the thermal conductance of the pellet-cladding gap and the fuel temperature. This is particularly important when analysing the fuel behaviour under mild over-power transients or load-follow operation. In the 1980s, axial gas mixing in LWR fuel

rods was extensively studied in a series of in-reactor experiments that were carried out in the Halden reactor, Norway [4–7]. In addition to these in-reactor studies, out-of-reactor experiments on gas mixing were also conducted on an electrically heated fuel rod simulator [8]. At the same time, computational models for axial gas transport and mixing were developed, with the aim to implement them in various fuel rod analysis programs [9–14]. It seems that these efforts were in vain, since most computer programs used for fuel rod thermal-mechanical analyses today do *not* model axial gas mixing [15]. The only exception seems to be the FEMAXI program, which has an optional model for gas mixing [12, 16]. Today, the standard modelling procedure is to assume instantaneous and complete mixing of the gas in the entire free volume of the fuel rod, i.e. the gas composition and pressure are assumed to be uniform along the pellet-cladding gap and in the fuel rod plena.

The second mechanism, bulk flow of gas caused by axial pressure gradients, is important mostly for off-normal and accident conditions, where it has the potential to affect cladding local deformation ("ballooning") and rupture in overheated axial sections of the fuel rod. Ballooning (large distension of a fairly short axial section of the cladding tube by action of internal overpressure) and subsequent rupture may occur under scenarios of LOCA and RIA that involve significant local overheating of the cladding, leading to local loss of material strength [1, 2, 17]. In these scenarios, axial bulk flow of gas can suppress or assist cladding ballooning, depending on whether extensive transient fission gas release takes place during the accident and at what time during the accident the ballooning occurs. If ballooning occurs early in the accident and transient fission gas release is limited, axial gas flow from the cold fuel rod plena to the hot ballooning section will assist the ballooning by providing gas that drives the local deformation. On the other hand, if extensive transient fission gas release occurs, which is typically the case for very high burnup fuel, axial gas flow may suppress the ballooning by reducing the otherwise high gas pressure that would arise locally in the overheated part of the fuel rod where the transient gas release occurs. Moreover, if the ballooning occurs at a late stage of the accident, in which the overheated cladding is gradually returning to normal temperature by progressive re-wetting, axial gas flow from the still overheated part of the rod to re-wetted and cool parts will suppress further ballooning.

The importance of axial gas flow to the ballooning and rupture of LWR fuel rods under LOCA was recognized early, and in the mid-1970s, computational models were developed and implemented in programs used for analysing the fuel rod behaviour under these accidents [18, 19]. A key parameter in these models was the axial flow resistance, and more specifically, how this resistance depended on burnup-related changes to the pellet-cladding gap width and the fuel pellet crack pattern. Experimental studies on the flow resistance were carried out in Germany, using fresh (unirradiated)  $\text{UO}_2$  fuel pellets in as-fabricated form,  $\text{Al}_2\text{O}_3$  pellets in as-fabricated and fragmented form, and granular  $\text{SiO}_2$  [20]. These studies showed that the gap geometry had a very strong influence on the axial gas flow, which was also expected from the computational models. This renders difficult to computationally model axial gas flow under LOCA, since the pellet-cladding gap width normally changes considerably with both space and time during the accident.

In the mid-1970s, axial gas flow experiments were also conducted in the USA on six full-length fuel rods that had been irradiated to a rod average burnup around  $25 \text{ MWd}(\text{kgU})^{-1}$  in a commercial pressurized water reactor (PWR) [21]. These experiments provided valuable data on the resistance associated with the tortuous flow path inside fuel rods with moder-

ate burnup. One of the rods was extensively characterized by use of metallography and ceramography, with the aim to quantitatively determine the axial flow path for the gas and provide data for model validation.

More recently, in-reactor LOCA simulation tests on LWR fuel rods have shown that axial gas flow may be very slow in fuel rods with higher burnup than those in the aforementioned experiments from the 1970s [22–24]. The reason is that the pellet-cladding gap, which makes up most of the axial flow channel for the gas in fuel rods charged with solid (non-annular) pellets, is virtually closed in high burnup fuel rods, at least as long as the cladding distension is limited. The gas flow is then confined to pellet cracks and the small annular clearance that may remain between the pellet and cladding due to the roughnesses of the two contacting surfaces. The implications of the restricted axial gas flow in some of these experiments have been studied by use of computational models [25].

Axial gas flow in high-burnup PWR fuel rods has recently also been studied experimentally at Oak Ridge National Laboratory, USA. These studies [26, 27] are part of a comprehensive research project, aimed at characterizing a wide spectrum of properties of spent nuclear fuel [28]. Gas flow experiments conducted at room temperature on eight PWR fuel rods with rod average burnups from 48 to 59 MWd(kgU)<sup>-1</sup> in this research project confirm that axial gas flow is restricted in high-burnup fuel rods. These experiments were not focussed on axial gas flow under accident conditions, but aimed to investigate internal gas flow kinetics under vacuum drying of failed and waterlogged fuel rods prior to dry storage.

## 1.2 Existing models for axial gas transport

Since the two mechanisms for axial gas flow mentioned above are relevant for different operating conditions of the fuel, computational models have usually been developed for either of the mechanisms. Exceptions are the models presented in [9, 11, 29], which considers both mechanisms simultaneously.

Examples of computational models intended specifically for diffusive mixing of gas species under uniform pressure can be found in [10, 13, 14]. In this report, however, we will focus on models for bulk flow of gas, caused by axial pressure gradients. For this mode of axial gas transport, two principally different kinds of models are currently in use. The two categories differ with regard to the assumption made regarding the axial flow path along the fuel rod [20]:

1. Models assuming axial gas flow in an idealized annular gap between the pellet and cladding [19, 25, 29];
2. Models assuming axial gas flow through a porous medium that completely fills the cladding tube (no distinct pellet-cladding gap) [26, 30–32].

Other differences also exist among the models, e.g. with regard to whether the flowing gas is assumed compressible or not: Compressibility is assumed in some models [25, 26, 29, 30], while in other models [31, 32], the gas is treated as incompressible. For models assuming axial gas flow in an annular gap, the assumed incompressibility makes the governing equations turn to the well-known Hagen-Poiseuille law in case of laminar flow conditions [33]. For models assuming flow through a porous medium, the incompressibility leads to Darcy's law as the governing equation for the flow. This law is common for

modelling *liquid* flow in porous media, for example groundwater or petroleum flow in soils [34], but it is usually not applied to gas flow in its original form. However, Darcy's law can easily be extended to compressible fluids, such as gases [35].

An essential feature of all models, irrespective of category, is that the axial flow depends strongly on the axial pressure gradient, the cross-sectional flow area within the cladding tube, the gas viscosity and frictional effects. The latter depend on both the flow channel properties and the velocity (i.e. turbulence) of the flowing gas. In the first category of models, the frictional effects are usually characterized by the non-dimensional Hagen number, which can be seen as the ratio of wall friction forces to overall viscous forces in the fluid. In the second category of models, frictional effects are lumped together with effects of the restricted flow path through the porous material and characterized by a fundamental material property: the axial permeability of the cracked fuel pellets that fill the cladding tube.

The first category of models have been shown to reproduce experimental data for axial gas flow in PWR fuel rods with low or intermediate burnup (rod average burnup  $\lesssim 25$  MWd(kgU) $^{-1}$ ), for which the estimated pellet-cladding gap width is typically  $\gtrsim 25$   $\mu\text{m}$  at zero rod power and room temperature [29]. For the second category of models, the situation is the opposite: they have been shown to reproduce axial gas flow in PWR fuel rods with rod average burnups beyond about 50 MWd(kgU) $^{-1}$ , for which the pellet-cladding gap is typically  $\lesssim 10$   $\mu\text{m}$  at zero rod power and room temperature [26, 32]. The fuel permeabilities reported from these studies (using argon or nitrogen gas at room temperature) range from  $1 \times 10^{-14}$   $\text{m}^2$  to  $2 \times 10^{-13}$   $\text{m}^2$ .

In conclusion, there is currently no computational model for axial bulk flow of gas in LWR fuel rods that has been validated and shown applicable to the entire range of pellet-cladding gap states expected over the lifetime of a typical LWR fuel rod. As will be shown in this report, analytical flow models as well as experimental data suggest that the axial gas permeability is extremely sensitive to the gap width, when the width is less than 10-15  $\mu\text{m}$ .

### 1.3 Scope and organization of the report

This report deals specifically with models for bulk flow of gas inside LWR fuel rods, which are applicable to modelling of typical conditions experienced by the fuel in design basis LOCA and RIA. The aim is to identify a suitable approach for modelling axial bulk flow of gas over the entire range of expected gap widths, i.e. from completely closed gaps in axial regions with intense pellet-cladding mechanical interaction to wide open gaps in axial regions with cladding ballooning; both gap conditions may hypothetically exist simultaneously in a single fuel rod during LOCA and RIA.

Section 2 of the report deals with the theoretical bases for the two principal modelling approaches described in section 1.2, i.e. models that consider axial flow of gas in an idealized annular pellet-cladding gap and models that consider flow in porous media. Of particular importance are inherent limitations of the models with regard to gap/crack geometry, flow velocity, gas pressure and axial pressure gradients. The presentation starts from the general conservation equations for mass, momentum and energy that any fluid should satisfy. Then, simplifying approximations of these equations that are commonly made in fuel rod

gas flow models are presented and discussed with regard to their physical significance and the restrictions on the applicability that they entail.

Section 3 is a review of experiments and data on axial gas transport inside LWR fuel rods. The experimental methods are reviewed and key results are summarized. In particular, the results of all reviewed studies are transformed into equivalent axial permeabilities for the fuel pellet column, which makes it possible to compare the results reported from different studies.

In section 4, we compare the two modelling approaches described in section 2. In particular, we investigate under which conditions the two modelling approaches provide similar results for the calculated axial gas flow. The objective is to delineate the conditions and model parameters that make the two modelling approaches provide consistent results, especially for conditions with a closed or nearly closed pellet-cladding gap.

Conclusions of the work are finally given in section 5, together with some recommendations for improving models for pressure-driven axial gas flow inside LWR fuel rods. These recommendations include numerical implementation of suitable models, validation and calibration of these models, and use of recent experimental data in the validation process.

The international system of units (SI) is used throughout the report, and symbols used in equations conform to prevalent nomenclature in international literature. All symbols and abbreviations are explained as they first appear in the text. However, to ease a non-linear reading of the report, a nomenclature is provided in section 6.



## 2 Modelling approaches for axial gas flow

Section 2.1 departs from the general conservation equations that any fluid should satisfy. These equations are then combined with constitutive relations that are appropriate for the gases and operating conditions expected in free volumes of LWR fuel rods. The resulting system of governing equations is then simplified by use of approximations afforded by the problem under study, viz. isothermal, quasi-stationary, one-dimensional creeping flow.

Section 2.2 deals with models for flow in annular ducts. The governing equations for laminar flow are theoretically derived. These equations are then compared with those applied in existing fuel rod gas flow models, and the differences are discussed. Finally, the equations are extended to turbulent flow and tested against data from gas flow experiments conducted on un-irradiated LWR fuel rod segments.

Section 2.3 deals with models for flow in porous and/or cracked media. The assumption of incompressible flow and its implications for axial gas flow in LWR fuel rods are discussed, and models for the permeability of porous and cracked media are reviewed.

### 2.1 Fundamental equations for gas flow

#### 2.1.1 General conservation equations

In this section, we present the general conservation equations for mass, momentum and energy that govern fluid flow. The notation used conforms, as far as possible, to prevalent nomenclature in international literature; the reader is referred to the list of symbols in section 6 for a definition of applied symbols. Unless otherwise stated, components of vectors and tensors (e.g. the velocity vector  $u_i$  and the Cauchy stress tensor  $\sigma_{ij}$ ) are related to a rectilinear cartesian coordinate system ( $i = x, y$  or  $z$ ). Einstein's summation convention is applied, meaning that repeated indices imply summation of the indexed vector/tensor components.

**Conservation of mass** A fluid with mass density  $\rho$ , which flows with a velocity defined by the components  $u_i$  with regard to cartesian coordinates  $x_i$ , should satisfy the continuity equation

$$\frac{D\rho}{Dt} = -\rho \frac{\partial u_i}{\partial x_i}, \quad (1)$$

where the left-hand-side material time derivative is defined by [33]

$$\frac{D\rho}{Dt} = \frac{\partial \rho}{\partial t} + u_j \frac{\partial \rho}{\partial x_j}. \quad (2)$$

The first right-hand-side term in eq. (2) describes the intrinsic variation of the density, independent of any flow. The second term, usually called the convective or advective derivative, describes the change in density caused by transport of the fluid in the flow. It may be non-zero also under stationary (time independent) flow conditions.

**Conservation of momentum** If the fluid is subject to body forces  $F_i$ , emanating e.g. from gravity, the momentum equation reads

$$\rho \frac{Du_i}{Dt} = \rho F_i + \frac{\partial \sigma_{ij}}{\partial x_j}, \quad (3)$$

where  $\sigma_{ij}$  is the Cauchy stress tensor. The components of this tensor are related to the state (pressure, temperature, velocity) of the fluid through a constitutive relation; see section 2.1.2 below.

**Conservation of energy** The total specific energy of the fluid,  $E$ , should in a general case satisfy the conservation equation

$$\rho \frac{DE}{Dt} = \rho u_j F_j + \frac{\partial (u_i \sigma_{ij})}{\partial x_j} + \frac{\partial}{\partial x_j} \left( \lambda \frac{\partial T}{\partial x_j} \right), \quad (4)$$

where  $T$  and  $\lambda$  are the temperature and thermal conductivity of the fluid. The total specific energy of the fluid comprises both internal energy and kinematic energy. It is usually expressed in terms of the fluid specific enthalpy,  $H$ , pressure,  $p$ , and velocity through

$$E = H - \frac{p}{\rho} + \frac{u_k u_k}{2}. \quad (5)$$

The above conservation equations are general and should apply at any position within the fluid. They provide five relations for totally sixteen unknown variables:  $p, \rho, T, u_i, \sigma_{ij}$  and either  $E$  or  $H$ . Consequently, eleven additional relations between these variables are needed to solve (close) the system of equations. These relations are specific to the considered fluid and usually termed constitutive relations.

### 2.1.2 Constitutive relations for the gas

As mentioned above, eleven independent relations are needed in addition to the conservation equations for mass, momentum and energy to determine the sixteen unknown variables. These additional relations define the properties of the fluid, and their complexity depends on the type of fluid under consideration (e.g. gas or liquid), and the level of detail needed for the analysis. The following presentation is restricted to constitutive relations suitable for the gas residing in free volumes inside LWR fuel rods, i.e. gas mixtures dominated by helium at temperatures and pressures typically below 1000 K and 10 MPa, respectively.

**Equation of state** The ideal gas law,

$$p(\rho, T) = \frac{R}{M} \rho T, \quad (6)$$

is usually sufficient for describing the relation between thermodynamic pressure, density and temperature of the free gas inside LWR fuel rods. In eq. (6),  $R$  is the universal gas constant ( $R = 8.134 \text{ J}(\text{molK})^{-1}$ ) and  $M$  is the molar mass ( $\text{kgmol}^{-1}$ ) of the gas.

**Enthalpy-temperature relationship** For an ideal gas, the specific enthalpy is independent of pressure. It is related only to temperature through

$$H(T) = c_p T, \quad (7)$$

where the heat capacity (specific heat) at constant pressure,  $c_p$ , can be considered constant. For helium,  $c_p = 5.19 \text{ kJ}(\text{kgK})^{-1}$  [36].

**Stress-velocity relationship** A fairly general relationship between the Cauchy stress tensor, thermodynamic pressure and flow velocity is given by

$$\sigma_{ij} = -p\delta_{ij} + \mu \left( \frac{\partial u_i}{\partial x_j} + \frac{\partial u_j}{\partial x_i} \right) + \Lambda \frac{\partial u_k}{\partial x_k} \delta_{ij}, \quad (8)$$

where  $\delta_{ij}$  is the Kroenecker delta

$$\delta_{ij} = \begin{cases} 0 & \text{for } i \neq j \\ 1 & \text{for } i = j \end{cases}, \quad (9)$$

and  $\mu$  and  $\Lambda$  are the dynamic and second viscosity coefficients of the fluid.

The first right-hand-side term in eq. (8) defines the stresses that would act on an infinitesimal element in a fluid at rest, provided that the element has the same density and temperature that it would experience if it were moving. The pressure  $p$  is the thermodynamic (or equilibrium) pressure, as calculated from eq. (6). As will be shown in section 2.1.3 below, in viscous fluids, it is not always identical to the mechanical pressure acting on the fluid element. The other two right-hand-side terms define stresses induced by viscosity through motion of the fluid. Equation (8) is the most general stress-velocity relation for Newtonian fluids, i.e. fluids where stresses depend linearly on the rate of strain tensor (second and third right-hand-side terms) [37].

The dynamic viscosity depends on temperature. For helium and hydrogen, the temperature dependence is fairly well described by relations with the simple analytical form

$$\mu = \mu_o \left( \frac{T}{T_o} \right)^n, \quad (10)$$

where  $\mu_o$  is the dynamic viscosity at temperature  $T_o$  and  $n$  is an empirical constant. For helium,  $n$  is in the range of 0.65 to 0.70, depending on the choice of reference temperature  $T_o$  and the temperature range of interest [36]. The second viscosity coefficient  $\Lambda$  in eq. (8) is usually not explicitly considered, since it is common to neglect terms that contain this coefficient. This is referred to as Stokes' hypothesis. It simplifies the momentum conservation equation and will be further discussed in section 2.1.3 below.

### 2.1.3 Common approximations

When modelling gas flow inside LWR fuel rods, the equations defined in sections 2.1.1 and 2.1.2 can be considerably simplified without losing much accuracy and significance. Here, we summarize the simplifying approximations that are commonly made in computational models for this particular application. These models are usually presented "as

is", without clearly stating what approximations and simplifications have been made when deriving their governing equations. Nor are the consequences of the approximations discussed.

Some of the simplifications presented in the following have been studied analytically with regard to e.g. loss of accuracy and inferred restrictions on the range of application by Reimann [38]. When applicable, the reader is referred to his report (in German) for further details.

**Isothermal conditions** It is common practice in models for axial gas flow inside LWR fuel rods to exclude the conservation equation for energy (4) from the solution procedure. The gas temperature distribution in the flow channel is consequently not calculated by the models, but inferred as a function of space and time from the (known) temperature distribution for the flow channel walls. Reimann analysed this approximation analytically for axial gas flow in a typical LWR fuel rod design from the 1970s, having an assumed radial pellet-cladding gap of 50  $\mu\text{m}$ . He came to the following main conclusions [38]:

- The axial transport of enthalpy and kinetic energy in the gap gas is negligible in comparison with radial heat transport between the gap gas and the pellet/cladding walls;
- For an assumed temperature difference of 200 K between the pellet and cladding sides of the gap, the radial heat transport and the radially varying gas temperature that it brings about have a negligible effect on the calculated axial mass flow: the relative difference from a simple approximate solution with uniform (radial average) gas temperature is only 0.2 %.

**Quasi-stationary conditions** It is also common practice to simplify the remaining conservation equations, i.e. for mass and momentum, by neglecting the time derivatives  $\partial/\partial t$ . This leads to a quasi-stationary solution, which follows a sequence of stationary (time-independent) solutions that are dictated by the time-dependent boundary conditions. The approximation is reasonable for axial gas flow inside LWR fuel rods, since the characteristic time for reaching stationary conditions is very short. More precisely, this characteristic time can be estimated from [33]

$$t_c \approx \frac{\rho}{\mu} \left( \frac{D_h}{2\lambda_1} \right)^2, \quad (11)$$

where  $D_h$  is the hydraulic diameter of the flow channel and  $\lambda_1 \approx 2.4$  is the first positive root to  $J_0$ , the zeroth order Bessel function of the first kind [39]. For an annual pellet-cladding gap with a radial width  $h$ , the hydraulic diameter is  $D_h = 2h$ . For a radial gap of  $h = 50 \mu\text{m}$ , filled with helium at 800 K and 5 MPa, we thus have  $D_h = 1 \times 10^{-4} \text{ m}$ ,  $\rho \approx 3 \text{ kgm}^{-3}$  and  $\mu \approx 4 \times 10^{-5} \text{ Pas}$  [36]. From eq. (11), we estimate the characteristic time for reaching stationary flow conditions to  $t_c \approx 32 \mu\text{s}$ . This time is very short, even in comparison with the time scale of worst-case reactivity initiated accidents [2]. Moreover, from eq. (11), we note that  $t_c$  will be even shorter for fuel rods with narrower pellet-cladding gaps.

**One-dimensional flow** As long as the pellet-cladding gap is open, the gap will be the dominating path for axial gas flow inside the fuel rod. In some computational models, the gap is treated as a continuous annular duct. In these models, the radial gap width may be treated as uniform along the tangential direction (axially symmetric geometry), or it may vary along the circumference due to eccentricity between the fuel pellet column and the cladding tube. In both cases, the gas flow is treated as entirely axial, which means that velocity components in the radial and tangential directions of the gap are neglected. Hence, radial flow of gas, e.g. caused by fission gas release from the fuel pellets, is not explicitly treated in the flow equations, but treated with an additional source/sink term in the continuity equation (1).

This is a rough idealization of the true pellet-cladding gap geometry and the gas flow within the gap. In reality, fuel pellets are cracked and the fragments are relocated from their original position, as shown in Figure 1. Consequently, the pellet-cladding gap does not provide a continuous annular duct for axial gas flow, but a tortuous flow path in the spaces between fuel pellet fragments and in the residual gap between the cladding inner surface and relocated fuel pellet fragments. This axial pathway will change considerably from one cracked pellet to another, which means that the predominantly axial gas flow will be locally diverted to regions with the lowest flow resistance by radial and tangential flow at a local scale. In models that consider axial flow in an idealized annular gap, this "tortuosity" effect is captured by empirically modifying flow friction parameters. Other models account for the tortuosity by considering flow through a porous medium rather than in an annual gap; see section 2.3.

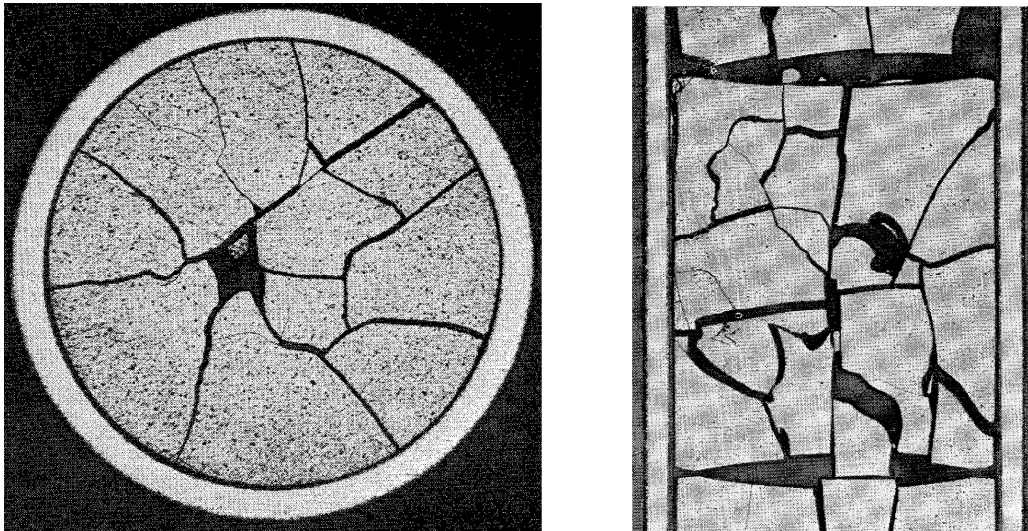


Figure 1: Typical fuel pellet crack pattern in low burnup (2.5 MWd/kgU)  $\text{UO}_2$  fuel, caused by normal reactor operation at high (40-45 kW/m) linear power. Pre-test condition of rod C6 in the FR2 LOCA test series [40].

**Stokes' hypothesis** In section 2.1.2, we presented the most general stress-velocity relationship for a Newtonian fluid; see eq. (8). By summing the diagonal elements of the stress tensor defined by this equation, we get

$$\sigma_{ii} = -3 \left( p - \left( \frac{2\mu}{3} + \Lambda \right) \frac{\partial u_k}{\partial x_k} \right). \quad (12)$$

By definition, the mechanical pressure experienced by a fluid element is  $-\sigma_{ii}/3$ , which means that the mechanical pressure resulting from eq. (12) is

$$p_{\text{mech}} = p - \left( \frac{2\mu}{3} + \Lambda \right) \frac{\partial u_k}{\partial x_k} = p - \mu_b \text{div} \mathbf{u}, \quad (13)$$

where  $\mu_b = 2\mu/3 + \Lambda$  is known as the bulk viscosity coefficient. Equation (13) states that the mechanical pressure differs from the thermodynamic pressure by viscous effects related to dilation ( $\text{div} \mathbf{u} > 0$ ) or contraction ( $\text{div} \mathbf{u} < 0$ ) of the volume element. Neglecting this difference between the mechanical and thermodynamic pressure makes mathematical treatment of compressible flow much easier. This was noticed by Stokes, who simply set  $\mu_b = 0$  [41]. This is known as Stokes' hypothesis, and it leads to the well-known Navier-Stokes equations for compressible flow [33]. However, Stokes' hypothesis that  $\mu_b = 0$  has no physical or experimental support, since  $\mu_b$  is non-negligible for all fluids but monatomic gases. Yet, the hypothesis is known to work well for modelling flows that satisfy the condition  $|p| \gg |\mu_b \text{div} \mathbf{u}|$ , which holds in most cases that do not involve shock waves or hypersonic flows.<sup>1</sup>

By use of Stokes' hypothesis, only the deviatoric part of the stress tensor is affected by viscosity. More precisely, the constitutive relation in eq. (8) can be written  $\sigma_{ij} = -p\delta_{ij} + \tau_{ij}$ , where the deviatoric stress tensor  $\tau_{ij}$  is calculated from the velocity gradients through

$$\tau_{ij} = \mu \left( \frac{\partial u_i}{\partial x_j} + \frac{\partial u_j}{\partial x_i} - \frac{2}{3} \frac{\partial u_k}{\partial x_k} \delta_{ij} \right). \quad (14)$$

**Additional simplifications to the momentum equation** In addition to Stokes' hypothesis, it is also common to simplify the conservation equation for momentum (3) by neglecting the body forces  $F_i$ . With regard to axial gas flow inside LWR fuel rods, these body forces are related to gravity. They are negligible in comparison with forces arising from axial pressure gradients in the fuel rod, caused by changes in axial distributions of temperature and fuel rod free gas volume.

Another common simplification to the momentum conservation equation is to neglect the advective inertia term, i.e. the second term of the left-hand-side material derivative in eq. (3)

$$\rho \frac{Du_i}{Dt} = \rho \frac{\partial u_i}{\partial t} + \rho u_j \frac{\partial u_i}{\partial x_j}. \quad (15)$$

This eliminates the non-linearity with regard to flow velocity, which considerably simplifies the solution of the equations. The resulting equations are known as Stokes' equations for creeping flow. They are applicable when advective inertial forces are small compared with viscous forces, which is typically the case when flow is slow, viscosity is high or the flow channel is narrow. More specifically, for flow in a duct with a typical cross-sectional dimension  $h$ , which may vary over a typical distance  $L$  along the flow direction, the linearization is justified when  $\rho u h^2 (\mu L)^{-1} \ll 1$ , where  $u$  is the typical flow velocity along the duct [43]. For axial gas flow along the pellet-cladding gap of an LWR nuclear fuel rod, typical values for  $h$  and  $L$  are  $3 \times 10^{-5}$  and  $1 \times 10^{-1}$  m. For helium at 800 K

<sup>1</sup>A notable exception is the damping of acoustic waves with high frequencies [42], the modelling of which requires  $\mu_b \neq 0$ , at the expense of numerical complexity.

and 5 MPa,  $\rho \approx 3 \text{ kgm}^{-3}$  and  $\mu \approx 4 \times 10^{-5} \text{ Pas}$  [36]. Hence, the linearization is justified when the axial gas flow velocity satisfies  $u \ll \mu L(\rho h^2)^{-1} = 1480 \text{ ms}^{-1}$ . This condition is definitively satisfied for axial gas flow inside the fuel rod.

## 2.2 Models for flow in annular ducts

### 2.2.1 Governing equations for laminar flow

With the aim to formulate a set of equations that models axial gas flow in the pellet-cladding gap with sufficient generality, yet reasonable complexity, we depart from the general equations described in sections 2.1.1 and 2.1.2 and apply the various simplifications to these equations that were presented and discussed in section 2.1.3.

More precisely, we consider quasi-stationary, one-dimensional flow in the axial ( $z$ ) direction. Henceforth, the axial flow velocity component will be referred to as  $u$ . The other two components are assumed to be zero, meaning that turbulence and departure from rectilinear axial flow by variations in the flow channel geometry along the axial direction (often referred to as conical flow) are neglected. For simplicity, we also neglect gravitational forces acting on the gas and exclude the conservation equation for energy (4). The gas temperature is assumed to be uniform across the gap, but expected to depend on axial position along the gap. From eqs. (6) and (10), it is clear that this implies that there are axial variations in the pressure-density ratio and viscosity. Finally, we neglect the advective inertia term in the momentum conservation equation (see eq. (15)) and apply Stokes' hypothesis for the stress-velocity relation for the gas.

Consider, as before, the conservation equations for mass and momentum in a cartesian coordinate system that is aligned with the principal directions of a narrow gap, as illustrated in Figure 2. The axial ( $z$ ) direction is the direction of flow ( $u$ ), whereas  $x$  is the direction across the gap. The fluid pressure and axial velocity are assumed to depend on both  $x$  and  $z$ , but not on  $y$ , since there is no variation in gap width, fluid properties and temperature along the  $y$ -axis. The mass conservation equation (1) under stationary one-dimensional flow in this geometry is simply

$$u \frac{\partial \rho}{\partial z} + \rho \frac{\partial u}{\partial z} = \frac{\partial}{\partial z}(\rho u) = 0, \quad (16)$$

which means that the axial mass flux is constant along the flow channel. This is true as long as the cross-sectional area of the flow channel does not change with  $z$  and there is no change in gap gas inventory by e.g. fission gas release from the fuel pellets. Otherwise, eq. (16) has to be modified to include these effects.

Consider now the momentum conservation equation (3), combined with the stress-velocity relationship in eq. (14) for a Newtonian fluid that obeys Stokes' hypothesis. Under one-dimensional stationary conditions, neglecting the advective inertia terms that are quadratic in  $u$ , the momentum equations for the  $x$  and  $z$  directions read

$$\frac{\partial p}{\partial x} = -\frac{2}{3} \frac{\partial}{\partial x} \left( \mu \frac{\partial u}{\partial z} \right) + \frac{\partial}{\partial z} \left( \mu \frac{\partial u}{\partial x} \right), \quad (17)$$

$$\frac{\partial p}{\partial z} = \frac{\partial}{\partial x} \left( \mu \frac{\partial u}{\partial x} \right) + \frac{4}{3} \frac{\partial}{\partial z} \left( \mu \frac{\partial u}{\partial z} \right). \quad (18)$$

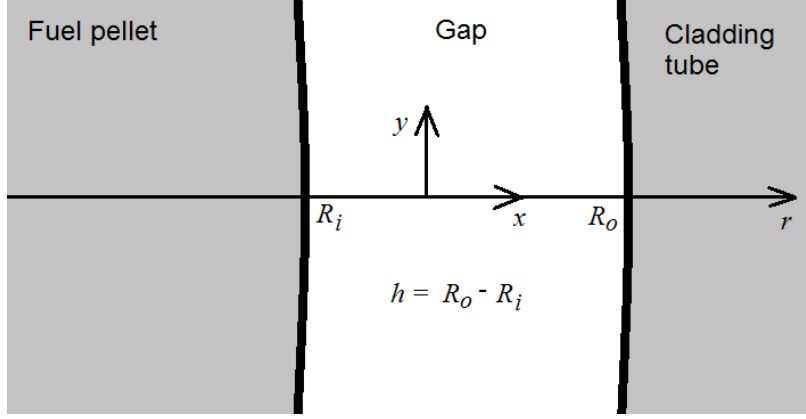


Figure 2: Pellet-cladding annular gap. For narrow gaps ( $R_o/R_i \rightarrow 1$ ), the cylindrical coordinate system  $(r, \theta, z)$  may be locally approximated by a cartesian system  $(x, y, z)$ .

To identify the magnitude of each term in eqs. (17) and (18), we normalize all variables with typical reference values, henceforth indexed with "o". The normalized variables are denoted with a bar, e.g.  $\bar{p} = p/p_o$ , etc. The normalized coordinates  $\bar{x}$  and  $\bar{z}$  are defined by  $\bar{x} = x/h$  and  $\bar{z} = z/L$ , where  $h$  and  $L$  are the typical width and length of the flow channel. Considering that  $\mu$  is assumed independent of  $x$ , the normalization of eqs. (17) and (18) results in

$$\frac{\partial \bar{p}}{\partial \bar{x}} = -\frac{2\bar{\alpha}\bar{\mu}}{3} \frac{\partial^2 \bar{u}}{\partial \bar{x} \partial \bar{z}} + \bar{\alpha} \frac{\partial}{\partial \bar{z}} \left( \bar{\mu} \frac{\partial \bar{u}}{\partial \bar{x}} \right), \quad (19)$$

$$\frac{\partial \bar{p}}{\partial \bar{z}} = \bar{\alpha}\bar{\mu} \left( \frac{L}{h} \right)^2 \frac{\partial^2 \bar{u}}{\partial \bar{x}^2} + \frac{4\bar{\alpha}}{3} \frac{\partial}{\partial \bar{z}} \left( \bar{\mu} \frac{\partial \bar{u}}{\partial \bar{z}} \right), \quad (20)$$

where the dimension-free quantity  $\bar{\alpha} = \mu_o u_o (L p_o)^{-1}$  is very small for typical gap gas conditions. Using the same example as before, helium at 800 K and 5 MPa,  $\rho \approx 3 \text{ kgm}^{-3}$  and  $\mu \approx 4 \times 10^{-5} \text{ Pas}$  [36]. This, together with  $L = 0.1 \text{ m}$  (typical length of axial segments used for discretizing fuel rods in computer analyses), gives  $\bar{\alpha} = u_o 8 \times 10^{-11}$ , where  $u_o$  is the typical gas flow velocity in  $\text{ms}^{-1}$ . Hence, it is safe to say that all right-hand-side terms in eqs. (19) and (20), except for one, are negligible. The non-negligible term contains the factor  $(L/h)^2$ , which for a typical gap width,  $h = 3 \times 10^{-5} \text{ m}$ , is about  $10^7$ .

Based on the above analysis, we may simplify the governing equations for axial gas flow in the pellet-cladding gap further by excluding the negligible right-hand-side terms in the non-normalized eqs. (17) and (18). The resulting system of simplified equations, expressed in cylindrical  $(r, z)$  rather than cartesian  $(x, y)$  coordinates, is

$$\frac{\partial(\rho u)}{\partial z} \approx 0, \quad (21)$$

$$\frac{\partial p}{\partial r} \approx 0, \quad (22)$$

$$\frac{\partial p}{\partial z} \approx \frac{\mu(z)}{r} \frac{\partial}{\partial r} \left( r \frac{\partial u}{\partial r} \right). \quad (23)$$

It is interesting to note that eq. (22) implies that the gas pressure is approximately constant across the gap. Since also the temperature is assumed constant across the gap, it follows from the ideal gas law in eq. (6) that the gas density is a function of axial position only.

Next, we seek a solution to eq. (23) in the pellet-cladding gap. We consider an idealized gap geometry, described by a concentric circular annular duct with inner and outer radius  $R_i$  and  $R_o$ , respectively. The radial gap width,  $h = R_o - R_i$ , is assumed to be much smaller than the axial extension,  $L$ , of the annulus. The boundary conditions for the axial flow velocity are  $u(r = R_i, z) = u(r = R_o, z) = 0$ , which are the well-known no-slip conditions for a viscous fluid. A solution to eq. (23) that satisfies these boundary conditions is

$$u(r, z) = -\frac{\partial p}{\partial z} \frac{1}{4\mu} \left[ R_i^2 - r^2 + \frac{(R_o^2 - R_i^2) \ln(r/R_i)}{\ln(R_o/R_i)} \right]. \quad (24)$$

The volumetric flow rate in the gap,  $Q$  [  $\text{m}^3\text{s}^{-1}$  ], can then be calculated by integrating the axial velocity across the cross-sectional flow area  $A$ :

$$\begin{aligned} Q(z) &= \int_A u(r, z) dA = 2\pi \int_{R_i}^{R_o} u(r, z) r dr \\ &= -\frac{\partial p}{\partial z} \frac{\pi}{8\mu} \left[ R_o^4 - R_i^4 - \frac{(R_o^2 - R_i^2)^2}{\ln(R_o/R_i)} \right]. \end{aligned} \quad (25)$$

Exact analytical solutions to eq. (23) with no-slip boundary conditions for other flow channel cross-sections are reviewed in [44, 45]. Moreover, a solution for an annular circular geometry that is not concentric is given by Reimann [38]. He considered an eccentricity  $\Delta_e$  between the centerlines of the fuel pellet column and the cladding tube. The pellet radius was  $R_i$  and the cladding tube inner radius  $R_o$ , which means that  $0 < \Delta_e < h = R_o - R_i$ . For this geometry, Reimann presented an approximate solution for the asymptotic case  $R_o/R_i \rightarrow 1$ , i.e. for a pellet-cladding gap that is nearly closed. He showed that the volumetric flow rate in this geometry is

$$Q(z) = -\frac{\partial p}{\partial z} \frac{\pi(R_o + R_i)(R_o - R_i)^3}{12\mu} \left[ 1 + \frac{3}{2} \left( \frac{\Delta_e}{h} \right)^2 \right]. \quad (26)$$

According to eq. (26), the volumetric flow rate increases by a factor 5/2 in a completely eccentric gap geometry ( $\Delta_e/h=1$ ), compared with a concentric geometry ( $\Delta_e/h=0$ ). This is a notable result, but it should be borne in mind that it is valid for an asymptotic case in a highly idealized gap geometry, where the flow is assumed to be laminar. The effect of pellet-cladding eccentricity also decreases in wider gaps; see section 2.2.3 below.

## 2.2.2 Approximations applied in existing fuel rod gas flow models

Equation (25) results from an exact solution to eq. (23) with no-slip boundary conditions at the walls of a concentric annular duct with arbitrary inner and outer radii  $R_i$  and  $R_o$ . To the author's best knowledge, no fuel rod analysis program with models for axial gas flow in an assumedly annular gap geometry makes use of this expression. Instead, approximate expressions for the volumetric flow rate  $Q$  are used, which are valid either for  $R_o/R_i \rightarrow 1$  (narrow pellet-cladding gap) or  $R_o/R_i \rightarrow \infty$  (flow channel resembling a simple circular tube).

For examples of the first kind, we first consider the gas flow model in the SSYST program [18], where  $Q$  is calculated from

$$Q(z) = -\frac{\partial p}{\partial z} \frac{\pi}{6\mu} R_i (R_o - R_i)^3. \quad (27)$$

This expression results from a first order Taylor series expansion of eq. (25), where it is assumed that  $\epsilon = R_o/R_i - 1$  turns towards zero. As another example, the recent GASMIX model [29] uses

$$Q(z) = -\frac{\partial p}{\partial z} \frac{8\pi}{\mu \text{Hg}} (R_o + R_i)(R_o - R_i)^3. \quad (28)$$

Here, Hg is the non-dimensional Hagen number, which characterizes the ratio of wall friction forces to overall viscous forces in the gas; see section 2.2.3 below. For the special case of Hg=96, eq. (28) is identical to a second-order Taylor series expansion of eq. (25). In fact, Hg=96 is a known result for laminar flow in a planar gap [38]. Moreover, we note that eq. (28) with Hg=96 is identical to eq. (26) if  $\Delta_e=0$  in the latter. The approximate expression in eq. (28) is used also in the (optional) axial gas flow model in the FRAPTRAN program [46], but it should be remarked that a factor 2 is erroneously included in the documentation as well as the numerical implementation of the equation. This error is in part compensated for by use of an empirically modified Hagen number in FRAPTRAN [46]: the erroneous factor in the fundamental equation is rectified by tuning Hg such that the model reproduces gas flow data.

An example of the second kind is provided by the FRELAX model [25]. In case an open pellet-cladding gap exists, this model calculates the volumetric flow rate from

$$Q(z) = -\frac{\partial p}{\partial z} \frac{\pi}{8\mu} (R_o - R_i)^4. \quad (29)$$

Equation (29) is not an approximation to eq. (25). It is derived from the Hagen-Poiseuille equation [33] for a circular tube with internal diameter  $D$ ,

$$Q(z) = -\frac{\partial p}{\partial z} \frac{\pi D^4}{128\mu}, \quad (30)$$

simply by substituting the internal diameter of the tube  $D$  with the hydraulic diameter  $D_h$  of the annular gap

$$D_h = \frac{4A}{P_w} = \frac{4\pi(R_o^2 - R_i^2)}{2\pi(R_o + R_i)} = 2(R_o - R_i), \quad (31)$$

where  $A$  is the cross-sectional flow area of the duct made up by the pellet-cladding annular gap, and  $P_w$  is its wetted perimeter.

Figure 3 shows the calculated volumetric flow rates from the approximate expressions in eqs. (27)-(29) divided by  $Q$  obtained from the exact solution in eq. (25). The ratios are plotted over a wide range of  $R_o/R_i$ . In fact, for application to ballooning fuel rods, only the range  $1 \lesssim R_o/R_i \lesssim 2$  is of interest: higher values are included here only to show the asymptotic behaviour when  $R_o/R_i \rightarrow \infty$ . It is clear from Figure 3 that the approximation for  $Q$  used in GASMIX and FRAPTRAN works well over a wide range of  $R_o/R_i$ , while the approximation in SSYST is restricted to narrow gaps, i.e. to  $R_o/R_i \approx 1$ . The approximation in FRELAX is useless for the range of  $R_o/R_i$  expected in ballooning fuel rods. It gives reasonable results only for  $R_o/R_i \gtrsim 3$ .

### 2.2.3 Extensions to turbulent flow

Equations (24) and (25) show that the assumption of laminar flow results in linear relationships between the axial pressure gradient and the axial flow velocity and volumetric flow

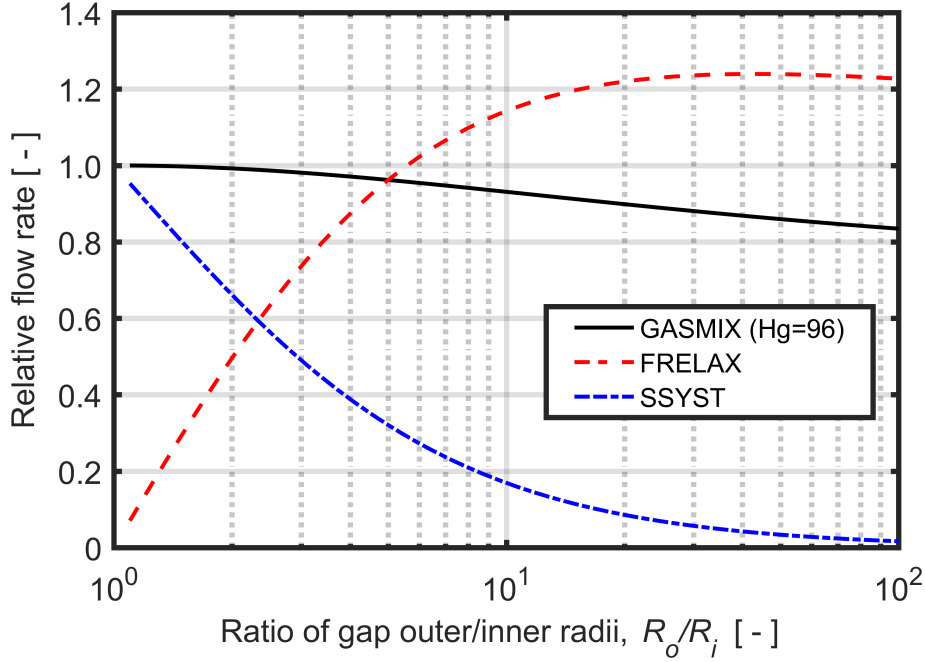


Figure 3: Volumetric flow rates,  $Q$ , from the approximate expressions in eqs. (27)-(29), divided by  $Q$  obtained from the exact analytical solution in eq. (25). Hence, values close to unity imply a good approximation to the exact solution.

rate, respectively. This assumption is valid at low velocities and flow rates, for which eqs. (24) and (25) work well. At higher velocities and flow rates, the flow becomes turbulent. This results in higher viscous loss and non-linear relationships between the axial pressure gradient and the axial flow velocity and flow rate.

For a general case with one-dimensional flow in the  $z$ -direction, these non-linear relationships can be characterized by use of the empirical Darcy-Weisbach equation

$$\frac{\partial p}{\partial z} = -f_D \frac{\rho \langle u \rangle^2}{2D_h}, \quad (32)$$

where  $\langle u \rangle = Q/A$  is the mean flow velocity over the flow channel cross-section and  $f_D$  is the Darcy friction factor, also known as the flow coefficient. This is a non-dimensional quantity that defines the friction losses. In general,  $f_D$  depends on the flow channel geometry, surface roughness of the channel walls and the flow regime, which in turn depends on the fluid properties and velocity, as characterized by the non-dimensional Reynolds number

$$\text{Re} = \frac{\rho D_h \langle u \rangle}{\mu}. \quad (33)$$

The Reynolds number expresses the ratio of inertial forces to viscous forces in the fluid. At low Reynolds numbers, viscous forces will attenuate perturbations in the one-dimensional laminar flow field and keep the flow laminar. At high Re, however, small perturbations in the laminar flow field will grow in an unstable manner. In wide circular pipes, stable laminar flow is known to always exist for  $\text{Re} \lesssim 2300$ . At higher numbers, a transition to turbulent flow takes place; the transition point in terms of Re depends on local disturbances in the flow, e.g. from surface roughness. For flows in narrow gaps, capillary tubes and porous media, the laminar-to-turbulent flow transition occurs at lower Reynolds numbers

than in wide pipes, due to increasing importance of these boundary disturbances [47]. Data from axial gas flow experiments on fresh (unirradiated) LWR fuel rods indicate that the flow remains laminar for Re up to about 600-1000 [20]. With  $D_h=6 \times 10^{-5}$  m and values for  $\rho$  and  $\mu$  representing helium at 800 K and 5 MPa, we find from eq. (33) that this corresponds to mean flow velocities of 130-220  $\text{ms}^{-1}$ .

Equation (32) is a general relation between the pressure gradient and the flow velocity, in which differences between flow regimes are accounted for by the friction factor  $f_D$ . For laminar flow,  $f_D$  can be calculated from analytical solutions for the flow velocity distribution. For turbulent flow and for the transition between laminar and turbulent flow,  $f_D$  must be estimated from empirical relations. These relations and their applicability constitute a research subject of its own. In the following, we restrict the presentation to relations that have proven useful for axial gas flow in the pellet-cladding gap [20].

**Laminar flow** For the case of laminar flow in an annular concentric duct with inner and outer radii  $R_i$  and  $R_o$ , we may use eq. (24) for calculating the mean flow velocity  $\langle u \rangle$ . Combining the result with eqs. (32)-(33), and recognizing that  $D_h=2(R_o - R_i)$  for this geometry, we find that

$$f_D = \frac{64 (R_o - R_i)^2}{\text{Re} [R_o^2 + R_i^2 - (R_o^2 - R_i^2)/\ln(R_o/R_i)]} = \frac{\text{Hg}}{\text{Re}}. \quad (34)$$

Hence, for laminar flow, the Darcy friction factor is simply the ratio of two non-dimensional numbers, where the Hagen number, Hg, is dependent on the flow channel geometry only. The Hagen number is plotted as a function of  $R_o/R_i$  in Figure 4. For a concentric gap, it goes from 96 for  $R_o/R_i \approx 1$  (narrow gap) to 64 for very large  $R_o/R_i$  (circular pipe) [20]. We recall from eq. (26) in section 2.2.1 that eccentricity between the fuel pellets and the cladding tube reduces the flow resistance. As shown in Figure 4, the reduction is significant for narrow gaps, but less important for wide gaps.

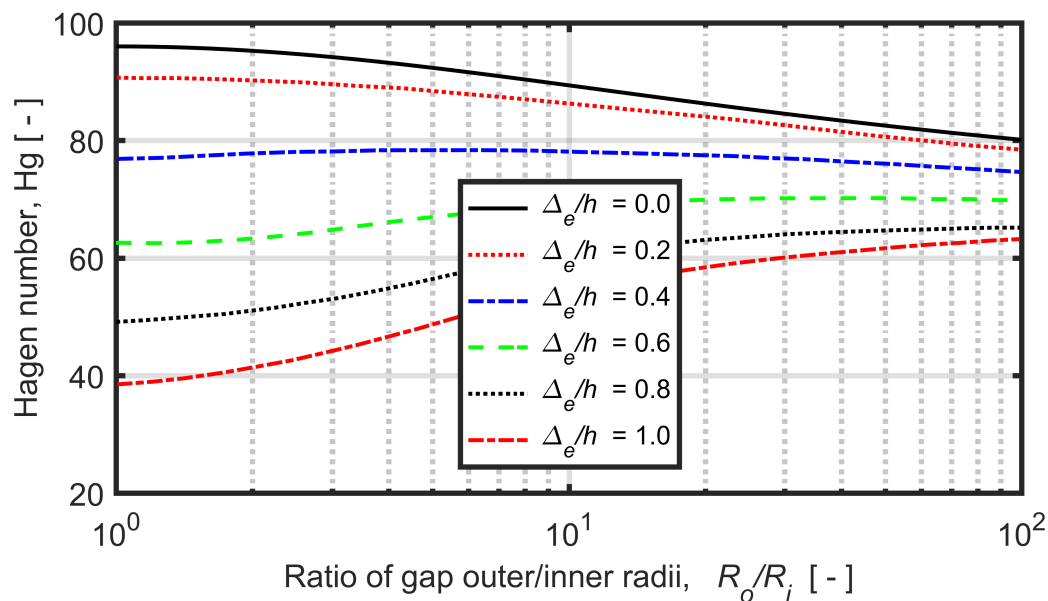


Figure 4: Hagen number for laminar flow in a circular annular duct with outer/inner radii  $R_o/R_i$  and relative eccentricity  $\Delta_e/h$ ; see eqs. (26), (34) and [20].

**Turbulent flow** In a flow channel with rough surfaces, the friction factor will become dependent on the surface roughness as the Reynolds number increases and the flow turns turbulent. At the same time,  $f_D$  becomes less dependent on Re as the Reynolds number increases: in fully turbulent flow, the friction factor is independent of Re. It is also independent of the cross-sectional shape of the flow channel: only the hydraulic diameter and the surface roughness of the flow channel walls are important. This behaviour is captured by the Colebrook (or Colebrook-White) equation for  $f_D$  [48]

$$\frac{1}{\sqrt{f_D}} = 1.14 - 2 \log_{10} \left( \frac{\epsilon}{D_h} + \frac{9.32}{\text{Re} \sqrt{f_D}} \right), \quad (35)$$

where  $\epsilon$  is an effective surface roughness for the flow channel. Equation (35) is an implicit expression for  $f_D$  that has to be solved numerically. Various approximations to eq. (35) are available, by which  $f_D$  can be calculated explicitly [49].

Equations (34) and (35) are plotted in Figure 5, together with measured data for  $f_D$  from gas flow experiments on a 0.5 m long fuel rod segment charged with solid  $\text{UO}_2$  fuel pellets in as-fabricated condition [20]. The experiments were carried out with stationary gas flow at room temperature, using He and Ar gas at pressures ranging from 0.2 to 5.9 MPa. The geometry of the tested  $\text{UO}_2$  fuel rod segment is summarized in Table 1.

Table 1: Geometry of fuel rod segments used for axial gas flow experiments in [20].

Fuel pellets:			
Material		$\text{UO}_2$	$\text{Al}_2\text{O}_3$
Outer radius	[ mm ]	4.570	4.553
Height (length)	[ mm ]	10.90	11.00
Surface roughness	[ $\mu\text{m}$ ]	5 - 7	10-25
Cladding tube:			
Material		Zircaloy-4	
Inner radius	[ mm ]	4.652	
Surface roughness	[ $\mu\text{m}$ ]	1.2-1.7	
Flow channel characteristics:			
Axial length	[ mm ]	500	500
Hydraulic diameter	[ mm ]	0.164	0.198
Outer/inner radius ratio ( $R_o/R_i$ )	[ - ]	1.018	1.022

From Figure 5, it is clear that the data are fairly well reproduced by eqs. (34) and (35), if reasonable values for the Hagen number  $H_g$  and the effective surface roughness  $\epsilon$  are used for the flow channel. More precisely, the data corresponding to the laminar flow regime ( $\text{Re} \lesssim 1000$ ) fall between the curves calculated through eq. (34) with  $H_g=64$  and 96, i.e. values expected for a narrow annular gap with some eccentricity between the fuel pellets and the cladding; confer Figure 4. The data corresponding to the turbulent flow regime fall between the curves calculated through Colebrooks relation in eq. (35) with  $\epsilon/D_h=0.004$  and 0.015. Since  $D_h=164 \mu\text{m}$  in these tests (cladding deformations caused by the internal overpressure are not considered here), these curves correspond to effective surface roughnesses of 0.7 and 2.5  $\mu\text{m}$ . These values are comparable to the reported surface

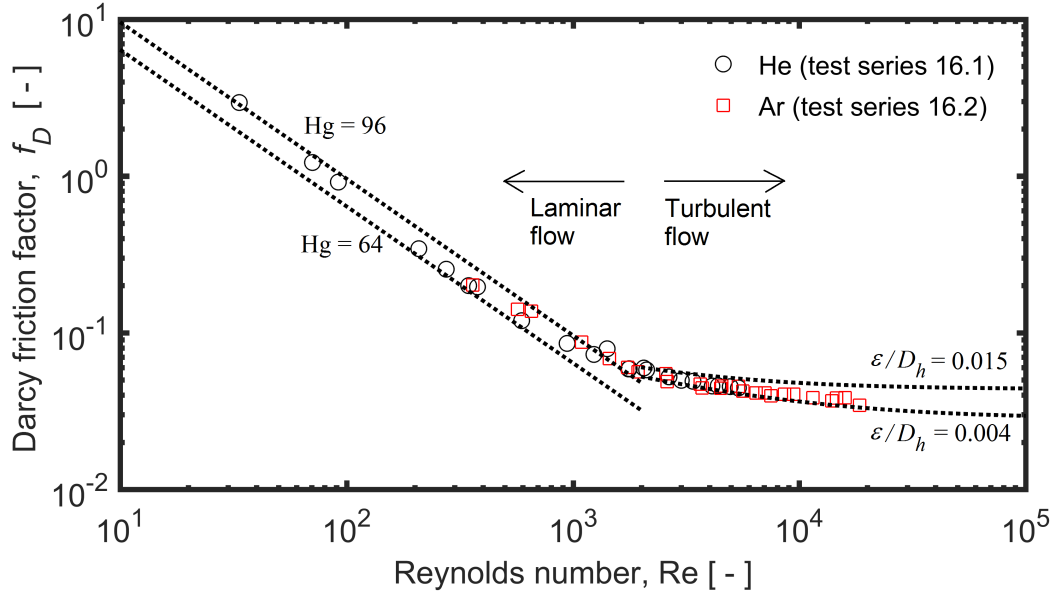


Figure 5: Moody diagram, showing Darcy friction factor versus Reynolds number. Dashed lines: Calculated results from eqs. (34) and (35). Symbols: Measured data for a 0.5 m long fuel rod segment charged with solid  $\text{UO}_2$  fuel pellets in as-fabricated condition [20]. The test setup is summarized in Table 1.

roughness of the cladding tube, but smaller than that reported for the  $\text{UO}_2$  fuel pellets; see Table 1.

Two remarks should be made on the data from [20] shown in Figure 5. Firstly, we note that there are few data points for helium in the turbulent flow regime. Due to the low density of helium and the narrow flow channel, high pressures in combination with steep pressure gradients are needed to achieve Reynolds numbers characteristic of turbulent flow; see eq. (33). Turbulent flow in the pellet-cladding gap of LWR fuel rods therefore seems unlikely, at least as long as the gap gas is dominated by He and the cladding tube distension is limited. Secondly, the data in Figure 5 show a smooth and monotonic transition from laminar to turbulent flow for Reynolds numbers between about 600 and 2000. This kind of transition is typical for flows in channels with normal, commercial grade, surface conditions. With highly polished surfaces, the transition is more complex: its abrupt, non-monotonic and unstable [48]. As shown in Figure 5, the transition region is fairly well reproduced by the intersection of the calculated lines from eqs. (34) and (35).

#### 2.2.4 Application to LWR fuel rods

From the model-data comparisons in section 2.2.3, we conclude that the axial gas flow in the pellet-cladding gap is predominantly laminar. Turbulent flow in the open gap regime is expected only in cases with very steep axial pressure gradients. Due to the large mass flux that such pressure gradients would induce along the an open pellet-cladding gap, the turbulent flow would be transitory, as the pressure gradients would be rapidly equilibrated by gas flow inside the fuel rod. Turbulent flow in the gap can be maintained over a longer period of time only in experiments with external gas supply, such as in [20].

We also conclude from the model-data comparisons in section 2.2.3 that the relation be-

tween flow rate and pressure gradient for laminar flow in as-fabricated (unirradiated) fuel rods is fairly well described by Hagen-Poiseuille type of equations for one-dimensional flow in annular ducts, such as eq. (25) or its approximation for narrow gaps, eq. (28). Based on the experimental data available in [20], it seems that the Hagen number is in the range from 64 to 96 for the flow channel made up of the pellet-cladding gap in as-fabricated LWR fuel rods. Equation (28) is informative in that it shows that the volumetric flow rate  $Q$  depends on the pellet-cladding gap size ( $R_o - R_i$ ) raised to the power of 3. Consequently, it is essential that the pellet-cladding gap size is accurately determined (measured or calculated), in order to accurately calculate the flow rate through eq. (25) or eq. (28).

When LWR fuel rods are taken into operation and brought up to power, the fuel pellets experience a significant radial temperature gradient that induces thermo-elastic stresses in the ceramic material. Tensile stresses are found at the cold outer surface of the pellet, predominantly in the hoop direction. These stresses cause radial cracks to form at a linear heat generation rate of 5-6 kWm<sup>-1</sup>. The cracking proceeds as the power is increased, and the strength of the temperature gradient caused by the applied power dictates how many fragments need be created to keep the tensile stresses below the fracture threshold for the material [50, 51]. Build-up of internal stresses by differential swelling and weakening of the material by element transmutation and by accumulation of gaseous fission products along grain boundaries contribute to pellet cracking at higher fuel burnup [52]. Hence, pellets in fuel rods that have experienced in-reactor operation are more or less fragmented. It is therefore worthwhile to investigate to what extent eqs. (25) and (28) can reproduce gas flow inside LWR fuel rods that contain cracked fuel pellets.

To this end, we consider gas flow tests conducted on fuel rod segments charged with Al<sub>2</sub>O<sub>3</sub> pellets in cracked as well as solid (uncracked) condition, reported in [20]. The tests are similar to those performed with solid UO<sub>2</sub> fuel pellets, discussed in section 2.2.3: they were carried out with stationary gas flow at room temperature, using He and Ar gas at pressures ranging from 0.2 to 6.0 MPa. The geometry of the tested Al<sub>2</sub>O<sub>3</sub> fuel rod segments is summarized in Table 1. The 0.5 m long test section was charged either with solid (uncracked) pellets or with pellets that were manually cracked by use of a cape chisel. The pellets were cracked one-by-one while contained in a short cladding tube segment. The pellet fragments were then carefully loaded into the 0.5 m long test section, without changing their relative positions. On average, each pellet was broken into 3 fragments [20].

Figure 6 shows the Darcy friction factor versus Reynolds number, measured for the solid and cracked Al<sub>2</sub>O<sub>3</sub> pellets [20]. It is clear that the friction factor is about an order of magnitude higher for the cracked pellets than for the solid pellets. Moreover, the data for the cracked pellets do not follow the same trend with regard to Re as the solid pellets; see also Figure 5 with gas flow data for solid UO<sub>2</sub> fuel pellets. The data for the cracked pellets do not follow the -1 slope in the logarithmic  $f_D$ -Re plot, which means that eqs. (25) and (28) are less appropriate for modelling the gas flow in fuel rods with cracked pellets, even if the Hagen number is significantly increased. This is illustrated by the dashed line, calculated with Hg=890, in Figure 6. This particular value is taken from the GASMIX model, where Hg is considered to be a decreasing function of the pellet-cladding gap width. In the GASMIX model, Hg=890 is the maximum value, applied for gap widths less than 10 μm [29].

A somewhat better agreement with the trend for gas flow data in cracked fuel pellets can be achieved by using the Darcy-Weisbach equation (32) together with empirical relations for

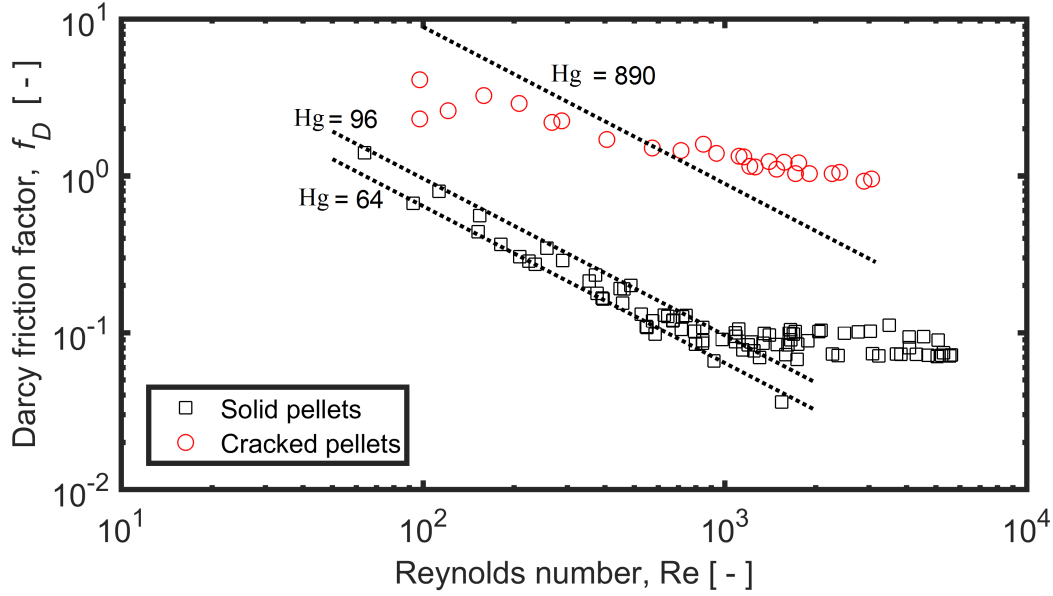


Figure 6: Moody diagram, showing Darcy friction factor versus Reynolds number. Dashed lines: Calculated results for laminar flow from eq. (34), using different Hagen numbers. Symbols: Measured data for 0.5 m long fuel rod segments charged with either solid (uncracked) or cracked  $\text{Al}_2\text{O}_3$  fuel pellets [20]. The test setup is summarized in Table 1.

the friction factor that originate from experiments on gas flow through granular materials. This kind of flow is relevant for filters, chemical reactors, etc., in which gas is flowing through particle beds. In [20], four different correlations for  $f_D$ , formulated for gas flow through particle beds, were tested against the gas flow data for cracked  $\text{Al}_2\text{O}_3$  presented in Figure 6 as well as data for spherical  $\text{SiO}_2$  beads with an average diameter of 1.25 mm that were charged into the 0.5 m long cladding segment. These model-data comparisons showed that all tested correlations reproduced the measured data for the small  $\text{SiO}_2$  beads accurately, but that they generally overestimated the flow resistance of the cracked pellets. In terms of  $f_D$ , the best performing correlation typically overestimated the data for cracked fuel pellets by a factor of two [20]. The main reasons for this discrepancy were identified in [20], and may be summarized as follows:

- The tested correlations for  $f_D$  in [20] are intended for and calibrated against gas flow in particle beds, which typically have a void fraction of 0.3-0.4. The void fraction of the cracked fuel pellet column inside an LWR fuel rod is typically less than 0.05, unless cladding ballooning occurs;
- Even with cracked pellets, most of the gas flows through the residual pellet-cladding gap, which has a lower flow resistance than the tortuous fuel pellet cracks. With only a few pellet cracks/fragments, as in the tests, the flow geometry is far from that of a wide particle bed treated by the correlations;
- A key parameter in all correlations is the mean particle size (or surface area to volume ratio). While this parameter is fairly well known and uniform for particle beds, it is poorly defined and varies from one pellet to another for cracked fuel pellets [52].

The reader is referred to [20] for details on the applied correlations and conclusions from the model-data comparisons. A review of more appropriate models for flow in cracked media is given in section 2.3 below.

A final comment should be made on the application of the Hagen-Poiseuille type of flow equations, such as eqs. (25)-(29), in computational analyses of LWR fuel rods. These analyses involve integration of the equations along the fuel rods, which are typically discretized into 20-40 axial segments in the computations. Calculations of various thermal-mechanical properties are usually carried out for each axial segment separately, considering segment-to-segment interaction only for a few properties, such as axial flow of coolant water and gap gas, as well as axial forces in the cladding tube and the fuel pellet column. This is usually referred to as "quasi 2D" or "1 1/2D" modelling of the fuel rod [53].

When integrating any of eqs. (25)-(29) along the fuel rod, it is fruitful to consider axial mass flow,  $\dot{m}$  [kgs<sup>-1</sup>], rather than volumetric flow,  $Q$ , if the fluid is compressible. Using  $\dot{m} = \rho Q$  and the ideal gas law (6), we may re-write any of eqs. (25)-(29) on the general form

$$\dot{m} = -\frac{M}{R} \frac{\mathcal{F}(z)}{T(z)\mu(z)} p \frac{\partial p}{\partial z}, \quad (36)$$

where the geometry-dependent function  $\mathcal{F}(z)$  [m<sup>4</sup>] contains  $R_i$  and  $R_o$ , which may depend on the axial position  $z$ . For example, with eq. (25), we have

$$\mathcal{F}(z) = \frac{\pi}{8} \left[ R_o^4(z) - R_i^4(z) - \frac{(R_o^2(z) - R_i^2(z))^2}{\ln(R_o(z)/R_i(z))} \right]. \quad (37)$$

Equation (36) is separable in variables and may be integrated from  $z_L$  to  $z_U$ , where the corresponding gas pressures are  $p_L$  and  $p_U$ :

$$p_U^2 - p_L^2 = -\frac{2R}{M} \int_{z_L}^{z_U} \frac{\dot{m}(z)\mu(z)T(z)}{\mathcal{F}(z)} dz. \quad (38)$$

If no fission gas is released from the fuel pellets to the gap in the considered segment  $z_L < z < z_U$ , then  $\dot{m}$  is independent of  $z$  and may be moved out of the integral. Here, it is tacitly assumed that the molar mass  $M$  is independent of  $z$ , which means that the gas in the fuel rod void volume is assumed to have uniform composition over the considered axial segment. When integrating eq. (38) along the entire fuel rod, one may consider the properties within the integral as either constant or axially varying within each axial segment. Which approach to use depends on how temperatures and deformations are calculated for each axial segment. These calculations are done in other parts of the applied computer program, and the calculated results are usually provided as segment-wise averages. However, exceptions exist [53].

### 2.3 Models for flow in porous and/or cracked media

Fluid flow through porous and/or cracked media is a phenomenon with many important practical applications. Most of these applications concern liquid fluids, e.g. in the fields of hydrology and petroleum engineering, while applications to gaseous fluids comprise drying operations, filtration and combustion [34, 54, 55]. Plenty of models for flow of various fluids in various types of porous media exist. They are largely empirically based and adapted to applications involving a specific fluid and/or a specific type of porous medium. However, the most widely used models are fairly general and have been theoretically shown to be approximations to the Navier-Stokes equations [56, 57].

### 2.3.1 Governing equations for gas flow in porous media

Consider a solid material with porosity (void) volume fraction  $\phi$ , in which the porosity is interconnected and permeable for gas. Consider, as before, one-dimensional gas flow in the axial ( $z$ ) direction. Nearly all models for this kind of gas flow are based on the mass conservation equation

$$\phi \frac{\partial \rho}{\partial t} + \frac{\partial(\rho \tilde{u})}{\partial z} = 0, \quad (39)$$

combined with some approximation of the momentum equation. A fairly general expression for the latter, capturing most of these approximations, is given by

$$-\frac{\partial p}{\partial z} = \alpha \mu \tilde{u} + \beta \rho |\tilde{u}| \tilde{u}, \quad (40)$$

where  $\alpha$  [ $\text{m}^{-2}$ ] and  $\beta$  [ $\text{m}^{-1}$ ] are model parameters that depend on properties of the porous medium and the flowing gas. The property  $\tilde{u}$  is the superficial (or filtration) velocity, defined through  $\tilde{u} = Q/\tilde{A}$ , where  $Q$  is the volumetric flow rate and  $\tilde{A}$  is the gross cross-sectional area of the flow channel that comprises the porous material. Since the gas flows through a tortuous network of pores that provide a significantly smaller *true* cross-sectional flow area,  $A$ , than  $\tilde{A}$ , the true gas velocity is higher than  $\tilde{u}$ . In fact,  $\tilde{u} = \phi \bar{u}$ , where  $\bar{u}$  is usually referred to as pore velocity, i.e. the average axial velocity of the gas within the pore network. The true local gas velocity is usually higher than  $\bar{u}$ , since the local flow through the winding network is generally not aligned with the axial direction.

For axial gas flow inside LWR fuel rods, the time derivative in the left-hand-side of eq. (39) can be neglected, which means that quasi-stationary conditions are considered. This approximation makes eq. (39) identical to eq. (21), although expressed in terms of superficial rather than true axial velocity. Also eq. (40) may be simplified in some cases. The first term in the right-hand-side of eq. (40) represents the pressure drop caused by viscous forces, while the second term represents that caused by inertial forces. The latter can usually be neglected for small Reynolds numbers: we recall from section 2.2.3 that the Reynolds number expresses the ratio of inertial to viscous forces in the fluid. To illustrate this, we may define the Reynolds number in terms of parameters related to the flow through the porous medium by letting  $\text{Re} = \rho \tilde{u} d / \mu$ , where  $d$  is a characteristic pore dimension in the material. Similar to the Darcy-Weisbach equation (32), we consider a friction factor for the porous material, defined by

$$f_P = -\frac{\partial p}{\partial z} / \frac{\rho \tilde{u}^2}{2d}. \quad (41)$$

Substituting  $\partial p / \partial z$  from eq. (40) and using the above definition of  $\text{Re}$ , eq. (41) results in

$$f_P = 2d^2 \left( \frac{\alpha}{\text{Re}} + \frac{\beta}{d} \right). \quad (42)$$

Obviously, the first term within the right-hand-side brackets is important for low Reynolds numbers, where  $f_P$  will be inversely proportional to  $\text{Re}$ . We recognize this behaviour from laminar flow in annular ducts; see eq. (34). For high Reynolds numbers (turbulent flow), the second right-hand-side term in eq. (42) dominates. This is similar to turbulent flow in annular ducts; see sections 2.2.3 and 2.2.4. In the following, we review some widely used forms of eq. (40), together with relations for the model parameters  $\alpha$ ,  $\beta$  and  $f_P$ . More extensive reviews of phenomenological models for flow in porous media can be found in [55, 58].

### 2.3.2 Common approximations to the momentum conservation equation

**Darcy's law** Without doubt, the most common approximation to the momentum conservation equation (40) for fluid flow in porous media is Darcy's law, which states that the pressure gradient is proportional to the superficial velocity of the fluid

$$-\frac{\partial p}{\partial z} \approx \alpha \mu \tilde{u} = \frac{\mu}{\kappa} \tilde{u}. \quad (43)$$

Here,  $\kappa = \alpha^{-1}$  [m<sup>2</sup>] is a material property of the porous medium termed specific permeability, or simply permeability. Equation (43) originates from Henry Darcy, who noted the proportionality between pressure drop and superficial flow velocity in experiments on water flow through sand. Later, Morris Muskat separated the proportionality constant into viscosity (fluid dependent) and permeability (porous media dependent), which significantly improved the usefulness of the equation. Darcy's law can be theoretically derived from Stoke's equations for creeping flow (see section 2.1.3) by averaging techniques [56].

Since inertial forces are neglected in Darcy's law, the law is restricted to laminar flow. Experience from flow in porous media shows that the linear relationship between pressure drop and superficial velocity becomes questionable when the ratio  $Re/(1-\phi)$  is in the range from 1 to 10 [55]. The point at which the deviations from linearity become significant depends not only on  $Re$  and  $\phi$ , but also on the properties of the pore network. We recall that the Reynolds number is here calculated from  $Re = \rho \tilde{u} d / \mu$ , which means that effects of pore size ( $d$ ) are included in  $Re$ . In porous media flow, the transition from a linear to a non-linear relationship between pressure drop and superficial flow velocity is not related to a transition from laminar to turbulent flow as we know it from flow in straight ducts. The reason is that the flow in the latter is much different from the flow along tortuous paths in a porous medium, which is characterized by eddies and recirculation zones [55, 59].

**Darcy's law with consideration of Knudsen diffusion** For gas flowing through porous materials with very fine pores or capillaries, particle-wall interactions become frequent and contribute to the gas flow by a phenomenon known as Knudsen diffusion [55]. The contribution gets significant when the mean free path,  $\lambda_f$  [m], of the gas molecules is comparable to, or larger than, the characteristic dimension of the pores,  $d$ . More precisely, a transition from continuum flow to rarified flow occurs when the Knudsen number,  $Kn = \lambda_f / d$ , goes from about 0.01 to 1 [35]. In the rarified flow regime, the contribution of Knudsen diffusion can be accounted for by modifying the permeability used in Darcy's law. Hence, an effective permeability,  $\kappa_e$ , is introduced, which is defined through

$$\kappa_e = \kappa \left( 1 + \frac{D_K \mu}{\kappa p} \right), \quad (44)$$

where  $D_K$  [m<sup>2</sup>s<sup>-1</sup>] is the Knudsen diffusivity of the gas. For a gas with molecular mass  $M$  [kgmol<sup>-1</sup>] flowing through a capillary with diameter  $d$ , this diffusivity may be calculated through

$$D_K = \frac{d}{3} \sqrt{\frac{8RT}{\pi M}}. \quad (45)$$

It is clear from eqs. (44) and (45) that the effective permeability depends not only on the properties of the porous material, but also on the properties of the flowing gas. Equation

(44) is often written as  $\kappa_e = \kappa(1+b/p)$ , where  $b = D_K\mu/\kappa$  [Pa] is known as the Klinkenberg parameter [60].

As mentioned above, the contribution from Knudsen diffusion becomes noticeable when  $\text{Kn}=\lambda_f/d$  goes from about 0.01 to 1. To estimate the typical pore size for which the phenomenon is relevant, we may calculate the mean free path from kinetic theory of gases, viz.

$$\lambda_f(p, T, d_k) = \frac{k_B T}{\sqrt{2}\pi p d_k^2}. \quad (46)$$

Here,  $k_B$  is the Boltzmann constant ( $1.3806 \times 10^{-23} \text{ JK}^{-1}$ ) and  $d_k$  is the kinetic diameter of the gas molecule. Typical values for  $d_k$  in the gas mixtures expected inside LWR fuel rods range from 2.6 Å (helium) to 4.0 Å (xenon). Assuming a typical gas temperature of 800 K and a typical pressure of 5.0 MPa inside the fuel rod, eq. (46) suggests that  $\lambda_f$  is in the range from 3 to 7 nm for the gas mixtures of interest. These numbers indicate that Knudsen diffusion would start to be relevant for pores smaller than about 0.5  $\mu\text{m}$ , and that the phenomenon would be significant for pores with a typical size of 5 nm. Since the pores and voids inside LWR fuel rods are expected to be larger than this, we may conclude that Knudsen diffusion is irrelevant for the gas transport. Hence, there is no need to modify the permeability of the porous material by use of eqs. (44) and (45).

**Forchheimer equation** Philipp Forchheimer [61] extended Darcy's law by including the quadratic term of  $\tilde{u}$  in eq. (40). As already mentioned, this term is related to inertial effects that come into play at higher flow velocities, and eq. (40) is known as the Forchheimer or Darcy-Forchheimer equation. The coefficient  $\beta$  in eq. (40) is sometimes replaced by  $k_I = \beta^{-1}$ , where  $k_I$  [m] is referred to as the inertial permeability of the porous material. The inertial permeability is known to correlate with the viscous permeability ( $\kappa$ ) of the material [59]. Forchheimer's equation can be derived theoretically from the Navier-Stokes equations (see section 2.1.3) by averaging techniques [57].

In section 3.2.4, the Forchheimer equation is applied to the axial gas flow experiments reported in [20], i.e. the experiments that were assessed by use of Hagen-Poiseuille type flow models in section 2.2.4.

### 2.3.3 Application to LWR fuel rods

Existing models for axial gas flow inside LWR fuel rods that treat the fuel pellet column as a porous medium use Darcy's law (43) as an approximation to the momentum conservation equation. The permeability of the fuel pellet column is in the models treated as an input parameter that the analyst has to provide, based on a very scarce experimental database; see section 3. For example, the axial gas flow model in the SCANAIR program [31] makes use of two permeability values that have to be provided by the user as input: one (high) value is used by the model in parts of the fuel rod where the pellet-cladding gap is open, while another (low) value is used in parts where the gap is closed [62]. Some data on the permeability of the fuel pellet column are reported from integral gas flow experiments on discharged LWR fuel rods, and more data can be generated by analysing additional tests and experiments; see section 3. However, the database is scant.

Among published gas flow models that treat the fuel pellet column as a porous medium, differences exist with regard to whether the flowing gas is assumed compressible or not: compressibility is assumed in [26, 30], while in other models [31, 32], the gas is assumed incompressible. To explore the significance of this difference, we depart from the governing equations presented in section 2.3.1. Similar to our treatment of the Hagen-Poiseuille flow equations in section 2.2.4, we consider the axial mass flow,  $\dot{m} = \rho Q = \rho \tilde{u} \tilde{A}$  [kgs<sup>-1</sup>]. Under steady-state conditions,  $\dot{m}$  is constant, provided that no fission gas is released from the fuel pellets. Substituting the mass flow into the momentum equation (40), we get

$$-\rho \frac{\partial p}{\partial z} = \frac{\dot{m}}{\tilde{A}^2} \left( \alpha \mu \tilde{A} + \beta |\dot{m}| \right), \quad (47)$$

which combined with the ideal gas law in eq. (6) results in

$$-p dp = \frac{\dot{m} R T}{M \tilde{A}^2} \left( \alpha \mu \tilde{A} + \beta |\dot{m}| \right) dz. \quad (48)$$

Equation (48) may be integrated from  $z_L$  to  $z_U$ , where the corresponding gas pressures are  $p_L$  and  $p_U$ :

$$p_U^2 - p_L^2 = -\frac{2R}{M} \int_{z_L}^{z_U} \frac{\dot{m} T (\alpha \mu \tilde{A} + \beta |\dot{m}|)}{\tilde{A}^2} dz. \quad (49)$$

In a general case, all parameters inside the integral in eq. (49) may depend on the axial coordinate  $z$ . We note that eq. (49) is similar to eq. (38), which describes Hagen-Poiseuille flow. The comments regarding evaluation of the integral in eq. (38) apply also to eq. (49): the evaluation should be adapted to the way the fuel rod is axially discretized in the fuel rod analysis computer program hosting the gas flow model.

The quadratic left-hand-side terms in eq. (49) result from the assumption of gas compressibility, as defined by the ideal gas law in eq. (6). Let us instead assume that the gas is incompressible and that the density is  $\rho_o$ , independent of the pressure variation along the axial segment from  $z_L$  to  $z_U$ . This assumption applied in eq. (47) leads after integration to linear pressure terms in the left-hand side, viz.

$$p_U - p_L = -\frac{1}{\rho_o} \int_{z_L}^{z_U} \frac{\dot{m} (\alpha \mu \tilde{A} + \beta |\dot{m}|)}{\tilde{A}^2} dz. \quad (50)$$

In axial gas flow models that assume incompressible flow,  $\rho_o$  is calculated through the ideal gas law, either using the known inlet pressure  $p_L$  or the average pressure  $(p_L + p_U)/2$ . In the latter case, iterations are needed over  $p_U$ , since eq. (50) is used for calculating  $p_U$ , based on  $p_L$  and known properties  $(T, \tilde{A}, \dot{m})$  for the axial segment extending from  $z_L$  to  $z_U$ . In fact, if we assume uniform gas temperature  $T_o$  in the segment and calculate  $\rho_o$  from the ideal gas law based on  $T_o$  and the average pressure  $(p_L + p_U)/2$ , eq. (50) results in

$$p_U^2 - p_L^2 = -\frac{2RT_o}{M} \int_{z_L}^{z_U} \frac{\dot{m} (\alpha \mu \tilde{A} + \beta |\dot{m}|)}{\tilde{A}^2} dz. \quad (51)$$

This expression is identical to eq. (49), except for the temperature, which is here assumed to be uniform for  $z_L < z < z_U$  and therefore appears outside the integral.

The above analysis suggests that the differences in calculated gas pressure, resulting from assuming compressible versus incompressible flow, depend on two factors:

- Axial variations in gas temperature along the considered axial segment of the fuel rod. If significant temperature variations exist, the axial variation in pressure will be more accurately calculated with assumption of compressibility, i.e. when the gas pressure is calculated through eq. (49);
- The way the gas density is calculated with regard to pressure, when incompressible flow is assumed, i.e. how  $\rho_o$  in eq. (50) is calculated. If the density is calculated based on *average* gas pressure in the considered axial segment, by use of iterations, the results calculated by the incompressible and compressible flow models will generally be small. As shown above, in case of uniform temperature within the segment, the calculated results will be *identical* if  $\rho_o$  is calculated based on the average gas pressure.

### 2.3.4 Models for permeability of porous and/or cracked materials

Empirical and semi-empirical models for the permeability of porous and/or cracked materials exist in the literature. The models usually emanate from applications with practical importance and apply to two principally different types of materials, as summarized below. The models provide estimates for the specific permeability,  $\kappa$ , or the friction factor,  $f_P$ , and in some cases also for the inertial permeability,  $\kappa_I$ , of the considered material, based on fundamental properties like porosity, average pore size or aperture (width) of cracks in the material. Most of the models are intended for liquid flow, which means that they have more experimental support for liquids than for gases.

**Models for permeability of particle beds** Flow through particle beds is a phenomenon with great practical importance in disciplines like hydrogeology, petroleum engineering, combustion and filtration. As a consequence, a large number of models or empirical correlations have over the years been proposed for estimating the permeability of particle beds. In 2015, Erdim and co-workers published a comprehensive review and assessment of 38 models and correlations of this kind [58]. The reader is referred to this review and the references therein for information on available models and correlations, which have emerged over the last century. The best models provide fairly good estimates of the permeability, based only on a few key parameters of the particle bed, such as porosity (void fraction) and particle size. The success can be understood from the fact that most particle beds are spatially uniform (except for boundary effects) and isotropic.

Unfortunately, permeability models for particle beds have limited applicability to axial gas flow inside LWR fuel rods. The main reason is that particle beds have void fractions of 0.3-0.4, which is far higher than the void fractions expected in LWR fuel rods, unless cladding ballooning with subsequent crumbling of the fuel pellet column into the balloon occurs [52]. The crumbled fuel in the balloon resembles a particle bed, but as long as the as-fabricated geometry of the fuel rod is retained, the void fraction made up of pellet cracks, the pellet-cladding radial gap and interpellet axial gaps is normally less than 0.05. Moreover, permeability models for particle beds usually contain the mean particle size (or surface area to volume ratio) as a key parameter. While this parameter is fairly well known and uniform for particle beds, it is poorly defined and varies from one pellet to another for cracked fuel pellets [52].

**Models for permeability of cracked media** In geological materials with low porosity and porosity-related permeability, such as bedrock, liquid flow takes place predominantly through a network of discrete cracks (joints) in the material [63]. Cracks may also affect fluid flow in porous media, partly by providing additional flow paths, partly by affecting the pressure gradients that drive the flow through uncracked regions of the material. Fluid flow in cracked media is of interest in hydrogeology, not least with regard to potential transport of radioactive substances from deep geological repositories for nuclear waste. In fact, useful data for calibration of permeability models for rock fractures were produced in the international Stripa project, carried out in the Stripa decommissioned iron ore mine in Sweden from 1980 to 1992 [64, 65]. This project was a cooperative research and development project among several member countries of the Nuclear Energy Agency (NEA) of the OECD. It was managed by the Swedish Nuclear Fuel and Waste Management Company (SKB), under the auspices of the NEA [66].

Models for the permeability of cracked media are based on estimates for the permeability of idealized cracks [43]. These estimates are combined with geometric fracture network modelling, from which an equivalent permeability of the cracked material can be calculated. In this calculation, an estimate for the matrix permeability may be added, in case the material is porous; see e.g. [67, 68]. The result of the calculation is an equivalent permeability tensor, since the orientation of individual cracks makes the permeability anisotropic (direction dependent). Moreover, this tensor will vary considerably with space, due to the discrete nature of the cracks. In fact, it is not always possible to define average properties of the material, due to the fractal nature of the crack geometry and the resulting indeterminate homogenization scale [69]. Consequently, the equivalent permeability cannot be considered as an intrinsic property of the cracked material, but varies with both position and scale of the sample.

The equivalent permeability tensor for a piece of cracked material is usually calculated by use of computer models, based on an assumed or measured configuration of the crack network in the considered sample. For illustration, we may consider the work by Thomas et al. [70], who calculated the permeability tensor for a 1.98 mm long axial section of a cracked  $\text{UO}_2$  fuel pellet, sampled from a discharged advanced gas-cooled reactor (AGR) fuel rod. The pellets in this fuel design are annular, with an inner and outer radius of 3.175 and 7.250 mm, respectively. To produce a three-dimensional (3D) model of the crack network in the 1.98 mm long axial section of the sampled pellet, the end of the pellet was photographed, ground and polished in five stages, producing detailed images of the 2D crack patterns at axial positions of 0, 0.57, 1.24, 1.62 and 1.98 mm from the pellet end. Based on the five photographs, the cracks were traced and reconstructed in 3D [70]. This reconstruction was used as input to a finite-element based computer program, which was used for calculating the flow through the porous fuel matrix and the crack network simultaneously. The approach is illustrated in Figure 7. Other important input parameters to the calculations were the crack width (aperture), which was assumed to be either 10 or 20  $\mu\text{m}$  for all cracks, and the permeability of the porous  $\text{UO}_2$  matrix, which was assumed to be either  $1.5 \times 10^{-14}$  or  $5.6 \times 10^{-13} \text{ m}^2$ . These matrix permeabilities were estimated, based on fuel porosities of 4 and 15 %, respectively. The low porosity value corresponds to the typical as-fabricated porosity of the pellet, while the high value represents regions that have experienced high fission gas release, containing a network of vented but still interconnected fission gas bubbles. Large uncertainties exist for the crack aperture and the matrix permeability, which motivated the parametric study with regard to these properties.

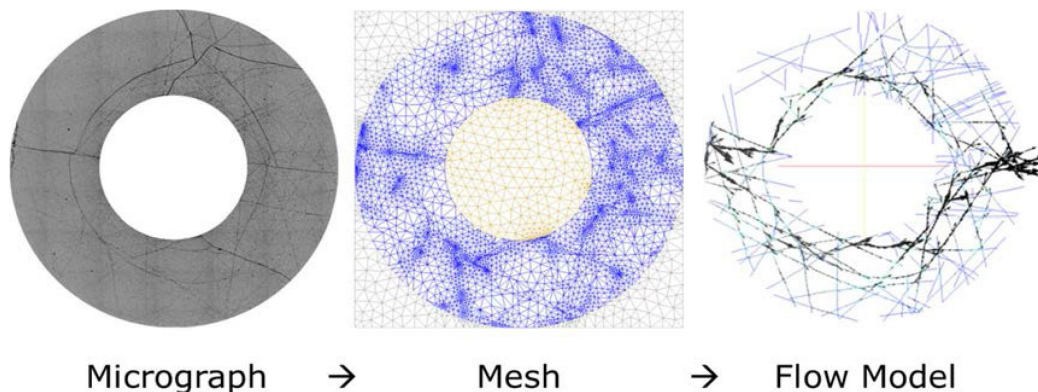


Figure 7: Approach used by Thomas et al. [70] for calculating flow in a porous and cracked axial section of a used AGR fuel pellet [71].

Using postulated pressure gradients along three orthogonal directions as boundary conditions, Thomas and co-workers calculated the permeability tensor for the considered fuel pellet sample. Various combinations of assumed crack apertures and  $\text{UO}_2$  matrix porosities were used in the calculations. The main results are summarized in Table 2, where the presented permeability refers to the average of the three eigenvalues of the calculated permeability tensor,  $\kappa$ , or in other words, to  $\text{trace}(\kappa)/3$ . The calculated permeability was in fact fairly isotropic, except for the case with low matrix porosity and large crack aperture. For this case, the cracks contribute significantly to the overall permeability and their orientation results in a notable anisotropy for the permeability. In Table 2, calculated results are presented also for the hypothetical case without any cracks at all (aperture equal to zero), which leads to isotropic permeability.

Table 2: Summary of calculated results for the equivalent permeability of a cracked  $\text{UO}_2$  fuel sample, assuming different combinations of matrix porosities and crack apertures [70].

Matrix porosity [%]	Crack aperture [ $\mu\text{m}$ ]	Equivalent permeability [ $10^{-14} \text{ m}^2$ ]
4	0	1.50
15	0	56.0
4	10	2.73
15	10	57.2
4	20	11.4
15	20	65.7

Most of the calculated results in Table 2 are in reasonable agreement with measured data from axial gas flow experiments on discharged LWR fuel rods; see section 3. The exceptions are the results calculated for materials with completely closed cracks. From in-reactor gas flow experiments on high-burnup fuel rods at high operating power, we expect the permeability to be in the range from  $10^{-16}$  to  $10^{-15} \text{ m}^2$  for materials with closed cracks; see section 3.2.2. The calculated permeabilities in Table 2 for zero crack apertures are several orders of magnitude higher. As a matter of fact, the calculated results in Table 2 suggest

that fuel porosity is more important than cracks for the equivalent permeability of the considered sample. The cracks make a significant contribution to the equivalent permeability only for the case with low (4 %) porosity. It is difficult to judge whether this is realistic or not, but it seems that the contribution to the equivalent permeability from flow along the cracks is partly offset by the reduction in pressure gradient that is caused by the cracks: Since the pressure gradient is the driving force for flow through the pores within the fuel pellet fragments, the contribution from pore flow decreases when the pressure gradient across fragments is reduced by the existence of cracks.

The calculated permeabilities in Table 2 for zero crack apertures may also be compared with measured data for high-porosity  $\text{UO}_2$  presented in the early 1970s by Graham [72]. He measured the permeability of sintered, un-irradiated  $\text{UO}_2$  with porosities of 15 and 49 %, and reported permeabilities of  $4.1 \times 10^{-16}$  and  $2.5 \times 10^{-13} \text{ m}^2$  for these two materials [72]. These results corroborate our conclusion that the permeability of cracked  $\text{UO}_2$  with closed cracks and porosities around 15 % should be in the range from  $10^{-16}$  to  $10^{-15} \text{ m}^2$ , i.e. much lower than the calculated values in Table 2.

Still, the computational study by Thomas and co-workers [70] is interesting, since it illustrates that the equivalent permeability of cracked fuel pellets can be calculated, based on detailed information on the porosity and crack distribution in the material. However, the effort expended in producing this information as input to the presented computational study on a single small-scale fuel sample is significant, and the flow modelling itself is complex. Consequently, it seems impracticable to use this computational approach for generating reliable correlations for the equivalent permeability of cracked fuel pellets with regard to key parameters like fuel porosity and the density, orientation, connectivity and aperture of pellet cracks. It should also be noted that calculated results from studies on other materials are difficult to apply for estimating the axial permeability of the fuel pellet column. The reason is that the pellet-cladding radial gap and the interpellet axial gaps provide distinct flowpaths that have no counterparts in other materials.



## 3 Data for axial permeability of the fuel pellet column

To the author's best knowledge, there are currently only two studies in the open literature that report measured gas permeabilities for the fuel pellet column in LWR fuel rods. In both studies, which are summarized below in section 3.1, the permeability was measured out-of-reactor by use of gas flow experiments on full-length discharged  $\text{UO}_2$  fuel rods with fairly high burnup ( $> 50 \text{ MWd}(\text{kgU})^{-1}$  rod average). Unfortunately, the results of these studies are not particularly useful for model formulation and calibration. Firstly, they are restricted to room temperature and zero-power conditions. Secondly, they provide an integral value for the permeability over the entire active (fuelled) length of the investigated fuel rods. The permeability is expected to vary along the rod as a consequence of the axial variation of fuel rod power and coolant temperature during operation. Thirdly, information on the tested fuel rods is scarce. Data on their operating power histories and axial power profiles are unavailable in open literature, which makes it difficult to properly assess differences in measured permeability among the tested rods in light of possible differences in their operating lives.

Similar out-of-reactor studies have been done in the past on discharged LWR fuel rods with lower burnup, but results from these studies are reported in terms of parameters relevant for flow in annular ducts, such as hydraulic diameter or Hagen number, rather than permeability. In section 3.2, some of these results are transformed into permeabilities and compared with existing data. In the same section, data on the hydraulic diameter obtained from in-reactor gas flow experiments in the Halden reactor, Norway, are reviewed and transformed into permeabilities. These data provide useful information regarding the effect of fuel rod power on gas permeability.

### 3.1 Direct measurements

#### 3.1.1 Rondinella et al (2015)

In a conference paper from 2015, Rondinella and co-workers reported gas permeability determined for a discharged PWR  $\text{UO}_2$  fuel rod with an average burnup of  $52 \text{ MWd}(\text{kgU})^{-1}$  [32]. The paper is brief, and further information on the experiment seems unavailable in open literature. The axial permeability along the full-length fuel rod was determined at room temperature by connecting gas chambers to each end of the rod, as illustrated in Figure 8. A high constant pressure,  $p_1$ , was maintained in one of the chambers, while the pressure rise in the second chamber,  $p_2(t)$ , was recorded versus time. By applying Darcy's law for a compressible gas, an analytical expression for  $p_2(t)$  can be found [26]

$$p_2(t) = p_1 \frac{(1 - C_o e^{-\kappa\eta t})}{(1 + C_o e^{-\kappa\eta t})}, \quad (52)$$

where

$$\eta = p_1 \tilde{A} / (\mu L V_2), \quad (53)$$

and

$$C_o = (p_1 - p_2(t = 0))/(p_1 + p_2(t = 0)), \quad (54)$$

where  $L$  is the active length of the rod and  $\tilde{A}$  is the cross-sectional area inside the cladding tube. For a known geometry of the test setup and any combination of  $p_1$  and  $p_2(t = 0)$ , eqs. (52) - (54) can be used for determining  $\kappa$  by fitting the calculated results to the measured time history of  $p_2$ . In fact, Rondinella et al. used a simpler analytical expression for  $p_2(t)$  when evaluating their tests. The expression, taken from the work of Calogivic [73], does not apply to the test setup in Figure 8. Consequently, we use eqs. (52) - (54) for evaluating the tests.

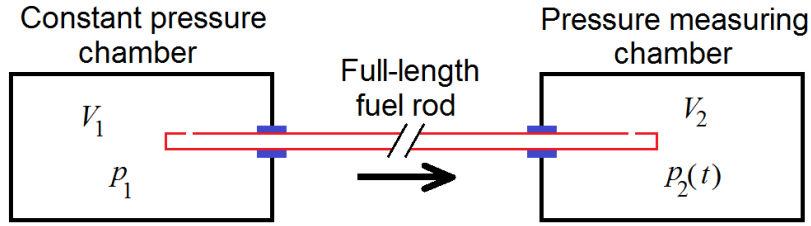


Figure 8: Schematic design of test rigs used for axial gas flow experiments by Rondinella et al. [32] and Montgomery & Morris [26].

Five tests with  $p_1$  in the range from 0.2 to 1.1 MPa were carried out with nitrogen gas at room temperature. The initial pressure in the measuring chamber,  $p_2(t = 0)$ , was 0.1 MPa in all tests. The measured time histories for  $p_2$  are shown in Figure 9, together with calculated results from eqs. (52) - (54), in which  $\kappa = 2.5 \times 10^{-13} \text{ m}^2$  is used. Other parameters used in the calculations are those reported for the test rig by Rondinella et al. [32]:  $L = 3.5 \text{ m}$ ,  $\tilde{A} = 7.01 \times 10^{-5} \text{ m}^2$ ,  $V_2 = 1.25 \times 10^{-5} \text{ m}^3$  and  $\mu = 1.79 \times 10^{-5} \text{ Pas}$ .

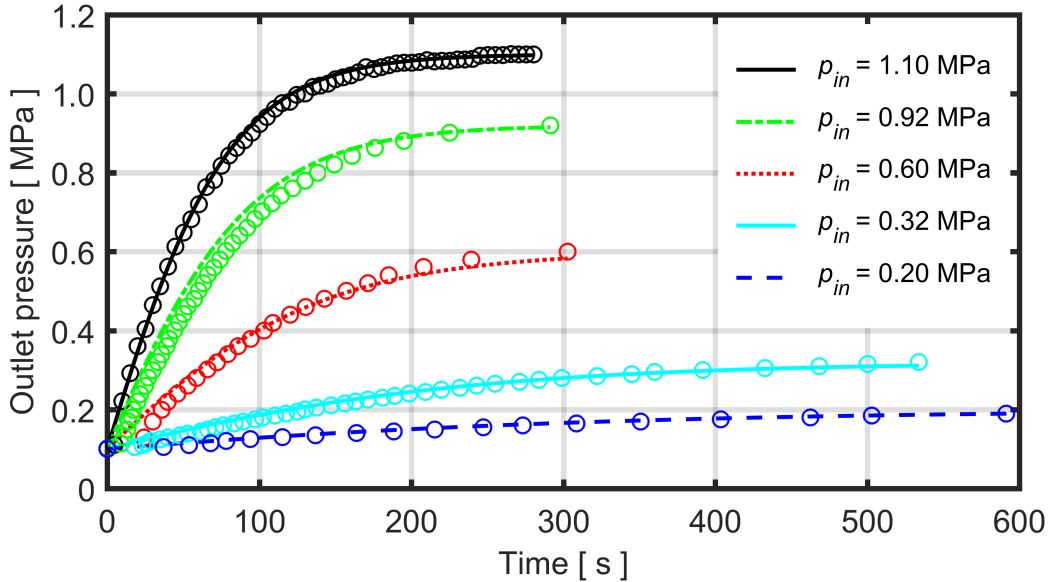


Figure 9: Measured outlet pressure histories,  $p_2(t)$ , from axial gas flow tests on a 52 MWd(kgU)<sup>-1</sup> PWR UO<sub>2</sub> fuel rod [32], in comparison with calculated results from Darcy's law for a compressible gas, using a permeability of  $2.5 \times 10^{-13} \text{ m}^2$  throughout the calculations.

From Figure 9, it is clear that Darcy's law for a compressible gas reproduces the measured data quite well, when  $\kappa = 2.5 \times 10^{-13} \text{ m}^2$  is used in the calculations. From the figure, it is

also clear that there is a slight delay in the pressure rise at beginning of the tests, especially for the tests done with low differential pressure. Rondinella and co-workers [32] provide no explanation or interpretation of this delay.

### 3.1.2 Montgomery & Morris (2019)

As part of an extensive study [74] aimed at characterizing spent PWR fuel with high burnup, axial gas flow experiments were conducted on eight discharged PWR  $\text{UO}_2$  fuel rods with rod average burnups from 51 to 59  $\text{MWd}(\text{kgU})^{-1}$  [26, 27]. All investigated rods were of  $17 \times 17$  fuel assembly design, but they had different cladding materials and represented fuel rod designs operated in the North Anna Nuclear Power Station, USA, from the late 1980s to about 2010.

The experimental setup used by Montgomery and Morris [26] was principally the same as described above in Figure 8, and eqs. (52) - (54) were used for determining the permeability of the fuel pellet column in each rod. Argon gas was used in the experiments, which were conducted at room temperature. Key data for the gas and the test rig are  $\mu = 2.42 \times 10^{-5}$  Pas,  $L = 3.65$  m,  $\tilde{A} = 5.15 \times 10^{-5}$   $\text{m}^2$ ,  $V_2 = 3.77 \times 10^{-5}$   $\text{m}^3$  and  $p_2(t = 0) = 0$ .

Most of the tests were conducted with  $p_1 = 0.10$  MPa, but three of the rods were tested also at higher pressures, up to 2.89 MPa. The influence of  $p_1$  on the measured permeability was generally small. The permeability was determined for each test separately by fitting eqs. (52) - (54) to each recorded time history for  $p_2$ . An example is given in Figure 10, which shows measured versus calculated curves for  $p_2(t)$  in three tests carried out on rod 30AK09 at different pressures. The calculated curves for all pressures were generated with  $\kappa = 1.06 \times 10^{-14}$   $\text{m}^2$ , which corresponds to the average best-estimate value for this particular rod, obtained from four tests at different pressures. This average value for  $\kappa$  reproduces the three tests shown in Figure 10 with fair accuracy: the individual best-estimate values for  $\kappa$  in the three tests ranged from 1.02 to  $1.11 \times 10^{-14}$   $\text{m}^2$  [26].

Best-estimate values for the permeability in each tested fuel rod are presented in Table 3, together with key data for the fuel rods. The measured permeabilities range from  $1.06 \times 10^{-14}$  to  $9.96 \times 10^{-14}$   $\text{m}^2$ , with an average value of  $4.25 \times 10^{-14}$   $\text{m}^2$  for the eight tested rods. This is about 1/6 of the permeability reported by Rondinella et al. [32] for a PWR fuel rod with similar burnup; see section 3.1.1 above. There is no clear correlation between permeability and fuel rod burnup for the eight tested rods. This is not surprising, considering that the burnup range spanned by the rods, 51-59  $\text{MWd}(\text{kgU})^{-1}$ , is narrow.

Since information on the operating lives of the tested rods, such as power histories, is unavailable in open literature, it is not possible to assess differences in measured permeability among the tested rods with regard to possible differences in their operating lives. However, in their paper, Montgomery and Morris [26] present two parameters that are said to characterize the operating life of each tested rod. The first parameter is the rod lifetime maximum high duty core index (HDCI). This parameter is normally used for characterizing the thermal load in the entire core when evaluating cladding corrosion performance in PWR cores [75]. In this context, HDCI is defined as the average cladding surface heat flux in the peak power fuel assembly, divided by the coolant flow and exit temperature. However, it seems that the HDCI values presented in [26] and reproduced in Table 3 are calculated for individual fuel rods, but no details are given on this issue, neither in [26], nor in the technical

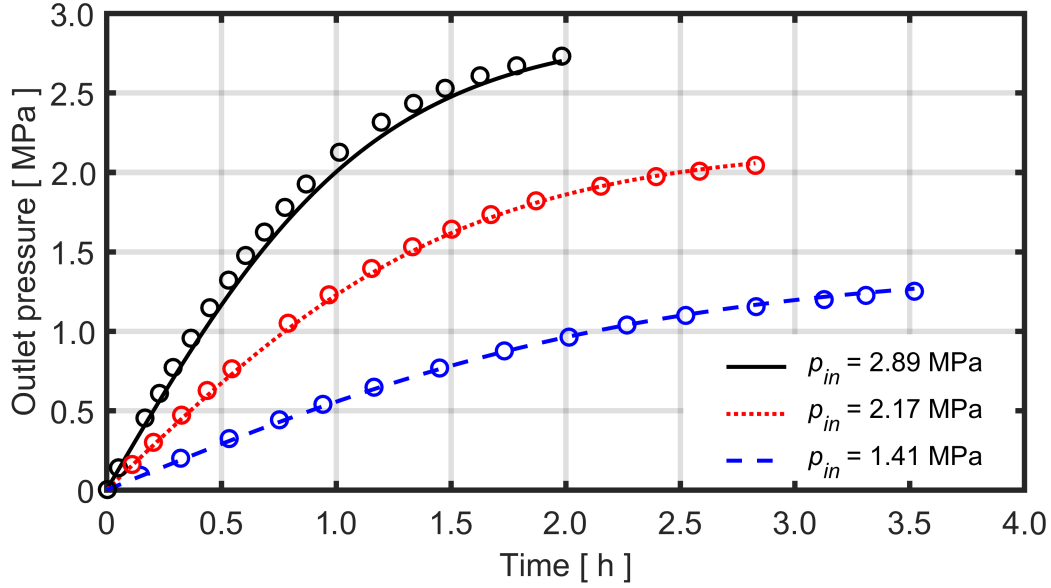


Figure 10: Measured outlet pressure histories,  $p_2(t)$ , from axial gas flow tests on fuel rod 30AK09 [26], in comparison with calculated results from Darcy's law for a compressible gas, using a permeability of  $1.06 \times 10^{-14} \text{ m}^2$  throughout the calculations.

Table 3: Best-estimate values for axial permeability in eight high-burnup PWR fuel rods of  $17 \times 17$  design, determined from axial gas flow tests at room temperature [26]. Type of power history defines high (H) or low (L) operating rod power in each reactor cycle. HDCI: High Duty Core Index [  $\text{Btu}(\text{ft}^2 \text{ gal } ^\circ\text{F})^{-1}$  ].

Fuel rod ID	Cladding tube material	Pre-test heat treatment	Rod average burnup [ $\text{MWd}(\text{kgU})^{-1}$ ]	Type of power history	Rod max lifetime HDCI	Fuel permeability [ $10^{-14} \text{ m}^2$ ]
F35P17	Std Zr-4	Yes	56.9	?-?-?-?	—	9.96
3A1F05	LT Zr-4	No	51.4	H-H	148	8.32
3F9N05	ZIRLO	Yes	54.3	H-H-L	114	7.30
6U3K09	ZIRLO	No	54.5	H-L-L	116	1.89
3D8E14	ZIRLO	No	58.9	H-L-L	113	4.08
30AE14	M5	Yes	54.3	H-H-L	114	2.40
30AD05	M5	No	54.1	H-H-L	113	1.15
30AK09	M5	No	52.8	H-H-L	111	1.06

reports (e.g. [27]) that document details of the experiments. In any case, the correlation between the presented values for HDCI and measured permeabilities is weak. We note that [26] contains a very high HDCI (167) for rod F35P17, which in the background report [27] is presented merely as an *estimate*, without support by proper calculations.

The second parameter used for characterizing the operating life of the examined fuel rods in [26] is the calculated middle-of-cycle operational lifetime assembly average fuel rod centerline temperature. This temperature is reported to range from 716 to 783 K for the eight tested fuel rods. These numbers are very low and most likely in error, but unfortunately, no information is provided on how they were calculated. Nevertheless, the measured permeabilities correlate with the reported temperatures. In conclusion, detailed information on the operating lives of the tested fuel rods, enabling computer modelling, is needed in order

to firmly attribute differences in measured permeability among the rods to parameters and effects that depend on the power history experienced by each rod. Among these parameters are pellet crack density and porosity (known to depend on fuel burnup and peak LHGR experienced during operation), and cold pellet-cladding gap width (known to depend on fuel burnup and end-of-life LHGR).

Three of the fuel rods in Table 3 were subjected to a pre-test heat treatment, intended to simulate dry storage canister loading procedures [26]. More precisely, the three rods were slowly heated from room temperature to 673 K at a rate of  $\approx 10 \text{ Kh}^{-1}$ , held at 673 K for 8 h, and finally cooled to room temperature at a rate of  $-3.7 \text{ Kh}^{-1}$ . As can be seen from Table 3, the heat treated rods had higher permeabilities than rods of similar design that were tested without prior heat treatment. We also note from Table 3 that older fuel designs, with standard (std) and low-tin (LT) Zircaloy-4 (Zr-4) cladding, had higher permeabilities than newer designs with ZIRLO and M5 cladding.

## 3.2 Other data

### 3.2.1 Double gas expansion tests by Desgranges et al. (2005)

In a 2005 paper, Desgranges and co-workers at CEA, France, proposed a new method for measuring the free volume and its gas content inside irradiated LWR fuel rods [30]. The method, which has particular advantages for application to high-burnup fuel rods with restricted axial gas flow, also provides the permeability of the fuel pellet column as a by-product from the measurements: the investigators did not present any permeability data in [30], but their presented results are sufficient for calculating the permeability by simple means.

More precisely, the investigators used a test setup similar<sup>2</sup> to that in Figure 8, and they evaluated the rate of change for  $p_2$  through

$$\frac{dp_2}{dt} = \frac{\mathcal{A}_D}{2LV_2} (p_1^2 - p_2^2), \quad (55)$$

where the proportionality coefficient  $\mathcal{A}_D$  [ $\text{m}^4\text{Pa}^{-1}\text{s}^{-1}$ ] was fitted to the measured data. It can be easily shown [26] that this coefficient is related to the fuel pellet column permeability through  $\kappa = \mu\mathcal{A}_D/\tilde{A}$ , where  $\mu$  is the dynamic viscosity of the gas and  $\tilde{A}$  is the internal cross-sectional area of the cladding tube.

To illustrate their new method, Desgranges and co-workers presented measurements on a  $17 \times 17$  PWR  $\text{UO}_2$  fuel rod with Zircaloy-4 cladding, irradiated during three operating reactor cycles to a burnup of about  $40 \text{ MWd}(\text{kgU})^{-1}$ . Helium at room temperature was used in the measurements, which were carried out in two steps, resulting in different final pressures for  $p_2$ . The coefficient  $\mathcal{A}_D$  was determined by fitting to the measured data from each step. The results reported for  $\mathcal{A}_D$  in [30] are reproduced in Table 4, together with corresponding values for the fuel pellet column permeability. The latter are calculated from  $\kappa = \mu\mathcal{A}_D/\tilde{A}$ , using  $\mu = 2.0 \times 10^{-5} \text{ Pas}$  [36] and  $\tilde{A} = 5.4 \times 10^{-5} \text{ m}^2$ .

<sup>2</sup>No constant pressure chamber was used by Desgranges and co-workers. The fuel rod internal volume replaced  $V_1$  in Figure 8, which means that the pressure  $p_1$  was not constant.

The resulting values for  $\kappa$  in Table 4 obviously fall between the permeabilities reported by Rondinella et al. [32] and Montgomery & Morris [26]; see sections 3.1.1 and 3.1.2. Moreover, there is a significant difference, i.e. larger than experimental uncertainties, between the permeabilities determined in Step 1 (high pressure) and Step 2 (low pressure). The reason for this difference is unclear. It is not explained or discussed in the paper by Desgranges and co-workers [30].

Table 4: Measured values for the proportionality coefficient  $\mathcal{A}_D$  in eq. (55) from [30] and corresponding values for the fuel pellet column permeability,  $\kappa$ .

Measurement step	$p_2(t = \infty)$ [ MPa ]	$\mathcal{A}_D$ [ $10^{-13} \text{ m}^4\text{Pa}^{-1}\text{s}^{-1}$ ]	$\kappa = \mu\mathcal{A}_D/\tilde{A}$ [ $10^{-14} \text{ m}^2$ ]
1	2.15	$3.6 \pm 0.4$	$13.3 \pm 1.5$
2	0.23	$5.3 \pm 0.5$	$19.6 \pm 1.9$

### 3.2.2 Halden in-reactor gas flow experiments

Beginning in the 1970s, gas flow rigs in the form of instrumented fuel assemblies (IFAs) have been used in the Halden test reactor, Norway, for in-reactor measurements of various properties, such as the pellet-cladding gap width, in operating fuel rods. A review of the gas flow rigs, the conducted experiments and the most important results is provided in [76]. In the gas flow rigs, a known and steady flow of He or Ar gas is maintained between the ends of each test rod in the rig, while the pressures at each end are measured. The measured pressure drop and the known gas flow rate are then used for calculating the average hydraulic diameter,  $D_h$ , for each test rod by assuming laminar flow in a planar gap. More precisely, from eq. (26) with  $\Delta_e=0$ , we find the relation used by the Halden staff for evaluating the hydraulic diameter  $D_h=2h=2(R_o - R_i)$  from the measured pressure drop and volumetric flow rate  $Q$

$$Q(z) = -\frac{\partial p}{\partial z} \frac{\pi(R_o + R_i)D_h^3}{96\mu}. \quad (56)$$

Here,  $R_i$  is the pellet radius and  $R_o$  is the cladding inner radius, as shown in Figure 2. Figure 11 is a summary of data on  $D_h$ , measured at hot standby conditions (zero power, temperature  $\approx 510$  K) during the operating lives of four test rods in the IFA-430 and IFA-504 gas flow rigs [77]. Figure 11 clearly shows that the measured hydraulic diameters are close to the as-fabricated diametral gaps ( $2h$ , indicated in the figure legend) when the rods are first taken into operation, but that  $D_h$  is drastically reduced early in life, due to fuel cracking and outward radial relocation of the pellet fragments when the fuel is brought up to power. Then, there is a period of fairly slow reduction of  $D_h$ , caused by solid swelling of the fuel pellets: the dashed lines in Figure 11 indicate typical fuel swelling rates caused by solid fission products in the  $\text{UO}_2$  matrix. The cladding creep-down is very slow in the Halden reactor, due to its low fast neutron flux and low coolant pressure. In PWRs, where cladding creep-down is fast, we expect a faster reduction of  $D_h$  with increasing burnup than shown in Figure 11.

At higher burnup, beyond about  $30 \text{ MWd}(\text{kgUO}_2)^{-1}$ , the measured data in Figure 11 suggest that  $D_h$  tends to a plateau value of 50-70  $\mu\text{m}$ . However, the trend is broken by the last four data points for test rod 504-2. The broken trend can be understood from the power

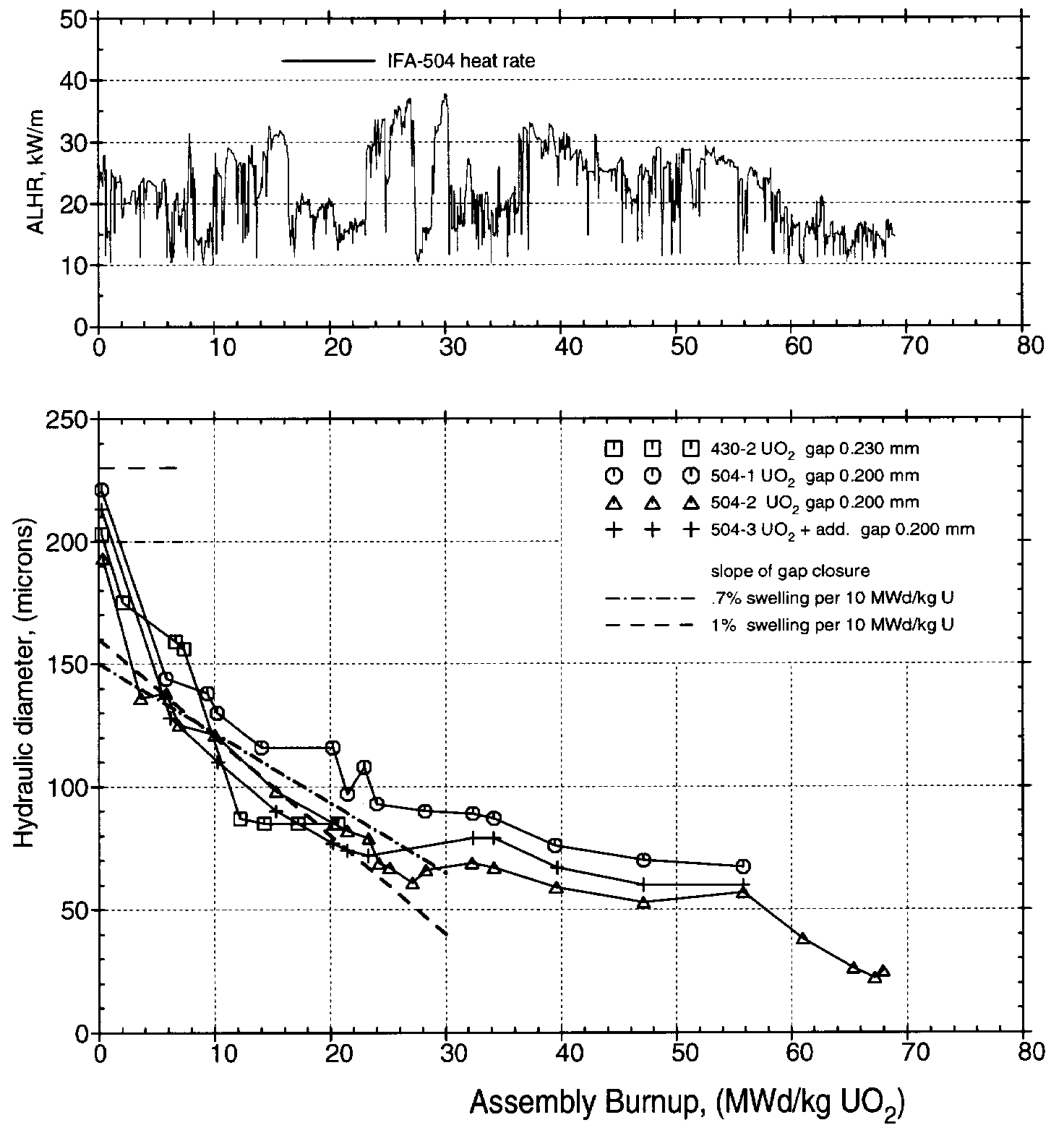


Figure 11: Measured data for hydraulic diameter  $D_h$ , obtained from two gas flow rigs in the Halden reactor [77]. The data pertain to hot standby conditions, i.e. zero power and  $\approx 510$  K. The upper panel shows the average linear heat generation rate for the instrumented fuel assembly 504 (IFA-504) versus assembly burnup.

history of IFA-504, as shown in the upper panel of Figure 11. The linear heat generation rate is significantly lowered beyond  $58 \text{ MWd}(\text{kgUO}_2)^{-1}$ . In high-burnup fuel, the pellet and cladding are usually in contact when the rod is operating at nominal power. For this reason, the zero-power hydraulic diameter shown in the lower panel is controlled by the differential shrinkage between the pellet and cladding when the fuel rod is downrated from operating power to zero power [77]. Hence, downrating from low operating power at high burnup leaves a small zero-power hydraulic diameter, as is the case for the last four data points for test rod 504-2 in Figure 11.

The hydraulic diameter measurements reported from the Halden gas flow rigs may be transformed into equivalent fuel pellet column permeabilities by comparing eq. (56) with Darcy's law in eq. (43), where  $\tilde{u} = Q/\tilde{A}$  and

$$Q(z) = -\frac{\partial p}{\partial z} \frac{\kappa \tilde{A}}{\mu}. \quad (57)$$

As before,  $\tilde{A} = \pi R_o^2$  is the internal cross-sectional area of the cladding tube. By combining eqs. (56) and (57), we find the relation

$$\kappa = \frac{(R_o + R_i) D_h^3}{96 R_o^2}, \quad (58)$$

by which measured values for  $D_h$  can be converted into equivalent permeability, if the test rod dimensions are known. Here, we consider Halden test rod 504-2, which had the as-fabricated dimensions  $R_i = 5.295 \text{ mm}$  and  $R_o = 5.395 \text{ mm}$ . With these numbers, eq. (58) yields  $\kappa = 3.826 D_h^3$ , where  $\kappa$  and  $D_h$  are in units of  $\text{m}^2$  and  $\text{m}$ , respectively.

Figure 12 shows  $\kappa$  for test rod 504-2, plotted versus average burnup for the instrumented fuel assembly 504. It is interesting to note that the zero-power permeability drops from about  $1 \times 10^{-12} \text{ m}^2$  to  $3 - 7 \times 10^{-14} \text{ m}^2$  at a burnup beyond  $65 \text{ MWd}(\text{kgU})^{-1}$ . The drop is caused by the reduction in power from about  $25 \text{ kWm}^{-1}$  to  $15 \text{ kWm}^{-1}$  that the fuel rod experienced at this burnup; confer the upper panel of Figure 11 and note that the unit for burnup is different in Figures 11 and 12. The permeability values measured after the power reduction, i.e.  $3 - 7 \times 10^{-14} \text{ m}^2$ , are similar to those reported for high-burnup PWR fuel rods by Montgomery & Morris; see Table 3. The permeabilities measured before the power reduction, i.e.  $\approx 1 \times 10^{-12} \text{ m}^2$ , are higher than those obtained in other studies on high-burnup fuel rods; confer with data presented in sections 3.1.1-3.2.1. This can be understood from the fact that a linear heat generation rate of  $25\text{-}30 \text{ kWm}^{-1}$  is exceptionally high for a fuel rod with  $40\text{-}65 \text{ MWd}(\text{kgU})^{-1}$  burnup, as was the case for test rod 504-2. It is more than likely that the commercial PWR fuel rods investigated by Rondinella et al. [32], Montgomery & Morris [26] and Desgranges et al. [30] experienced significantly lower end-of-life power.

The permeability data for test rod 504-2 in Figure 12 underline the importance of the past power history to the zero-power axial permeability for high-burnup fuel rods. In particular, the data show that differences in reported zero-power permeability between the studies reviewed in sections 3.1.1-3.2.1 may very well be explained by differences in end-of-life power among the tested fuel rods. As already mentioned, information on the power histories of the tested fuel rods is unfortunately unavailable in the open literature, which means that possible causes to the observed differences in permeability cannot be properly assessed.

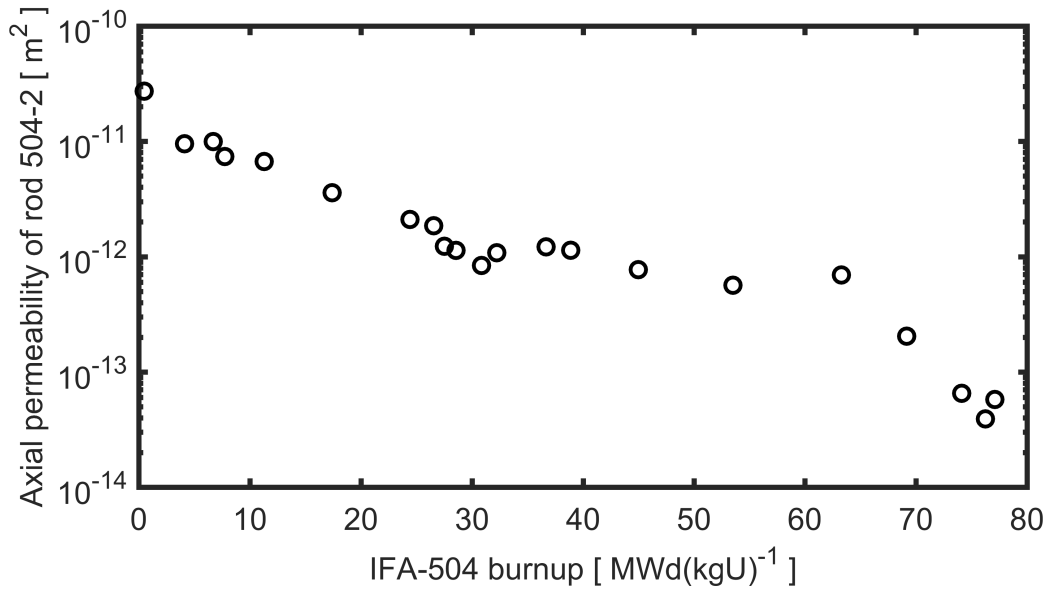


Figure 12: Zero-power permeability of the fuel pellet column in Halden test rod 504-2, calculated from the measured hydraulic diameter data in Figure 11 by use of eq. (58). Note that the unit used for the abscissa is here changed from  $\text{MWd}(\text{kgUO}_2)^{-1}$  to the more common  $\text{MWd}(\text{kgU})^{-1}$ .

To the author's best knowledge, the Halden gas flow experiments are currently the only available sources of information regarding axial gas transport inside fuel rods that operate at power. Figure 13 is an example, taken from [77]. It shows the hydraulic diameter versus LHGR, measured for the Halden 504-2 test rod at a rod average burnup of  $75 \text{ MWd}(\text{kgU})^{-1}$ . The measurements, which were done during decreasing power, show that a residual flow path, corresponding to  $D_h \approx 3\text{-}4 \mu\text{m}$ , exists for LHGRs above  $11 \text{ kWm}^{-1}$ , even when the pellet and cladding are in firm contact. When the LHGR is reduced below  $11 \text{ kWm}^{-1}$ , the hydraulic diameter increases rapidly and non-linearly as a result of gap opening. This transitory stage passes into a more gradual increase of  $D_h$  with decreasing power below  $10 \text{ kWm}^{-1}$ . This stage exhibits a linear relationship between hydraulic diameter and rod power. It ends with a zero-power hydraulic diameter of about  $30 \mu\text{m}$ , which agrees with the high-burnup data for rod 504-2 presented in Figure 11.

As before, we may transform the data for  $D_h$  in Figure 13 into an equivalent permeability by use of eq. (58). The results are shown in Figure 14. The permeability increases by almost two orders of magnitude when the LHGR is lowered from  $11$  to  $9 \text{ kWm}^{-1}$  and the pellet-cladding gap opens. When the rod power is further reduced,  $\kappa$  increases by another order of magnitude. These results indicate that axial gas flow inside LWR fuel rods with solid (non-annular) fuel pellets is extremely sensitive to the state of the pellet-cladding gap, when the gap is passing from closed to open or vice versa. With regard to modelling and computational analyses, the results presented in Figure 14 underline the importance of accurate gap state predictions for reliable calculations of axial gas flow.

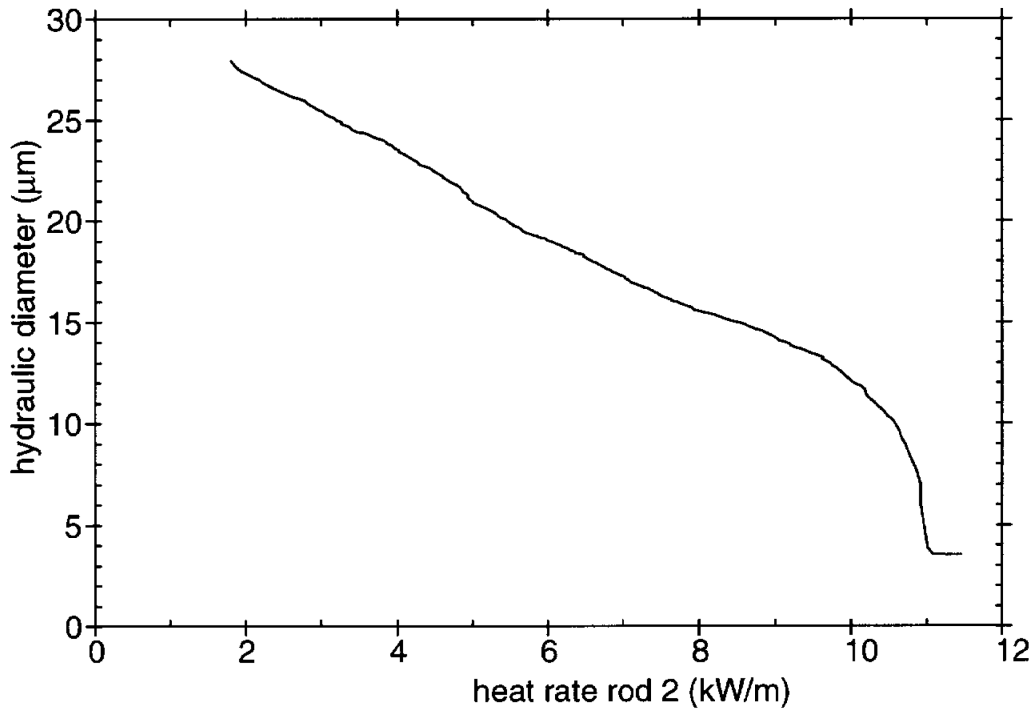


Figure 13: In-reactor measurement of hydraulic diameter for the Halden 504-2 test rod. The measurements were done during decreasing power at a fuel rod burnup of  $75 \text{ MWd}(\text{kgU})^{-1}$  [77].

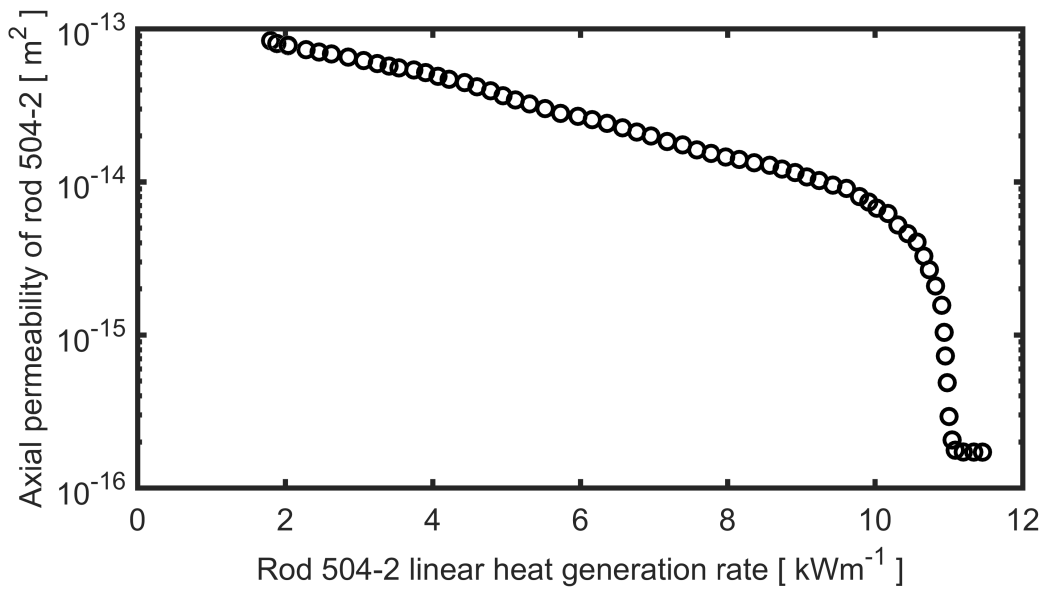


Figure 14: Permeability of the fuel pellet column in Halden test rod 504-2 versus LHGR, calculated from the measured hydraulic diameter data in Figure 13 by use of eq. (58).

### 3.2.3 INEL out-of-reactor gas flow experiments

In the late 1970s, out-of-reactor axial gas flow experiments were conducted on six discharged PWR UO<sub>2</sub> fuel rods at Idaho National Engineering Laboratory (INEL), USA [21]. All investigated rods belonged to the same fuel assembly, which means that they were of identical design and had experienced very similar operating conditions. For three of the fuel rods, the zero-power hydraulic diameter was measured by the same technique as used in the Halden gas flow rigs: a steady axial flow of gas was forced through the full-length rods, and the hydraulic diameter was determined from the resulting pressure difference by use of eq. (56). Measurements were done with both He and Ar at average pressures between 2.6 and 5.6 MPa. Most tests were done at room temperature, but some were done at 533 K [21].

Table 5 summarizes key results obtained from the tested fuel rods. The rod average axial permeability is calculated from the measured values for  $D_h$  through eq. (58), using  $R_i=4.648$  and  $R_o=4.673$  mm. These numbers represent the average deformed dimensions of the tested fuel rods [21]. The fuel burnup of the tested rods is significantly lower than in the tests reviewed in previous subsections. As expected from the low burnup, the measured hydraulic diameters and the equivalent permeabilities are fairly large. In fact, the results for  $D_h$  and  $\kappa$  in Table 5 agree fairly well with the data for Halden test rod 504-2 at a burnup of about 27 MWd(kgU)<sup>-1</sup>; compare with the Halden results in Figures 11 and 12.

Table 5: Rod average properties determined for three discharged PWR UO<sub>2</sub> fuel rods, subjected to out-of-reactor steady-state axial gas flow tests at INEL [21].

Rod ID	Burnup [ MWd(kgU) <sup>-1</sup> ]	$D_h$ [ $\mu\text{m}$ ]	$\kappa$ [ $10^{-14} \text{ m}^2$ ]
M-4	26.5	60	96
L-4	27.2	64	120
K-4	27.3	48	49

The data on  $D_h$  and  $\kappa$  presented in Table 5 are rod average values, determined from the measured pressure differences between the ends of the full-length fuel rods. In addition to these rod average measurements, the variation of  $D_h$  along the tested fuel rods was determined by use of eight additional pressure transducers that were connected to drilled pressure taps, distributed evenly along the active part of the rods. The average hydraulic diameter between neighbouring pressure taps, i.e. over  $\approx 35$  cm long axial segments, could thereby be determined from the local pressure difference between each pair of neighbouring taps. An example for test rod K-4 is shown in Figure 15. The measured hydraulic diameter ranges from about 40  $\mu\text{m}$  in the central part of the rod to 70-80  $\mu\text{m}$  at the ends. This variation for  $D_h$  can be understood from the axial variations in fuel pellet swelling and cladding tube creep-down during the operating life of the fuel rod. Some information on the operating life, e.g. fuel assembly axial power profiles for the two operating cycles, is available in [21], but very little information is provided on the power history of the fuel. Figure 16 shows the axial variation in permeability, corresponding to the measured variation for  $D_h$ .

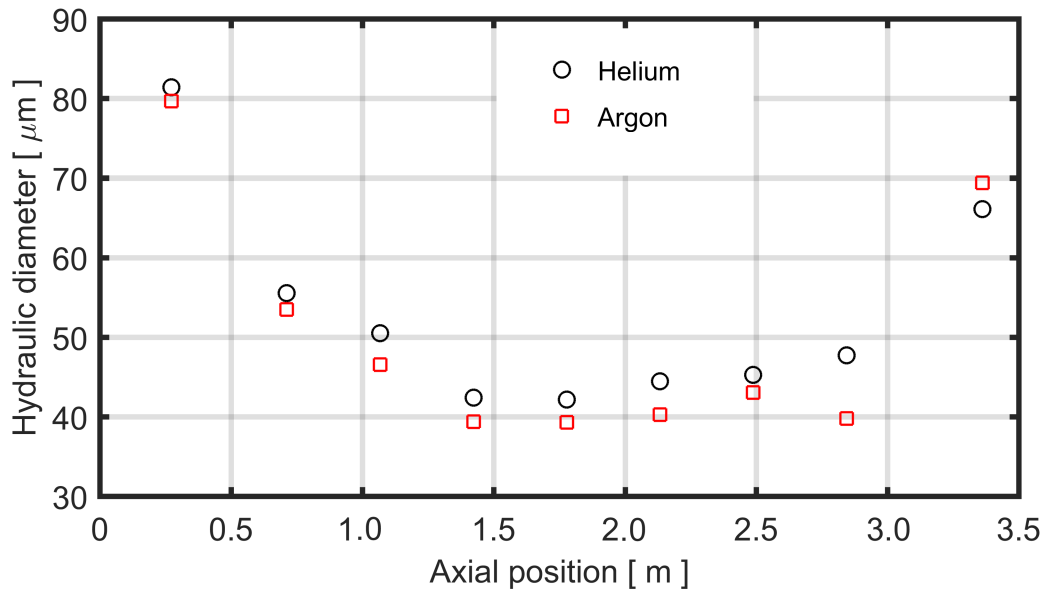


Figure 15: Axial variation in zero-power hydraulic diameter for test rod K-4, determined from steady-state gas flow tests with He and Ar at room temperature [21].

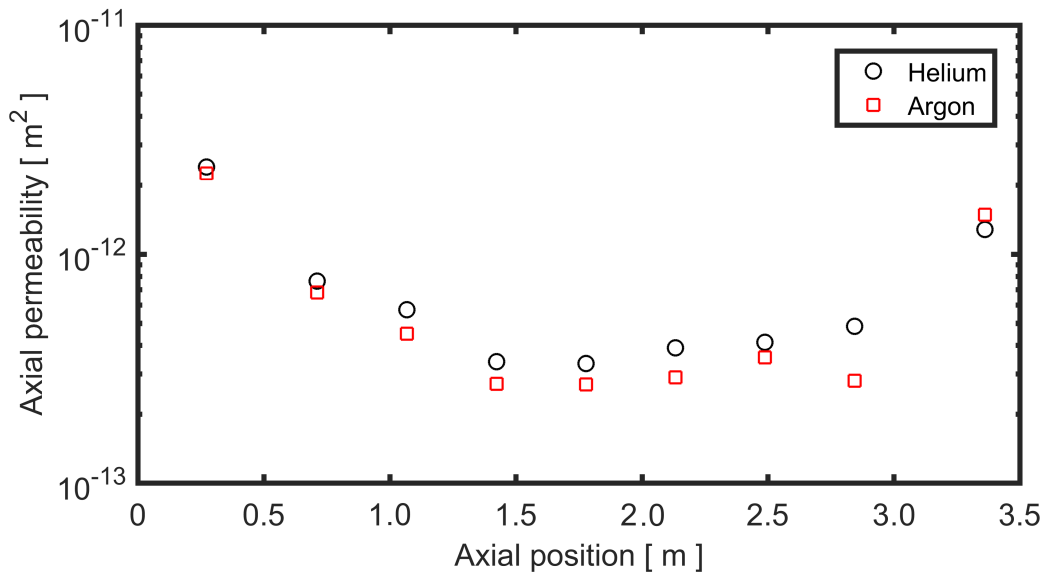


Figure 16: Axial variation of the zero-power permeability for the fuel pellet column in rod K-4, calculated from the measured hydraulic diameter data in Figure 15 by use of eq. (58) [21].

The INEL steady-state gas flow tests were conducted at average gas pressures between 2.6 and 5.6 MPa. The applied pressure difference between the two ends of the fuel rods was also varied, leading to Reynolds numbers between 5 and 300 [21]. Tests with high Reynolds numbers generally resulted in apparently lower values for  $D_h$ , as illustrated by Figure 17. The reason is the increasing flow resistance with increasing  $Re$ , caused by turbulence, as discussed in section 2.2.3. We note from Figure 17 that  $Re > 50$  could only be achieved with argon in the INEL steady-state gas flow tests. Due to the low density of helium, very high pressure gradients would have been needed to reach  $Re > 50$  with helium in the INEL test rods, due their fairly narrow pellet-cladding gap. This corroborates the conclusion from section 2.2.3 that turbulent flow in the pellet-cladding gap of LWR fuel rods is unlikely, as long as the gap gas is dominated by helium and the cladding distension is limited.

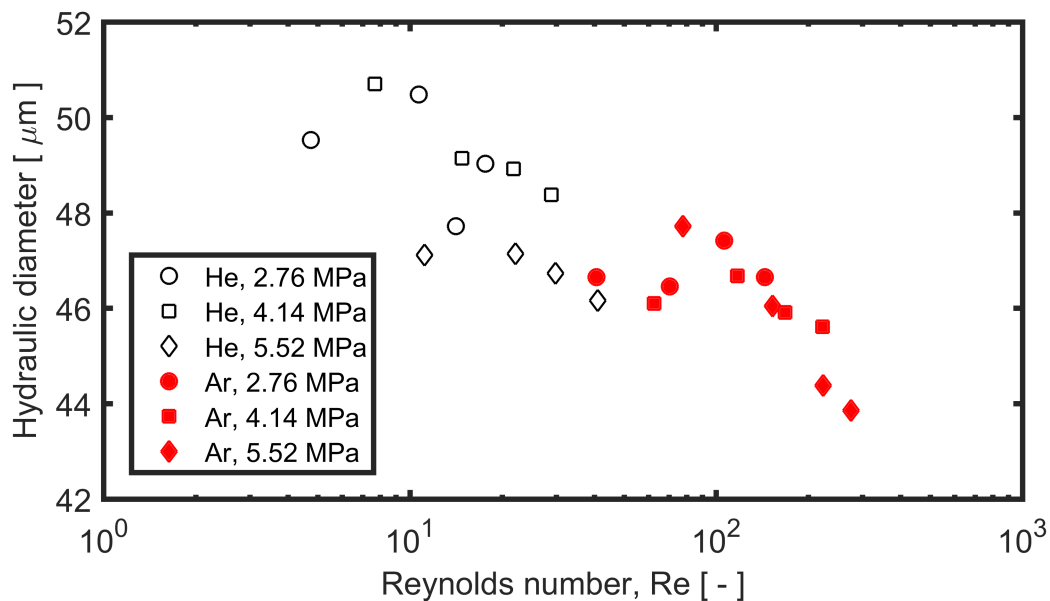


Figure 17: Effect of Reynolds number on zero-power axial average hydraulic diameter for test rod K-4, determined from steady-state gas flow tests at room temperature [21]. The pressures indicated in the legend are axial average pressures; the axial pressure differences varied in relation to  $Re$ .

### 3.2.4 KfK out-of-reactor gas flow experiments

Finally, we consider the data obtained from gas flow experiments conducted on fuel rod segments charged with  $Al_2O_3$  pellets in cracked as well as solid (uncracked) condition at Kernforschungszentrum Karlsruhe (KfK), Germany [20]. These data were used for assessing models for flow in annular ducts in section 2.2.4 of the report, and the experimental procedure is summarized in section 2.2.4. Here, we only recall that the experiments were carried out on 0.5 m long cladding tube segments that were charged with either solid (uncracked) or manually cracked  $Al_2O_3$  pellets. A steady and controlled mass flow of He or Ar gas at room temperature was forced through the segments, while the gas pressures at the two ends of the segments were measured.

The data on mass flow and corresponding inlet/outlet pressures, presented in Tables 3.3 and 4.4 of [20], can be used for assessing the Forchheimer equation, as given in its general form by eq. (49). Since the temperature, gas viscosity and cross-sectional area of the cladding

tube were uniform along the tested segments in the KfK experiments, this equation can here be simplified to

$$p_{in}^2 - p_{out}^2 = C_1 \dot{m} + C_2 \dot{m}^2, \quad (59)$$

where  $p_{in}$  and  $p_{out}$  are the inlet and outlet pressures and  $\dot{m}$  is the mass flow. The two coefficients  $C_1$  and  $C_2$  in eq. (59) are related to the Forchheimer parameters through

$$C_1 = \frac{2RLT\mu}{M\tilde{A}}\alpha, \quad (60)$$

$$C_2 = \frac{2RLT}{M\tilde{A}^2}\beta, \quad (61)$$

where all properties in the fractions are known:  $R = 8.134 \text{ J}(\text{molK})^{-1}$ ,  $L = 0.5 \text{ m}$ ,  $T = 295 \text{ K}$ ,  $\tilde{A} = 6.8 \times 10^{-5} \text{ m}^2$ ; see Table 1. For helium,  $M = 4.00 \times 10^{-3} \text{ kgmol}^{-1}$  and  $\mu = 2.0 \times 10^{-5} \text{ Pas}$  [36]. For argon,  $M = 3.99 \times 10^{-2} \text{ kgmol}^{-1}$  and  $\mu = 2.3 \times 10^{-5} \text{ Pas}$  [78].

By fitting  $C_1$  and  $C_2$  to the data on  $\dot{m}$ ,  $p_{in}$  and  $p_{out}$  from the experiments in [20], it is possible to determine best-estimate values for  $\alpha$  and  $\beta$  through eqs. (60)-(61). The experimental data and the resulting fits are shown in Figures 18 and 19. Clearly, there is a large spread in the measured data, particularly for the experiments conducted with solid (uncracked) pellets. It is believed that the eccentricity of the solid pellets may have changed from one test to another, leading to the spread in measured pressure drop. The data for cracked pellets do not suffer from this sensitivity. It is also clear from Figures 18 and 19 that the mass flow rates in many of the KfK tests were too high for being adequately described by the linear relationship between  $\dot{m}$  and  $p_{in}^2 - p_{out}^2$  assumed in Darcy's law: the quadratic term in Forchheimer's extension to the law is essential for reproducing the data with  $\dot{m}$  larger than 0.2-0.3  $\text{gs}^{-1}$ .

Best-fit values of  $\alpha$ ,  $\beta$  and  $\kappa = \alpha^{-1}$ , determined from the KfK experiments, are presented in Table 6. Three comments should be made on these results: Firstly, the differences between best-fit parameters obtained with helium vis-à-vis argon are large, unexpected and difficult to explain. From eqs. (60)-(61), the only expected differences between the gases are related to their molar mass and viscosity. Uncertainties in these properties are small, and cannot explain the large differences in  $\alpha$  and  $\beta$  obtained with helium vis-à-vis argon. Secondly, when comparing the results for solid (uncracked) vis-à-vis cracked fuel pellets, it is clear that  $\alpha$  is a factor  $\approx 2.5$  higher for the latter, while  $\beta$  is increased by a factor 3.0-3.5. This notable effect of cracking on the flow resistance is similar for helium and argon. Thirdly, the permeabilities in Table 6 compare quite well with the zero-burnup, zero-power permeability reported for the Halden test rod 504-2; see Figure 12.

Table 6: Values for parameters  $\alpha$  and  $\beta$  in the Forchheimer equation, obtained by fitting to data from KfK gas flow experiments [20].

State of pellet	Gas flow	$\alpha$ [ $10^{10} \text{ m}^{-2}$ ]	$\beta$ [ $10^5 \text{ m}^{-1}$ ]	$\kappa = \alpha^{-1}$ [ $10^{-11} \text{ m}^2$ ]
Solid	He	2.32	0.868	4.31
	Ar	3.21	0.672	3.12
Cracked	He	5.71	2.57	1.75
	Ar	8.49	2.39	1.18

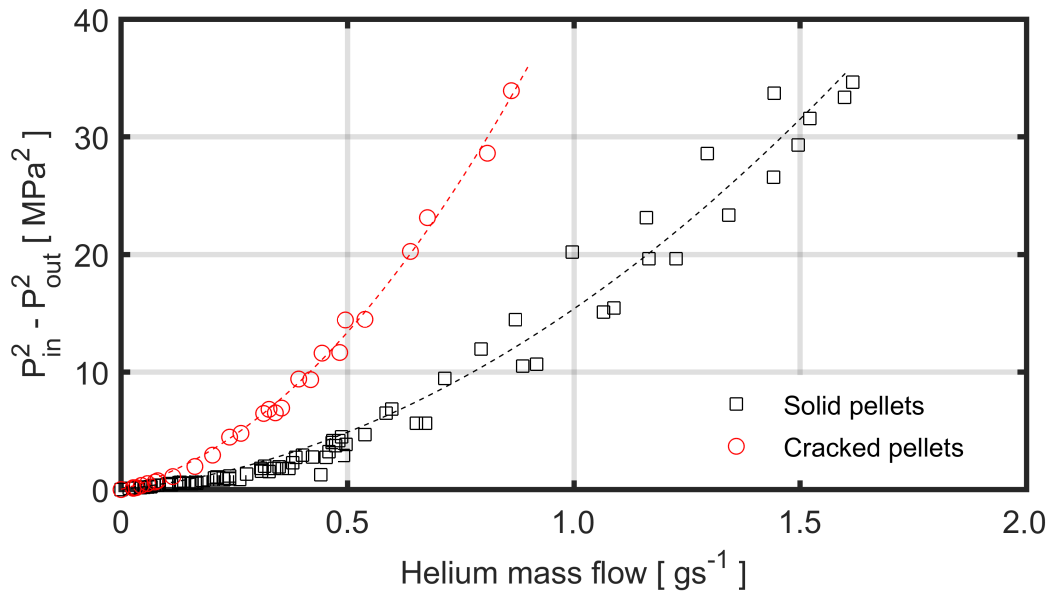


Figure 18: Symbols: Measured data from steady-state helium gas flow experiments on 0.5 m long fuel rod segments, charged with either solid (uncracked) or cracked Al<sub>2</sub>O<sub>3</sub> pellets [20]. Dashed lines: Quadratic fits to the data, according to the Forchheimer equation; see Table 6.

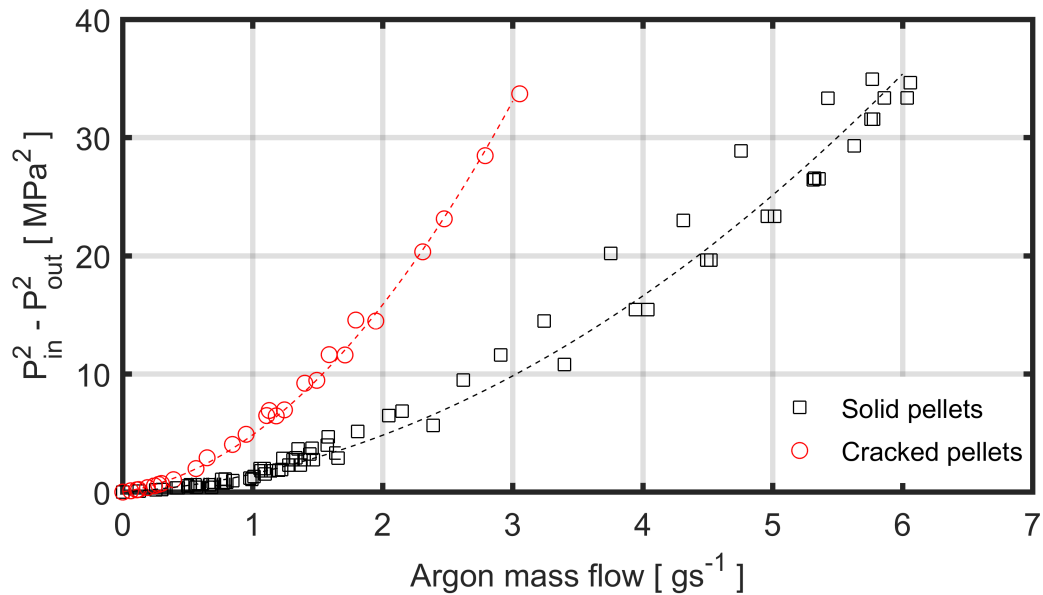


Figure 19: Symbols: Measured data from steady-state argon gas flow experiments on 0.5 m long fuel rod segments, charged with either solid (uncracked) or cracked Al<sub>2</sub>O<sub>3</sub> pellets [20]. Dashed lines: Quadratic fits to the data, according to the Forchheimer equation; see Table 6.



## 4 Comparison of modelling approaches

As described in section 2, there are currently two principally different approaches for modelling pressure-driven axial gas flow inside LWR fuel rods: the first approach is based on models for one-dimensional laminar flow in an idealized annular gap between the fuel pellets and the cladding tube, while the other assumes tortuous flow through a porous and/or cracked medium, constituted by the fragmented fuel pellets, that completely fills the cross-section of the cladding tube.

As will be shown in section 4.1, under conditions expected for most applications to gas flow inside LWR fuel rods, the two modelling approaches lead to similar functional relationships between the mass flow rate and the axial pressure gradient. The difference between the approaches is related only to the description of the axial gas transmissivity of the fuel pellet column. This is discussed in section 4.2, where comparisons are made between the descriptions.

### 4.1 Governing equations for mass flow rate

As described in section 2.1.3, several simplifying approximations to the governing conservation equations can be made when pressure-driven gas flow inside LWR fuel rods is modelled. Without losing much accuracy or significance, the flow may be considered as isothermal<sup>3</sup>, quasi-stationary and one-dimensional, and the gas may be assumed to obey the ideal gas law. It is also common to assume creeping flow, i.e. slow gas flow where advective inertia forces acting on the flowing gas are negligible in comparison with viscous forces. The latter assumption is justified for most expected flow conditions inside LWR fuel rods, but may be violated in cases of very steep axial pressure gradients in combination with wide pellet-cladding gaps. Such cases may possibly occur immediately after cladding burst under a LOCA, in parts of the fuel rod where the cladding tube has distended (ballooned) as a result of overheating and high internal overpressure.

As shown in section 2.2.4, under the simplifying conditions listed above, models for gas flow in annular ducts lead to the general expression

$$\dot{m} = -\frac{M\mathcal{T}(z)}{RT(z)\mu(z)} p \frac{\partial p}{\partial z}, \quad (62)$$

where  $\mathcal{T}(z)$  [m<sup>4</sup>] is a function that depends on the cross-sectional geometry of the flow channel. For example, for a concentric circular annular duct with inner and outer radius  $R_i$  and  $R_o$  (see Figure 2),  $\mathcal{T}(z)$  is defined by eq. (37). For non-concentric circular ducts,  $\mathcal{T}(z)$  may be expressed as

$$\mathcal{T}(z) = \frac{\pi (R_i(z) + R_o(z)) D_h^3(z)}{\text{Hg}(z)}, \quad (63)$$

where  $D_h = 2(R_o - R_i)$  is the hydraulic diameter of the flow channel and Hg is the non-dimensional Hagen number. For laminar flow, Hg depends on the flow channel cross-sectional geometry only, and it can be calculated analytically for various cross-sectional

---

<sup>3</sup>Here, isothermal means that the gas temperature is defined as a function of space and time from the known temperature distribution for the flow channel walls. It is not necessarily constant; see section 2.1.3.

configurations of the duct; see e.g. Figure 4. For more complex flow channel geometries, such as that afforded by a column of cracked fuel pellets inside an LWR fuel rod,  $H_g$  cannot be calculated from analytical expressions. In existing gas flow models for LWR fuel rods [29, 46],  $H_g$  is treated as an empirical parameter that is fitted to data from gas flow experiments; see e.g. Figure 6. This is, however, not an easy task, since the mass flow depends on the ratio  $D_h^3/H_g$  (see eq. (63)), where the hydraulic diameter  $D_h$  can be determined with exactitude only for fresh (un-irradiated) fuel rods.

As shown in section 2.3, models for flow through porous and/or cracked media are generally empirically based. Nevertheless, the most widely used models of this kind, Darcy's law and Forchheimer's equation, have been theoretically shown to be approximations to the Navier-Stokes equations [56, 57]. For cases with slow (creeping) flow of an ideal gas, models for flow in porous and/or cracked media result in a relation for the mass flow rate that is very similar to eq. (62), namely

$$\dot{m} = -\frac{M\tilde{A}(z)\kappa(z)}{RT(z)\mu(z)} p \frac{\partial p}{\partial z}. \quad (64)$$

Here,  $\tilde{A}(z)$  is the gross cross-sectional area of the flow channel, which is filled with a porous and/or cracked material with permeability  $\kappa(z)$ . Equation (64) follows from Darcy's law in eq. (43), applied to an ideal gas; see eq. (48) in section 2.3.3.

## 4.2 Transmissivity measures

By comparing eqs. (62) and (64), it is clear that the two modelling approaches lead to identical governing equations for the mass flow rate, provided that  $\mathcal{T} \equiv \tilde{A}\kappa$ . In studies of porous/cracked materials, the product  $\tilde{A}\kappa$  is usually referred to as *transmissivity* [43], and henceforth, we will use this name also for  $\mathcal{T}$ . The transmissivity thus refers to a specific component or configuration (in our case the cladding tube filled with cracked fuel pellets), whereas the permeability is a material property (in our case of the cracked pellets). For incompressible fluids, the transmissivity divided by fluid viscosity is the proportionality coefficient between the volumetric flow rate and the pressure gradient, and hence, a property that can be readily determined experimentally for a specific test setup [43].

Since the two modelling approaches result in equivalent governing equations, the approach to pursue can be selected based on whether  $\mathcal{T}$  or  $\tilde{A}\kappa$  is the best parameter to characterize the gas transmissivity inside the fuel rod. Two factors should thereby be considered: (i) the availability of experimental data for  $\mathcal{T}$  vis-à-vis  $\tilde{A}\kappa$ ; (ii) the possibility to estimate  $\mathcal{T}$  or  $\tilde{A}\kappa$  from results calculated by other sub-models in the fuel rod analysis software that hosts the axial gas flow model. While the availability of experimental data is comparable for  $\mathcal{T}$  and  $\tilde{A}\kappa$  (see section 3),  $\mathcal{T}$  has advantages with regard to model implementation in computer programs for fuel rod thermal-mechanical analysis. More precisely, for the idealized fuel rod geometry usually treated by these programs, i.e. a column of cylindrical fuel pellets concentrically contained within an axisymmetric cladding tube,  $\mathcal{T}$  can be calculated analytically from the radii of the pellet outer surface and the cladding inner surface, respectively. These analytical solutions may serve as estimates for  $\mathcal{T}$  in the true fuel rod geometry, which in most cases consists of densely packed fuel pellet fragments inside a cladding tube that may depart somewhat from axial symmetry. We recall from sections

2.2.1-2.2.2 that the analytical solutions show that  $\mathcal{T} \propto D_h^3$ , where  $D_h$  is the hydraulic diameter of the flow channel. For a general case,  $D_h = 4A/P_w$ , where  $A$  and  $P_w$  are the true cross-sectional flow area and the wetted perimeter of the flow channel. In any computer program for fuel rod thermal-mechanical analysis, it should be possible to estimate both  $A$  and  $P_w$  from calculated deformations and the typical size of fuel pellet fragments. The latter depends on the fuel pellet average burnup and peak LHGR experienced by the fuel during its lifetime; see e.g. Appendix A to [52] and references therein.

To assess the possibility of using the analytically derived relation  $\mathcal{T} \propto D_h^3$  for estimating the transmissivity of cracked fuel pellets, we may use the data from KfK out-of-reactor gas flow experiments, which were summarized in section 3.2.4. These experiments were conducted on 0.5 m long fuel rod segments that were charged with either solid (uncracked) or cracked  $\text{Al}_2\text{O}_3$  pellets. The latter were manually cracked one-by-one by use of a cape chisel. On average, each pellet was broken into three fragments [20]. We recall from Table 6 that the permeability of segments containing cracked pellets was about 40 % of that measured for segments containing solid pellets. Let us compare this finding with the calculated reduction in permeability obtained from the difference in hydraulic diameter between the idealized cross-sections for solid and cracked pellets shown in Figure 20. The assumed crack pattern increases the wetted perimeter from 57.8 to 85.2 mm, leading to a reduction of the hydraulic diameter from 0.198 to 0.135 mm. From the relation  $\mathcal{T} \propto D_h^3$ , we expect the transmissivity (or permeability) of the segments charged with cracked pellets to be  $(0.135/0.198)^3 = 0.32$  of that for segments with solid pellets. This predicted reduction is in reasonable agreement with the measured reduction for  $\kappa$  in the KfK experiments with helium and argon (0.41 and 0.38; see Table 6).

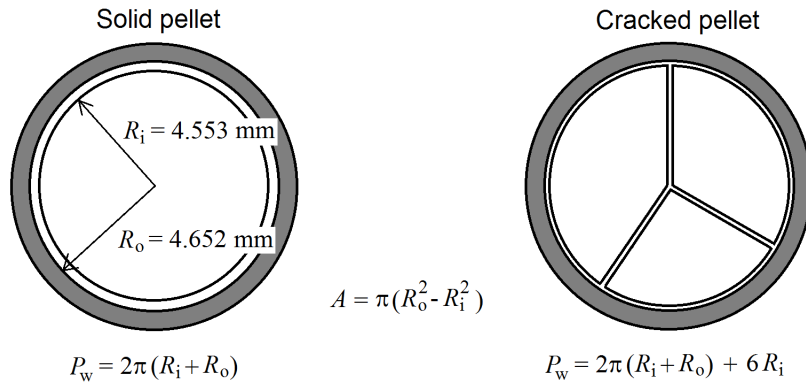


Figure 20: Schematic cross-sections for fuel rod segments containing solid and cracked pellets in KfK gas flow experiments [20]. On average, the cracked pellets were broken into three fragments.

Hence, with a Hagen-Poiseuille type duct flow model, it seems possible to link the transmissivity  $\mathcal{T}$  to parameters that can be readily calculated by the fuel rod analysis computer program that hosts the model. The situation is different for models for flow in porous and/or cracked media. While the gross cross-sectional area  $\tilde{A}$  is trivial to calculate from the cladding inner radius, there is no way to directly estimate the permeability of the fuel pellet column by simple means. As shown in section 2.3.4, the models needed for estimating  $\kappa$  in cracked media are complex and far beyond the scope of most computer programs used for fuel rod thermal-mechanical analysis. A feasible approach for estimating  $\kappa$  in such programs could be to use the correspondence between  $\mathcal{T}$  and  $\tilde{A}\kappa$  revealed by eqs. (62) and (64), combined with the estimates for  $\mathcal{T}$  and  $D_h$  discussed above. To illustrate this

correspondence, we make use of eq. (63) and set  $\mathcal{T} = \tilde{A}\kappa = \pi R_o^2 \kappa$ , which results in

$$\kappa = \frac{(R_i + R_o)D_h^3}{\text{Hg}R_o^2}. \quad (65)$$

We recall that eq. (65) was used with  $\text{Hg} = 96$  for assessing gas flow experiments in sections 3.2.2 and 3.2.3. This particular Hagen number was used in these sections, since the experimentalists used it in eq. (65) when evaluating their measured data. Consequently,  $\text{Hg} = 96$  reproduces their original data exactly. However, as shown in section 2.2.3, the Hagen number depends on the geometry assumed for the flow channel, and  $\text{Hg} = 96$  is valid for a narrow annular duct with concentric circular cross-section. Equation (65) is plotted in Figure 21 for two fixed values of  $\text{Hg}$  and for a case where  $\text{Hg}$  is assumed to depend on the hydraulic diameter through

$$\text{Hg}(D_h) = \begin{cases} 890 & \text{if } D_h < 20 \mu\text{m}, \\ 38.4 + \frac{2.146 \times 10^{-5}}{D_h^{1.617}} & \text{if } D_h \geq 20 \mu\text{m}. \end{cases} \quad (66)$$

Equation (66) is used in the GASMIX model for axial transport and mixing of gas inside LWR fuel rods [29]. It is empirically based on data from the INEL gas flow experiments presented in section 3.2.3. As shown in Figure 4, the values 38.4 and 96 constitute lower and upper limits for  $\text{Hg}$  in annular ducts with circular cross-section. Figure 21 suggests that the gas permeability is extremely sensitive to  $D_h$  when  $D_h$  is less than 20-25  $\mu\text{m}$ . This finding agrees with data from in-reactor gas flow experiments on high-burnup fuel rods with a closed or nearly closed pellet-cladding gap; see section 3.2.2.

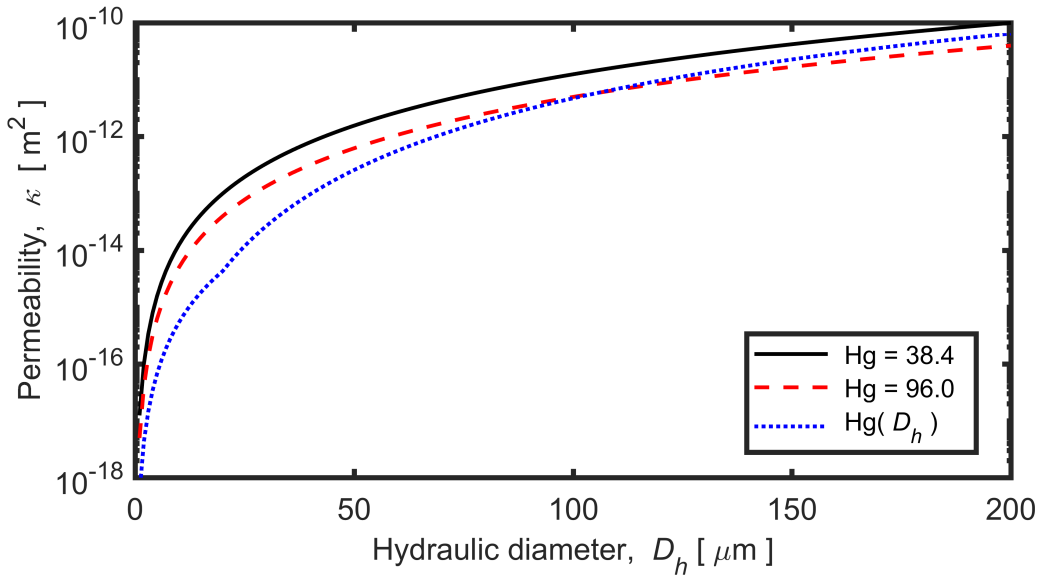


Figure 21: Equation (65) plotted for a typical 17×17-design PWR fuel rod ( $R_i = 4.15$  mm,  $R_o = 4.18$  mm) and various Hagen numbers. The blue dotted line refers to  $\text{Hg}(D_h)$  given by eq. (66).

# 5 Conclusions and outlook

## 5.1 Conclusions

In section 2.1 of the report, we departed from the fundamental conservation equations for mass, momentum and energy that, together with constitutive relations for the fluid, provide a system of equations for the sixteen variables that define the state of the flowing fluid in a general case. Simplifying approximations to these general equations, relevant for modelling of pressure-driven axial gas flow inside LWR fuel rods, were then introduced. More precisely, we showed that the conservation equation for energy could be omitted, since the gas temperature is controlled by the assumedly known temperature distributions of the fuel pellets and the cladding inner surface. We also showed that the flow may be assumed one-dimensional and quasi-stationary, without losing much accuracy or significance.

In section 2.2, we concluded that these simplifying approximations lead to the well-known Hagen-Poiseuille equation, provided that the gas flow is sufficiently slow to be laminar. Hence, the momentum conservation equation can be written

$$p \frac{\partial p}{\partial z} = - \frac{RT\mu}{M\mathcal{F}} \dot{m}, \quad (67)$$

where all properties except for the universal gas constant  $R$  may vary with time and axial position ( $z$ ) along the fuel rod. However, they are assumed uniform in the lateral ( $r, \theta$ )-plane, which means that they represent cross-sectional average properties. In section 2.2, we also showed that the axial gas transmissivity,  $\mathcal{F}$ , can be calculated analytically for simple cross-sectional geometries of the flow channel, such as an annular pellet-cladding gap. No analytical solutions exist for more complex geometries, but our analysis suggests that the analytical solutions for simple geometries may provide the basis for estimating  $\mathcal{F}$  for more complex geometries from properties that can be readily calculated by computer programs for thermal-mechanical fuel rod analysis; see section 4.2.

Equation (67) should be solved together with the conservation equation for mass, which in the fuel rod geometry may be expressed as

$$\frac{\partial \dot{m}}{\partial z} = \dot{r} - \frac{\partial}{\partial t} (\rho A), \quad (68)$$

where  $\dot{r}$  [ $\text{kg}(\text{ms})^{-1}$ ] is the local fuel fission gas release rate per unit length of the fuel pellet column. To close the set of equations for the unknown properties  $\dot{m}$ ,  $p$  and  $\rho$ , we apply the ideal gas law

$$\rho = \frac{Mp}{RT}, \quad (69)$$

which is applicable to the gas temperatures and pressures expected in fuel rod void volumes. Equations (67)-(69) are to be simultaneously solved for  $\dot{m}(t, z)$ ,  $p(t, z)$  and  $\rho(t, z)$ , based on  $T(t, z)$ ,  $A(t, z)$  and  $\dot{r}(t, z)$ , which are provided by the computer program that hosts the gas flow model. The viscosity  $\mu$  and transmissivity  $\mathcal{F}$  are calculated from the above mentioned properties by use of correlations. The numerical method to solve eqs. (67)-(69) should be adapted to the host program, in particular to how  $T$ ,  $A$  and  $\dot{r}$  are discretized with regard to space and time by other modules in the program.

In some existing models for pressure-driven axial gas flow inside LWR fuel rods, eq. (67) is replaced by empirically based simplifications to the momentum equation, which emanate from work on fluid flow through porous and/or cracked media. A fairly general relation of this kind is the Forchheimer equation

$$p \frac{\partial p}{\partial z} = -\frac{RT}{M} \left( \frac{\mu}{\tilde{A}\kappa} + \frac{\beta}{\tilde{A}^2} |\dot{m}| \right) \dot{m}, \quad (70)$$

where  $\kappa$  and  $\beta$  are material properties that characterize the permeability of the cracked fuel pellets that fill the cladding tube with internal cross-sectional area  $\tilde{A}$ . In cases with moderate mass flow rates  $\dot{m}$ , the non-linear term in the right-hand-side of eq. (70) can be neglected. The linearized equation is the well-known Darcy's law, which is the form of eq. (70) that is used in all existing fuel rod models for axial gas flow of this kind. The linearized form of eq. (70) is equivalent to eq. (67), provided that  $\mathcal{T} \equiv \tilde{A}\kappa$ . The linearized form is adequate for most expected flow conditions inside LWR fuel rods. The non-linear term is deemed relevant only for cases with very steep axial pressure gradients in combination with wide pellet-cladding gaps. Such cases may possibly occur immediately after cladding burst under loss-of-coolant accidents, in parts of the fuel rod with large cladding tube distension (ballooning).

Hence, the momentum equations resulting from the two modelling approaches, i.e. Hagen-Poiseuille vis-à-vis Darcy flow, are equivalent if  $\mathcal{T} \equiv \tilde{A}\kappa$ . As shown in section 4.2, the Hagen-Poiseuille approach has an advantage in that the axial gas transmissivity  $\mathcal{T}$  can be estimated from analytical solutions. More specifically, these solutions show that  $\mathcal{T} \propto D_h^3$ , where the hydraulic diameter is defined by  $D_h = 4A/P_w$ . Both the true cross-sectional flow area  $A$  and the wetted perimeter  $P_w$  are possible to estimate from calculated pellet and cladding deformations and the typical size of fuel pellet fragments, i.e. from parameters that can be readily computed by programs for fuel rod thermal-mechanical analyses.

Any model used for estimating  $\mathcal{T}$  (or the equivalent property  $\tilde{A}\kappa$ ) from parameters calculated by a fuel rod analysis program must be calibrated against data from axial gas flow experiments on LWR fuel rods. Our review of such experimental data in section 3 of the report showed that most of the current database consists of out-of-reactor gas flow experiments on discharged PWR UO<sub>2</sub> fuel rods. These experiments usually provide the rod average axial transmissivity, since the pressure difference and its associated gas flow rate are measured over the entire length of the rods. However, some data exist also for shorter sections of fuel rods. These data show that the transmissivity may vary by an order of magnitude along a fuel rod, as a consequence of axial variations in the rate of fuel pellet swelling and cladding tube creep-down. Figure 22 summarizes the current database from out-of-reactor gas flow experiments on discharged PWR fuel rods. This database covers fuel designs from the 1970s to about 2010, with rod average burnups from 26 to 59 MWd(kgU)<sup>-1</sup>, representing the increase in typical discharge burnups over these four decades. Evidently, the axial permeability decreases with burnup, as a result of pellet-cladding gap narrowing. This trend is also clear from the Halden IFA-504.2 in-reactor test, data from which are included in Figure 22 for comparison. In this test, the zero-power permeability was repeatedly measured during more than twenty years of continuous fuel rod operation in the Halden reactor.

Most of the spread for the zero-power permeability data in Figure 22 is deemed to result from differences in the end-of-life power among the tested fuel rods. In high-burnup fuel, the pellet and cladding are usually in contact when the fuel rod is operating at nominal

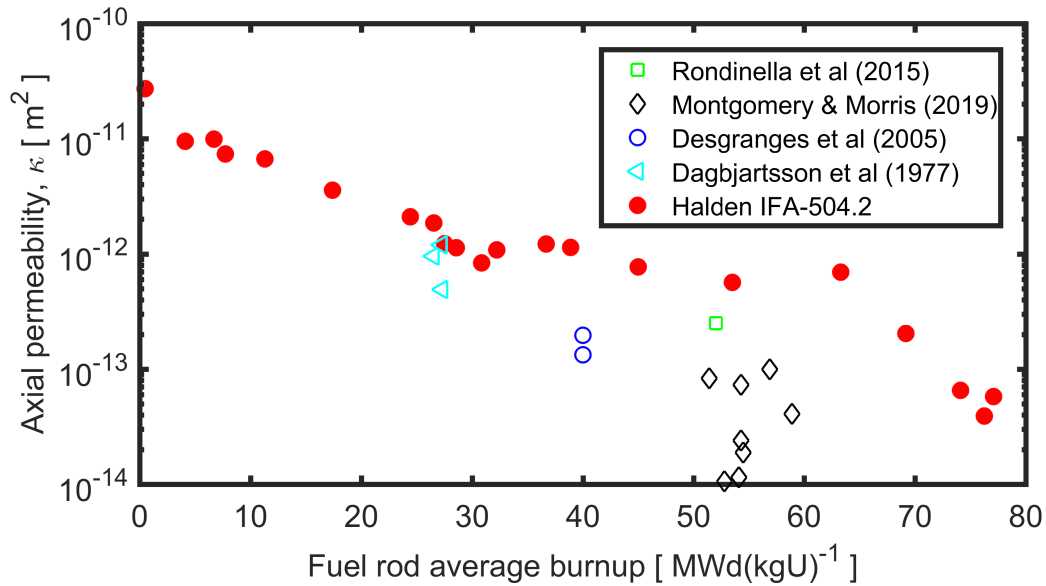


Figure 22: Open symbols: Rod average zero-power axial gas permeability, measured in out-of-reactor gas flow experiments on full-length discharged PWR  $\text{UO}_2$  fuel rods. Filled circles: Rodlet average zero-power axial gas permeability, measured in Halden IFA-504.2 in-reactor gas flow tests. See section 3 for a review of the data sources.

power. For this reason, the zero-power permeability shown in Figure 22 is controlled by the differential shrinkage between the pellet and cladding when the fuel rod is downrated from operating power to zero power prior to discharge. Downrating a high-burnup fuel rod from high operating power therefore results in a wide flow path and high zero-power permeability, as is the case for the IFA-504.2 test rod in the burnup range from 40 to 65  $\text{MWd}(\text{kgU})^{-1}$ ; see section 3.2.2. Hence, the past power history is very important for the zero-power or low-power axial permeability in high-burnup fuel rods. Information on the power histories of the tested fuel rods included in Figure 22 is unfortunately unavailable in the open literature, which means that possible causes to the observed differences in zero-power permeability cannot be properly assessed.

In addition to the zero-power permeability data obtained from out-of-reactor gas flow experiments on discharged PWR fuel rods, there are also useful data from Halden in-reactor measurements, more precisely from the gas flow rigs IFA-430 and IFA-504. To the author's best knowledge, these Halden gas flow experiments are currently the only available sources of information regarding axial gas transport inside fuel rods that operate at power. The Halden in-reactor permeability data suggest that axial gas flow inside LWR fuel rods with non-annular fuel pellets is extremely sensitive to the state of the pellet-cladding gap, when the gap is passing from closed to open or vice versa. This finding agrees with the  $\tilde{A}\kappa \equiv \mathcal{F} \propto D_h^3$  dependence obtained from analytical solutions for the transmissivity of annular ducts. With regard to modelling and computational analyses, these findings underline the importance of accurate gap state predictions for reliable calculations of axial gas flow.

Finally, there are also data from laboratory gas flow experiments on fuel rod segments charged with either uncracked or manually cracked  $\text{Al}_2\text{O}_3$  pellets. These data show that pellet cracking causes a significant reduction in axial gas transmissivity or permeability. Our analysis of these data shows that this reduction can be understood and modelled by the

increase in gas-solid interface area (wetted perimeter) brought about by the cracking; see section 4.2.

## 5.2 Outlook

The presented analysis of models and data for pressure-driven axial gas flow inside LWR fuel rods shows that most expected flow conditions can be adequately modelled with the fairly simple equations that are summarized in section 5.1. These equations are here formulated in terms of mass flow rate ( $\dot{m}$ ) and mass density ( $\rho$ ), which is the formulation normally found in the literature. However, when they are numerically solved in a computer program for fuel rod thermal-mechanical analysis, they should be formulated in terms of molar flow rate and molar density. This eliminates the molar mass ( $M$ ) from the equations, and hence, the need to calculate  $M$  from the gas composition in the fuel rod void volumes, which may vary with both space and time.

Under conditions of slow (creeping) gas flow, the linearized one-dimensional momentum equations obtained from Hagen-Poiseuille type models for flow in ducts and Darcy-Forchheimer type models for flow in porous media are equivalent: they differ only by the way the axial transmissivity/permeability of the flow channel is described. The axial transmissivity is a key parameter in both types of models, and as shown in this report, it is extremely sensitive to the state of the pellet-cladding gap, when the gap is passing from closed to open or vice versa. Our analysis of models and data indicates that the transmissivity can be estimated from parameters that are, or could readily be, calculated by programs for fuel rod thermal-mechanical analyses. Reasonable estimates can be made by use of analytical solutions for transmissivity of annular ducts, if these solutions are extended to account for the increased gas-solid interface area caused by fuel pellet cracking. Considering that the axial transmissivity is very sensitive to the pellet-cladding gap state, it is recommended that any model used for estimating the transmissivity from *calculated* gap state parameters (e.g. calculated pellet and cladding deformations, extent of pellet cracking and fragment relocation) is calibrated against gas flow data *together* with the fuel rod analysis program that computes these gap state parameters. Hence, calibration of transmissivity models separately and independently of a specific host program is deemed impracticable.

A handful of gas flow experiments on LWR fuel rods are reported in the open literature. Unfortunately, most of the public domain database is of limited value for model calibration and validation: Firstly, most data pertain to zero-power conditions. At zero rod power, there are usually void volumes between fuel pellet fragments, which provide a tortuous axial flow path also in high-burnup fuel. These voids shrink with increasing power, which leads to a significant reduction in axial gas transmissivity. This reduction is poorly known. Secondly, information on the operating histories of the tested fuel rods is unavailable in open literature. The operating histories, especially the end-of-life fuel rod power level and axial distribution, are important to the zero-power transmissivity. Power histories and background information on the tested fuel rods are therefore warranted. This information may exist, but it is currently unavailable in open sources. Thirdly, most experiments involve gas flow measurements over full-length fuel rods and produce only rod average values for the axial transmissivity. This is problematic, since a few sets of data on medium burnup fuel rods show that the transmissivity may vary by an order of magnitude along a fuel rod, as a result of the axial variations in fuel pellet swelling and cladding tube creep-down. Hence,

with regard to data for model validation, axial gas flow experiments on short, carefully characterized, fuel rod segments would be useful. A few experiments of this kind have been conducted within Part III of the Studsvik Cladding Integrity Project (SCIP-III), and similar experiments are planned for Part IV of the project [79]. These experiments are done by imposing a steady gas flow through short-length test rodlets, prior to LOCA simulation tests. The results of these experiments are available to SCIP participants, but they are not yet in the public domain.

The scope of this report is restricted to models and data for pressure-driven axial gas flow, which is one of the transport mechanisms for gas inside LWR fuel rods. The other mechanism, multi-component gas diffusion under isobaric conditions, is treated in a separate report [29].

**Acknowledgements** The work was sponsored by the Swedish Radiation Safety Authority (SSM) through research grant DNR SSM2021-817.



# 6 Nomenclature

## 6.1 Latin symbols

$A$	True cross-sectional flow area [m <sup>2</sup> ]
$\tilde{A}$	Gross cross-sectional area containing a porous/cracked solid [m <sup>2</sup> ]
$b$	Klinkenberg parameter, $b = D_K \mu / \kappa$ [Pa]
$c_p$	Heat capacity at constant pressure [J(kgK) <sup>-1</sup> ]
$d$	Characteristic pore dimension [m]
$d_k$	Kinetic diameter of gas molecule [m]
$D_h$	Hydraulic diameter, $D_h = 4A/P_w$ [m]
$D_K$	Knudsen diffusivity [m <sup>2</sup> s <sup>-1</sup> ]
$E$	Total specific energy [J(kg) <sup>-1</sup> ]
$f_D$	Darcy friction factor [-]
$f_P$	Friction factor for porous materials [-]
$F_i$	Body force component [N(kg) <sup>-1</sup> ]
$h$	Gap width [m]
$H$	Specific enthalpy [J(kg) <sup>-1</sup> ]
Hg	Hagen number [-]
$k_B$	Boltzmann constant, $1.3806 \times 10^{-23}$ [JK <sup>-1</sup> ]
$k_I$	Inertial permeability, $k_I = \beta^{-1}$ [m]
$L$	Axial length of flow channel [m]
$\dot{m}$	Mass flow rate [kgs <sup>-1</sup> ]
$M$	Molar mass of gas [kgmol <sup>-1</sup> ]
$p$	Pressure (thermodynamic) [Pa]
$P_w$	Wetted perimeter [m]
$Q$	Volumetric flow rate [m <sup>3</sup> s <sup>-1</sup> ]
$r$	Radial coordinate [m]
$\dot{r}$	Fuel fission gas release rate per unit axial length [kg(ms) <sup>-1</sup> ]
$R$	Universal gas constant, 8.134 [J(molK) <sup>-1</sup> ]
$R_i$	Radial position of annular gap inner surface [m]
$R_o$	Radial position of annular gap outer surface [m]

$Re$	Reynolds number [-]
$t$	Time [s]
$T$	Temperature [K]
$\mathcal{T}$	Gas transmissivity [ $m^4$ ]
$u$	Velocity [ $ms^{-1}$ ]
$\bar{u}$	Pore velocity [ $ms^{-1}$ ]
$\tilde{u}$	Superficial velocity, $\tilde{u} = Q/\tilde{A}$ [ $ms^{-1}$ ]
$V$	Volume [ $m^3$ ]
$x$	Cartesian coordinate [m]
$y$	Cartesian coordinate [m]
$z$	Axial coordinate (in flow direction) [m]

## 6.2 Greek symbols

$\alpha$	Parameter in Forchheimer's equation (40) [ $m^{-2}$ ]
$\bar{\alpha}$	Dimension-free parameter in eqs. (19)-(20) [-]
$\beta$	Parameter in Forchheimer's equation (40) [ $m^{-1}$ ]
$\Delta_e$	Eccentricity of annular gap [m]
$\epsilon$	Effective surface roughness [m]
$\eta$	Parameter in eq. (53) [ $m^{-2}s^{-1}$ ]
$\theta$	Azimuthal coordinate [rad]
$\kappa$	Permeability, $\kappa = \alpha^{-1}$ [ $m^2$ ]
$\lambda$	Thermal conductivity [ $W(mK)^{-1}$ ]
$\lambda_f$	Mean free path [m]
$\Lambda$	Second viscosity coefficient [Pas]
$\mu$	Dynamic viscosity [Pas]
$\mu_b$	Bulk viscosity coefficient [Pas]
$\rho$	Density [ $kgm^{-3}$ ]
$\sigma$	Cauchy stress [Pa]
$\tau$	Deviatoric stress [Pa]
$\phi$	Porosity volume fraction [-]

# References

- [1] Nuclear fuel behaviour under loss-of-coolant (LOCA) conditions. Report NEA No. 7483, OECD Nuclear Energy Agency, Paris, France, 2022. (In press).
- [2] Nuclear fuel behaviour under reactivity initiated accident (RIA) conditions. Report NEA No. 7575, OECD Nuclear Energy Agency, Paris, France, 2022. (In press).
- [3] J. L. Guillet and Y. Guerin, editors. *Nuclear Fuel - A Nuclear Energy Division Monograph*. Commissariat à l'Énergie Atomique et aux Énergies Alternatives (CEA), Saclay, Gif-sur-Yvette, France, 2009.
- [4] R. J. White, E. Skattum, and A. Haaland. Communication of fission products in the interior of a fuel rod, with particular emphasis on recent tests on the IFA-430 gas flow rig. Report HPR-325, OECD Halden Reactor Project, Halden, Norway, 1985.
- [5] J. C. Killeen and A. Haaland. Mixing of argon and helium in the interior of a fuel rod: results of experiments with the IFA-504 gas flow rig. Report HWR-172, OECD Halden Reactor Project, Halden, Norway, 1986.
- [6] J. C. Killeen and A. Haaland. Mixing of argon and helium in the interior of an operating fuel rod. Report HWR-186, OECD Halden Reactor Project, Halden, Norway, 1986.
- [7] J. C. Killeen. Thermal response of the gas flow rig IFA-504 to fission gas release. Report HWR-194, OECD Halden Reactor Project, Halden, Norway, 1987.
- [8] C. Vitanza, T. Johnsen, and J. M. Aasgaard. Interdiffusion of noble gases: results of an experiment to simulate dilution of fission gases in a fuel rod. Report HPR-295, OECD Halden Reactor Project, Halden, Norway, 1983.
- [9] M. Kinoshita. Axial transport of fission gas in LWR fuel rods. In *IAEA Specialists Meeting on Water Reactor Fuel Element Performance Computer Modelling*, IWGFPT/13, pages 387–396, Preston, UK, March 15-19, 1982. IAEA.
- [10] M. Kinoshita. Evaluation of axial fission gas transport in power ramping experiments. *Res Mechanica*, 19(3):219–226, 1986.
- [11] M. Nakamura, K. Hiramoto, and A. Maru. Evaluation of LWR fuel rod behavior under operational transient conditions. *Nucl. Engng. Design*, 80(1):49–63, 1984.
- [12] T. Nakajima. FEMAXI-IV: a computer code for the analysis of fuel rod behavior under transient conditions. *Nucl. Engng. Design*, 88(1):69–84, 1985.
- [13] N. Kjaer-Pedersen. The effect of axial diffusional delays on the overall fission gas release. In *IAEA Specialists Meeting on Water Reactor Fuel Element Performance Computer Modelling*, IWGFPT/13, pages 343–346, Preston, UK, March 15-19, 1982. IAEA.
- [14] K. Ito, Y. Iwano, H. Furuya, M. Sugisaki, and K. Hashizume. Simple model for describing axial fission gas transport in fuel rod. *J. Nucl. Sci. Techn.*, 22(1):73–75, 1985.

- [15] M. T. del Barrio and L. E. Herranz. Axial fission gas transport in nuclear fuel rods. *Defect and Diffusion Forum*, 283-286:262–267, 2009.
- [16] M. Suzuki, H. Saitou, Y. Udagawa, and F. Nagase. Light water reactor fuel analysis code FEMAXI-7; Model and structure. Report JAEA-Data/Code-2013-005, Japan Atomic Energy Agency, Tokai-mura, Japan, 2013.
- [17] A. Moal. Advanced models for the simulation of post-DNB phenomena during reactivity initiated accidents with SCANAIR. In *Proceedings of the 2010 LWR Fuel Performance Meeting/TopFuel/WRFPM*, pages 297–306, Orlando, FL, USA, September 26-29, 2010. American Nuclear Society.
- [18] W. Gulden et al. SSYST-1: A computer code system to analyse the fuel rod behaviour during a loss of coolant accident. Report KFK-2496, Kernforschungszentrum Karlsruhe, Karlsruhe, Germany, 1977. (in German).
- [19] J. A. Dearien, L. J. Siefken, M. P. Bohn, D. R. Coleman, and E. T. Laats. FRAP-T2: A computer code for the transient analysis of oxide fuel rods. Report TREE-NUREG-1040, Idaho National Engineering Laboratory, Idaho Falls, ID, USA, 1977.
- [20] E. Karb, G. Harbauer, W. Legner, L. Sepold, and K. Wagner. Theoretical and experimental investigations on gas flow in LWR fuel rods during loss-of-coolant accidents. Report KFK-2411, Kernforschungszentrum Karlsruhe, Karlsruhe, Germany, 1976. (in German).
- [21] S. J. Dagbjartsson, D. E. Owen, B. A. Murdock, and P. E. MacDonald. Axial gas flow in irradiated PWR fuel rods. Report TREE-NUREG-1158, Idaho National Engineering Laboratory, Idaho Falls, ID, USA, 1977.
- [22] W. Wiesenack, L. Kekkonen, and B. Oberländer. Axial gas transport and loss of pressure after ballooning rupture of high burn-up fuel rods subjected to LOCA conditions. In *Proceedings of the International Conference on the Physics of Reactors (PHYSOR'08)*, pages 2987–2992, Interlaken, Switzerland, September 14-19, 2008. Paul Scherrer Institut.
- [23] W. Wiesenack. Summary of the Halden Reactor Project LOCA test series IFA-650. Report HPR-380, OECD Halden Reactor Project, Halden, Norway, 2013.
- [24] Report on fuel fragmentation, relocation, dispersal. Report NEA/CSNI/R(2016)16, OECD Nuclear Energy Agency, Paris, France, 2016.
- [25] G. Khvostov, W. Wiesenack, M. A. Zimmermann, and G. Ledergerber. Some insights into the role of axial gas flow in fuel rod behaviour during the LOCA, based on Halden tests and calculations with the FALCON-PSI code. *Nucl. Engng. Design*, 241:1500–1507, 2009.
- [26] R. Montgomery and R. N. Morris. Measurement and modeling of the gas permeability of high burnup pressurized water reactor fuel rods. *J. Nucl. Mater.*, 523:206–215, 2019.
- [27] R. N. Morris and R. Montgomery. Sister rod destructive examinations (FY20), Appendix C: Rod internal pressure, void volume and gas transmission tests. Report ORNL/SPR-2020/1769, Oak Ridge National Laboratory, Oak Ridge, TN, USA, 2020.

- [28] J. M. Scaglione, R. A. Montgomery, and B. B. Bevard. Post irradiation examination plan for high burnup demonstration project sister rods. Report ORNL/SR-2016/111, Oak Ridge National Laboratory, Oak Ridge, TN, USA, 2016.
- [29] L. O. Jernkvist. Models for axial gas flow and mixing in LWR fuel rods. Research report 2020:02, Swedish Radiation Safety Authority, Stockholm, Sweden, 2020. Available at: [www.ssm.se](http://www.ssm.se).
- [30] L. Desgranges, M. H. Faure, and A. Thouroude. A new apparatus for determination of the free volume of a fuel rod using the double expansion method. *Nucl. Techn.*, 149:14–21, 2005.
- [31] A. Moal, V. Georgenthum, and O. Marchand. SCANAIR: A transient fuel performance code, Part one: General modelling description. *Nucl. Engng. Design*, 280:150–171, 2014.
- [32] V. V. Rondinella, D. Papaioannou, R. Nasyrow, W. Goll, and M. Rehm. Measurement of gas permeability along the axis of a spent fuel rod. In *Proceedings of the 2015 Water Reactor Fuel Performance Meeting (TopFuel-2015)*, volume 2, pages 217–225, Zürich, Switzerland, September 13-17, 2015. European Nuclear Society.
- [33] G. K. Batchelor. *An introduction to fluid dynamics*. Cambridge Mathematical Library. Cambridge University Press, Cambridge, UK, 3rd edition, 2000.
- [34] J. Bear. *Dynamics of Fluids in Porous Media*. Dover Publications, New York, USA, 1988.
- [35] J. E. Shepherd and D. R. Begeal. Transient compressible flow in porous materials. Report SAND83-1788, Sandia National Laboratories, Albuquerque, NM, USA, 1988.
- [36] H. Petersen. The properties of helium: density, specific heats, viscosity and thermal conductivity at pressures from 1 to 100 bar and from room temperature to about 1800 K. Risø report No. 224, Danish Atomic Energy Commission, Risø Research Establishment, Denmark, 1970.
- [37] J. Serrin. *Mathematical principles of classical fluid mechanics*, volume 3/8/1, chapter Fluid Dynamics I, Encyclopedia of Physics (C. Truesdell, Ed), pages 125–263. Springer, Berlin, Germany, 1959.
- [38] M. Reimann. Analytical investigation of annular gap gas flow during ballooning of zircaloy claddings. Report KFK-2280, Kernforschungszentrum Karlsruhe, Karlsruhe, Germany, 1976. (in German).
- [39] M. Abramowitz and I. A. Stegun. *Handbook of Mathematical Functions*. Dover, New York, 1964.
- [40] E. H. Karb, M. Prüssmann, L. Sepold, P. Hofmann, and G. Schanz. LWR fuel rod behavior in the FR2 in-pile tests, simulating the heatup phase of a LOCA. Report KFK-3346, Kernforschungszentrum Karlsruhe, Karlsruhe, Germany, 1983.
- [41] G. G. Stokes. On the theories of the internal friction of fluids in motion, and of the equilibrium and motion of elastic solids. *Trans. Camb. Philos. Soc.*, 8:287–319, 1845. Reprinted 2009 by Cambridge University Press, in: *Mathematical and Physical Papers - Cambridge Library Collection - Mathematics*, pp. 75-129.

- [42] G. Buresti. A note on Stokes' hypothesis. *Acta Mech.*, 226:3555–3559, 2015.
- [43] R. W. Zimmerman and G. S. Bodvarsson. Hydraulic conductivity of rock fractures. *Transport in Porous Media*, 23:1–30, 1996.
- [44] R. Berker. *Integration des equations du mouvement d'un fluide visqueux incompressible*, volume VIII/2, chapter Fluid Dynamics I, Encyclopedia of Physics (S. Flügge, C. Truesdell, Eds), pages 1–384. Springer, Berlin, Germany, 1963.
- [45] P. G. Drazin and N. Riley. *The Navier-Stokes equations: a classification of flows and exact solutions*. London Mathematical Society Lecture Note Series No. 334. Cambridge University Press, Cambridge, UK, 2006.
- [46] K. J. Geelhood, W. G. Luscher, J. M. Cuta, and I. E. Porter. FRAPTRAN-2.0: A computer code for the transient analysis of oxide fuel rods. Report PNNL-19400, Vol.1 Rev.2, Pacific Northwest National Laboratory, Richland, WA, USA, 2016.
- [47] A. Nagashima and I. Tanishita. Viscosity measurement of water and steam at high temperatures and high pressures. *Bull. JSME*, 12(54):1467–1478, 1969.
- [48] C. F. Colebrook. Turbulent flow in pipes, with particular reference to the transition region between the smooth and rough pipe laws. *J. Institution Civil Engineers*, 11(4):133–156, 1939.
- [49] D. Brkić. Review of explicit approximations to the Colebrook relation for flow friction. *J. Petroleum Sci. Engng.*, 77(1):34–38, 2011.
- [50] G. P. Mezzi. Thermoelastic stresses in pellet fragments and conditions for fragments formation. *Nucl. Engng. Des.*, 73:83–93, 1983.
- [51] M. Oguma. Cracking and relocation behaviour of nuclear fuel pellets during rise to power. *Nucl. Engng. Des.*, 76:35–45, 1983.
- [52] L. O. Jernkvist and A. R. Massih. Models for axial relocation of fragmented and pulverized fuel pellets in distending fuel rods and its effects on fuel rod heat load. Research report 2015:37, Swedish Radiation Safety Authority, Stockholm, Sweden, 2015. Available at: [www.ssm.se](http://www.ssm.se).
- [53] P. Van Uffelen and G. Pastore. *Comprehensive Nuclear Materials*, volume 2, chapter 2.13 Oxide fuel performance modeling and simulation, pages 363–416. Elsevier, 2nd edition, 2020.
- [54] M. Muskat. *The Flow of Homogeneous Fluids Through Porous Media*. McGraw-Hill, New York, NY, USA, 1937.
- [55] F. A. L. Dullien. *Porous Media: Fluid Transport and Pore Structure*. Academic Press, San Diego, CA, USA, 2nd edition, 1991.
- [56] S. Whitaker. Flow in porous media I: a theoretical derivation of Darcy's law. *Transport in Porous Media*, 1:3–25, 1986.
- [57] S. Whitaker. The Forchheimer equation: a theoretical development. *Transport in Porous Media*, 25:27–61, 1996.
- [58] E. Erdim, Ö. Akgiray, and I. Demir. A revisit of pressure drop-flow rate correlations for packed beds of spheres. *Powder Techn.*, 283:488–504, 2015.

- [59] J. Q. Zhou, Y. F. Chen, L. Wang, and M. B. Cardenas. Universal relationship between viscous and inertial permeability of geologic porous media. *Geophys. Res. Letters*, 46:1441–1448, 2019.
- [60] L. J. Klinkenberg. The permeability of porous media to liquids and gases. *Drilling and Production Practice*, pages 200–213, 1941. American Petroleum Institute.
- [61] P. Forchheimer. Wasserbewegung durch Boden. *Zeitschrift des Vereins deutscher Ingenieure*, 45:1782–1788, 1901.
- [62] A. Moal. SCANAIR reference documentation, Version V\_7\_10. Report IRSN/2020-00076, Institute de Radioprotection et de Sûreté Nucléaire (IRSN), Cadarache, Saint-Paul-lez-Durance, France, 2020.
- [63] J. Bear, C. F. Tsang, and G. de Marsily, editors. *Flow and Contaminant Transport in Fractured Rock*. Academic Press, San Diego, CA, USA, 1993.
- [64] E. Hakami. Aperture distribution of rock fractures. Doctoral thesis TRITA-AMI PHD 1003, Royal Institute of Technology, Division of Engineering Geology, Department of Civil and Environmental Engineering, Stockholm, Sweden, 1995.
- [65] E. Hakami and E. Larsson. Aperture measurements and flow experiments on a single natural fracture. *Int. J. Rock Mechanics and Mining Sciences and Geomechanics Abstracts*, 33(4):395–404, 1996.
- [66] C. Fairhurst, F. Gera, P. Gnirk, M. Gray, and B. Stillborg. OECD/NEA International Stripa Project 1980-1992: Overview volume 1: Executive summary. Report ISBN 91-971906-2-4, Swedish Nuclear Fuel and Waste Management Company (SKB), Stockholm, Sweden, 1993. Available at: [www.skb.se](http://www.skb.se).
- [67] P. Renard and G. de Marsily. Calculating equivalent permeability: a review. *Advances in Water Resources*, 20(5-6):253–278, 1997.
- [68] P. S. Lang, A. Paluszny, and R. W. Zimmerman. Permeability tensor of three-dimensional fractured porous rock and a comparison to trace map predictions. *J. Geophys. Res. Solid Earth*, 119:6288–6307, 2014.
- [69] E. Bonnet, O. Bour, N. E. Odling, P. Davy, I. Main, P. Cowie, and B. Berkowitz. Scaling of fracture systems in geological media. *Reviews of Geophysics*, 39(3):347–383, 2001.
- [70] R. N. Thomas, A. Paluszny, D. Hambley, F. M. Hawthorne, and R. W. Zimmerman. Permeability of observed three dimensional fracture networks in spent fuel pins. *J. Nucl. Mater.*, 510:613–622, 2018.
- [71] Spent fuel performance assessment and research: Final report of a coordinated research project (SPAR-IV). Report IAEA-TECDOC-1975, International Atomic Energy Agency, Vienna, Austria, 2021.
- [72] R. A. Graham. A quantitative determination of the effects of microstructure on the gas permeability of UO<sub>2</sub> and Ni sinter bodies. Master thesis (OCoLC)13996415, Materials Science and Engineering, University of Florida, Gainesville, FL, USA, 1973.

- [73] V. Calogovic. Gas permeability measurement of porous materials (concrete) by time-variable pressure difference method. *Cement and Concrete Res.*, 25(5):1054–1062, 1995.
- [74] High burnup dry storage cask research and development project: Final test plan. Contract DE-NE-0000593, Electric Power Research Institute, Palo Alto, CA, USA, 2014.
- [75] Fuel reliability guidelines: PWR fuel cladding corrosion and crud. Report 3002002795, Rev. 1, Electric Power Research Institute, Palo Alto, CA, USA, 2014.
- [76] J. A. Turnbull and R. J. White. The thermal performance of the gas flow rigs: A review of experiments and their analyses. Report HWR-715, OECD Halden Reactor Project, Halden, Norway, 2002.
- [77] W. Wiesenack. Separate effect studies at the Halden reactor project related to fuel thermal performance and modelling. In *Proceedings of a Seminar on Thermal Performance of High-Burnup LWR Fuel*, pages 197–207, Cadarache, France, March 3-6, 1998. OECD Nuclear Energy Agency.
- [78] M. Hongo. Viscosity of argon and argon-ammonia mixtures under pressure. *Review Physical Chem. of Japan*, 48(2):63–71, 1978.
- [79] OECD Nuclear Energy Agency. Studsvik Cladding Integrity Project. [https://www.oecd-nea.org/jcms/pl\\_25445/studsvik-cladding-integrity-project-scip](https://www.oecd-nea.org/jcms/pl_25445/studsvik-cladding-integrity-project-scip), 2022.



The Swedish Radiation Safety Authority has a comprehensive responsibility to ensure that society is safe from the effects of radiation. The Authority works from the effects of radiation. The Authority works to achieve radiation safety in a number of areas: nuclear power, medical care as well as commercial products and services. The Authority also works to achieve protection from natural radiation and to increase the level of radiation safety internationally.

The Swedish Radiation Safety Authority works proactively and preventively to protect people and the environment from the harmful effects of radiation, now and in the future. The Authority issues regulations and supervises compliance, while also supporting research, providing training and information, and issuing advice. Often, activities involving radiation require licences issued by the Authority. The Swedish Radiation Safety Authority maintains emergency preparedness around the clock with the aim of limiting the aftermath of radiation accidents and the unintentional spreading of radioactive substances. The Authority participates in international co-operation in order to promote radiation safety and finances projects aiming to raise the level of radiation safety in certain Eastern European countries.

The Authority reports to the Ministry of the Environment and has around 300 employees with competencies in the fields of engineering, natural and behavioral sciences, law, economics and communications. We have received quality, environmental and working environment certification.

Publikationer utgivna av Strålsäkerhetsmyndigheten kan laddas ned via [stralsakerhetsmyndigheten.se](https://stralsakerhetsmyndigheten.se) eller beställas genom att skicka e-post till [registrator@ssm.se](mailto:registrator@ssm.se) om du vill ha broschyren i alternativt format, som punktskrift eller daisy.

**Strålsäkerhetsmyndigheten**  
**Swedish Radiation Safety Authority**  
SE-171 16 Stockholm  
Phone: 08-799 40 00  
Web: [ssm.se](https://ssm.se)  
E-mail: [registrator@ssm.se](mailto:registrator@ssm.se)

©Strålsäkerhetsmyndigheten